Chapter III:
A General View of Structural and Catalytic Results

This chapter will give a general view of the structural characteristics and the catalytic activity of the molybdate –type catalysts investigated in this work. Additional experimental data are detailed in Appendixes III-V.

More detailed and complementary data related to the solid solutions of Ni and Co molybdates in silica-dispersed and bulk catalysts prepared by sol-gel, impregnation and citrate method an their characterization and catalytic activity in propane ODH are given in Appendix III.

For more details concerning Ni and/or Co molybdates modified by bismuth and/or lanthanides and their characterization and catalytic activity in propane ODH see Appendix IV.

Appendix V reports complementary data related to the preparation and catalytic activity of Ni-Co molybdates supported on alumina, magnesia, titania, zirconia and mixed alumina-magnesia.

III.1 Overview of the structural and textural results

III.1.1 Introduction

The first part of this overview is devoted to a detailed physico-chemical characterization and the measurement of the catalytic activity of mixed Ni-Co molybdates, either as bulk phases (obtained by the citrate method) or dispersed in a silica matrix. For the dispersed catalysts, the sol-gel procedure will be compared to the classical impregnation method. The materials obtained by these routes will be compared from the point of view of their bulk and surface physico-chemical characteristics, by means of X-ray diffraction, Raman spectroscopy, surface area and porosity measurements and X-ray photoelectron spectroscopy. The results will demonstrate (i) the importance of mixed nickel-cobalt molybdates, and (ii) the interest of dispersing the active phase on a support.

Once these results will be established for silica-dispersed catalysts, analogous catalysts dispersed on various supports characterized by different acidities: Al_2O_3, MgO, TiO_2, ZrO_2, and also a mixed Al_2O_3-MgO support will be described. Alumina- and magnesia-based catalysts were prepared by impregnation and sol-gel methods, in order to evidence the influence of the preparation method on the textural properties. Because the sol-gel method allows in principle to modulate the composition of the support by combining different alkoxides in appropriate amounts, similar catalysts were

also dispersed on a mixed Al_2O_3-MgO (Al/Mg = 2) support, in order to check whether the sol-gel method is able to synthesize mixed supports with intermediate and tunable acidities, and to see if the individual properties of the alumina-supported and magnesia-supported catalysts could be combined in a synergetic way. To get a deeper insight into the support acidity effects, two other supports were also considered: titania and zirconia, but the catalysts were prepared only by impregnation.

The third part of this overview will be devoted (i) to the preparation of Ni and Co molybdate systems modified by lanthanides (La, Ce, Pr, Sm and Tb) and/or bismuth, and (ii) to their spectroscopic characterization (XRD, XPS, Raman spectroscopy). These catalysts were obtained by two different preparation methods, the sol-gel method, by which active phases are dispersed in a silica matrix, and the citrate method, used as a convenient and traditional way to obtain them as bulk phases. We will show that the involvement of a Ln-Mo-O phase in the formulation of Ni-Mo-O systems will also stabilize the β-phase.

III.1.2 Solid Solutions of Ni and Co Molybdates in Silica-dispersed and Bulk Catalysts prepared by Sol-gel, Impregnation and Citrate method

III.1.2.1 Citrate prepared catalysts

III.1.2.1.1 X-ray diffraction and BET specific surface areas

Table III.1 lists all the citrate-prepared catalysts with their respective BET specific surface areas and crystalline phases identified by X-ray diffraction. As indicated, the experimental specific surface areas of the mixed Ni-Co molybdates are generally lower than those of $NiMoO_4$ and higher than those of $CoMoO_4$, the only exception being $Ni_{0.5}Co_{0.5}MoO_4$ and $Ni_{0.45}Co_{0.55}MoO_4$, which present specific surface areas of 2.4 and 13 m^2g^{-1}, respectively.

To follow the phase transformations in function of temperature, XRD patterns were also recorded not only at room temperature but also between 303 K and 1073 K for both pure $NiMoO_4$ and $CoMoO_4$ samples. They are illustrated in fig.III.2 and III.3 for the Ni-Mo and the Co-Mo samples, respectively.

a) $NiMoO_4$

In the Ni-Mo-O system, the α-$NiMoO_4$ phase (file 33-0948) with octahedral Mo coordination is identified by XRD through its well-defined pattern displaying peaks at d-spacing values of 3.095, 3.513 and 2.746 Å (see fig.III.2, T = 303 K, peaks at 2θ = 28.56°, 25.36° and 32.6° respectively).

Table III.1: Composition, specific surface area and crystalline phases detected in simple and mixed Ni-Co molybdates prepared by the citrate method (calcination at 923 K).

Composition	Molar ratio	S_{BET} ($m^2 \cdot g^{-1}$)[a)]	Crystalline phases detected
Ni:Mo	1 :1	8.3	α-$NiMoO_4$
Co:Mo	1 :1	3.1	β-$CoMoO_4$
Ni:Co:Mo	0.75 :0.25: 1	4.0	α,β-$Ni_{0.75}Co_{0.25}MoO_4$
Ni:Co:Mo	0.50 :0.50: 1	2.4	α,β-$Ni_{0.50}Co_{0.50}MoO_4$
Ni:Co:Mo	0.45 :0.55: 1	13.0	β-$Ni_{0.45}Co_{0.55}MoO_4$
Ni:Co:Mo	0.40 :0.60: 1	5.7	β-$Ni_{0.40}Co_{0.60}MoO_4$
Ni:Co:Mo	0.35 :0.65: 1	5.4	β-$Ni_{0.35}Co_{0.65}MoO_4$
Ni:Co:Mo	0.25 :0.75: 1	3.3	β-$Ni_{0.25}Co_{0.75}MoO_4$

[a)] measurements with Kr at 77 K; ± 0.02 m^2g^{-1}

Upon heating, a phase transformation (α→β) is observed from 973 K, i.e. at a temperature which is about 80 K higher than that reported by Mazzocchia et al. for $NiMoO_4$ prepared by precipitation (53). In our case, at 973 K some peaks assigned to the α-phase (file 33-0948) are still present together with those related to the β-phase (file 45-0142), the latter phase being identified through its well-defined XRD pattern with peaks at 2θ = 23.35°, 25.56°, 26.57°, 27.20°, 28.45°, 32.13°, 33.72°, the strongest being at 26.57°. At 1073 K, the phase transformation is complete and only the peaks related to the β-phase are observed. When decreasing the temperature from 1073 K to 303 K, the opposite transformation (β→α) is observed, even if a small percentage of β-phase still remains. As far as the catalytic applications in propane ODH are concerned, it is important to point out that no phase transformation occurs in the temperature range 673-773 K, which corresponds to the range of usual operation for this reaction.

b) $CoMoO_4$

There are two major differences between the pure Ni and Co molybdates (fig. III.3): first, at room temperature, β-$CoMoO_4$ (file 21-0868) with tetrahedral Mo

coordination, evidenced by peaks at d-spacing values of 3.360, 3.81 and 3.490 Å (see fig.III.3, T = 303 K, peaks at 2θ = 26.44°, 23.36 and 25.36°) is identified instead of the α-phase (file 25-1434);

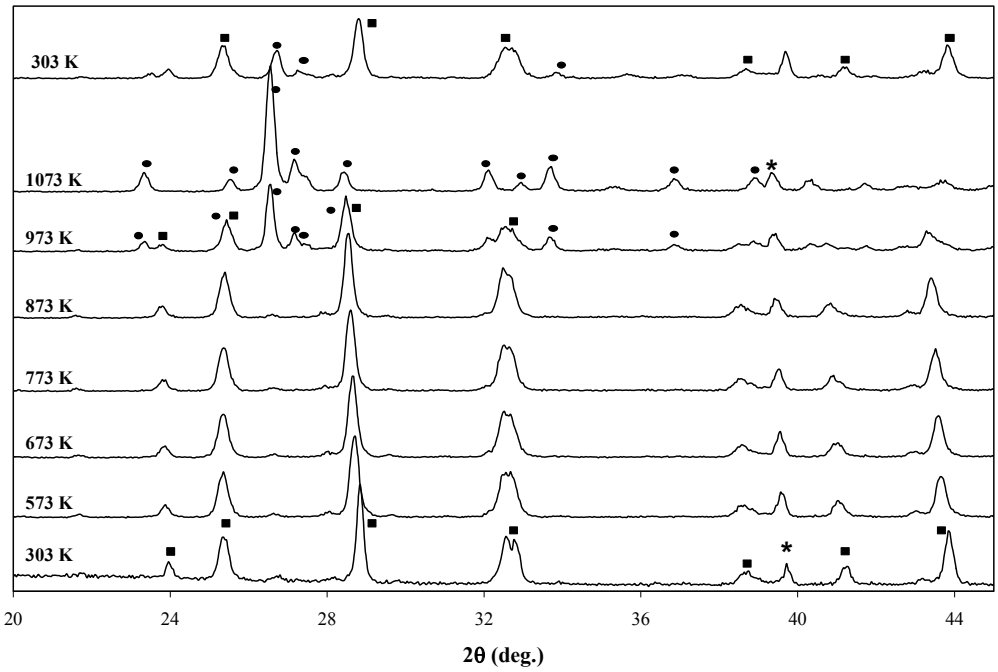

Fig.III.2: X-ray thermodiffractometry of $NiMoO_4$ prepared by the citrate method in the temperature range 303-1073 K. (•)β-$NiMoO_4$; (■) α-$NiMoO_4$; (*) Pt support.

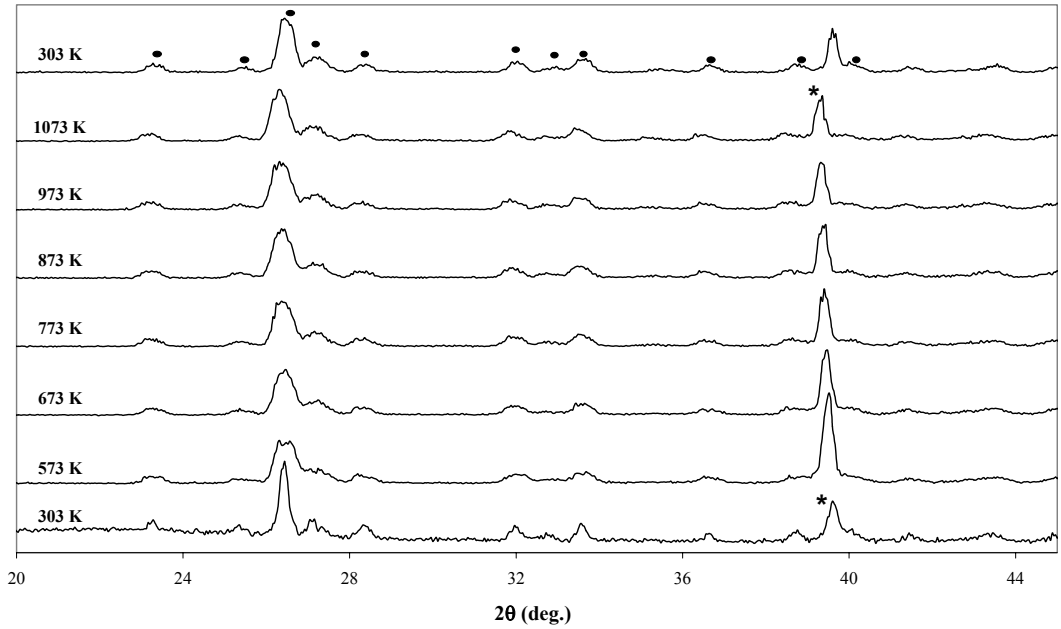

Fig.III.3: X-ray thermodiffractometry of $CoMoO_4$ prepared by the citrate method in the temperature range 303-1073 K. (•)β-$CoMoO_4$; (*) Pt support.

second, no phase transformation is observed. The fact that β-$NiMoO_4$, unlike the isotypic $CoMoO_4$ phase cannot be quenched at ambient temperature is clearly observed.

c) Mixed Ni-Co molybdates

A series of mixed nickel-cobalt molybdates corresponding to the formulation $Ni_{1-x}Co_xMoO_4$ where x =0, 0.25, 0.50, 0.55, 0.60, 0.65, 0.75 and 1, were also prepared by the citrate method.

As illustrated in fig. III.4, Vegard's law is respected in two different composition domains: the α-phase is detected in the range $0 \leq x \leq 0.5$, while the β-phase is observed in the range $0.25 \leq x \leq 1.0$. Fig. III.4 shows that a lattice expansion is observed when going from α-$NiMoO_4$ to α-$Ni_{0.5}Co_{0.5}MoO_4$, with a shift in (220) d-spacing from 3.092 Å to 3.109 Å. In the same way, lattice expansion is observed when going from β-$Ni_{0.75}Co_{0.25}MoO_4$ to β-$CoMoO_4$, as evidenced by the shift in the corresponding d-spacing from 3.344 Å to 3.374 Å. $Ni_{0.75}Co_{0.25}MoO_4$ and $Ni_{0.5}Co_{0.5}MoO_4$ are the only samples in which a mixture of both α and β-phase was detected.

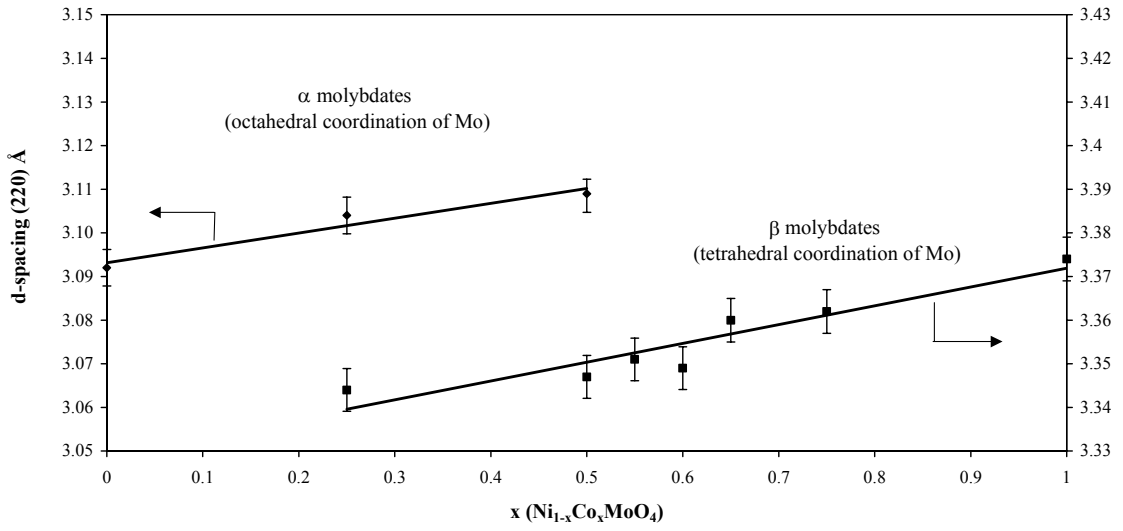

Fig.III.4: Verification of Vegard's law with the interreticular (220) d-spacing in $Ni_{1-x}Co_xMoO_4$ prepared by the citrate method. (♦)α-$Ni_{1-x}Co_xMoO_4$; (■) β-$Ni_{1-x}Co_xMoO_4$.

It should however be noted that in the case of $CoMoO_4$, the (220) and (002) lines are so close to each other (d_{220} = 3.362 Å and d_{002} = 3.361 Å) that they overlap. This behaviour is consistent with the increase in six-fold coordinated ionic radii of Ni^{2+} (0.69

Å) to Co^{2+} (0.74 Å), which is reflected in the linear increase of d-spacing with the Co/Ni ratio across each region. Since both the cell dimensions and the relative intensities representative of these two compounds vary linearly with Ni/Co atomic ratio, application of Vegard's Law (101) led us to conclude that the structures of the mixed nickel-cobalt molybdates in each domain are solid solutions of α-$NiMoO_4$ and α-$CoMoO_4$, on one hand, and of β-$NiMoO_4$ and β-$CoMoO_4$ on the other hand.

III.1.2.1.2 Raman spectroscopy

All our $Ni_{1-x}Co_xMoO_4$ samples have been analyzed by Raman spectroscopy. These data were analyzed by referring to results available in the literature (102-104) and also those obtained with pure phases from this work. They are all listed in table III.1 in Appendix III. It is observed that in all cases, the spectra characteristic of the solid solutions exhibit bands corresponding essentially to the β-phase. According to the literature sampling of α-$NiMoO_4$ is assumed to result in the formation of the so-called α'-phase, which is a distorted form of α-$NiMoO_4$ (102,104), and this has been confirmed in our case.

In all the other cases, the presence of the β-phase is inferred from the occurrence of two neighbour bands in the range 935-945 cm^{-1}, resulting in a broad band without clear resolution. The Raman spectra of catalysts whose XRD pattern revealed the presence of both α- and β-phases only displayed the bands corresponding essentially to the β-phase.

III.1.2.2 Catalysts prepared by sol-gel and impregnation method

III.1.2.2.1 X-ray diffraction and BET specific surface areas

Tables III.2 and table III.4 in Appendix III summarize the composition of all silica-dispersed catalysts prepared by sol-gel and impregnation method, their specific surface areas and main crystalline phases identified by X-ray diffraction.

Concerning the sol-gel prepared catalysts, in the simple Ni-Mo-Si and Co-Mo-Si samples, XRD identifies β-$NiMoO_4$ (file n° 45-0142) and β-$CoMoO_4$ (file n° 21-0868) with tetrahedral Mo coordination in both cases. In the series of silica-dispersed mixed Ni-Co molybdates, the (220) reflection is common to both structural types and a lattice expansion is observed within the series $Ni_{1-x}Co_xMoO_4$ (fig. III.5), as indicated by the shift in the d-spacing from 3.337 Å to 3.373 Å (in the samples characterized by Si/Mo =

20), when going from β-$NiMoO_4$ to β-$CoMoO_4$. This behaviour is common to all sol-gel samples, independently from the Si content.

As already observed for the catalysts prepared by the sol-gel method, also in the case of the analogous impregnated catalysts, application of Vegard's law is observed (fig.III.8 in Appendix III) and led us to conclude that the structures of these mixed Ni-Co molybdates are solid solutions of β-$NiMoO_4$ and β-$CoMoO_4$.

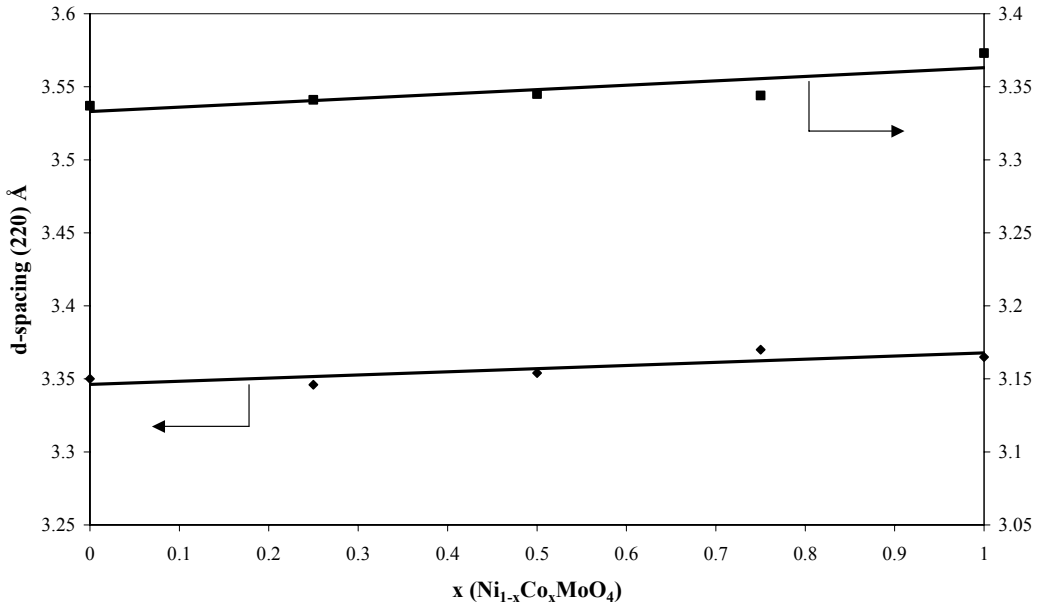

Fig.III.5: Verification of Vegard's law with the interreticular (220) d-spacing in silica dispersed β-$Ni_{1-x}Co_xMoO_4$ prepared by the sol-gel method. (♦) Si/Mo = 10; (■) Si/Mo = 20.

The surface area values of the impregnated samples lie in the range 171-196 m^2 g^{-1} i.e. values some 25 % lower than those of the catalysts prepared by the sol-gel method (216- 257 m^2 g^{-1}).

III.1.2.2.2 General comments on specific surface area and porosity measurements

The textural properties of selected SiO_2-supported samples are described in table III.4. These data were determined from complete nitrogen adsorption/desorption isotherms analyzed according to the BET method (for the sample surface area) and to the BJH method (for the pore volume and diameter). All isotherms exhibit the same overall shape corresponding to type IV in Brunauer's classification. Generally speaking, the pore distribution of all analysed catalysts is the same, with no significant difference: the majority of the pores of the samples is characterized by a diameter close to the

average diameter given in table III.2. For comparison, the textural characterizations performed on a pure silica sample prepared by the same sol-gel procedure and calcined at 1073 K during 20 hours indicated a mesoporous structure with a BET specific surface area of 215 m^2g^{-1}, an average pore diameter of 5.1 nm (tubular shape) and an average pore volume 0.35 cm^3g^{-1}.

The influence of the loading of active phase in silica on the textural characteristics is quite important. Figures III.5-6 and 7 in Appendix III display the evolution of the specific surface area (SBET), the volume of the pores (Vp) and the diameter of the pores (Dp) of some samples with respect to their silicon content (Si/Mo). First, in all SiO_2-dispersed molybdates, the silicon content plays the most important role in the S_{BET} values, the higher the silicon content, the higher the S_{BET} value. The influence of the Ni/Co composition in $Ni_{1-x}Co_xMoO_4/SiO_2$ samples is also well marked: in the catalysts characterized by the (Si/Mo) ratio of 10 or 20, the higher S_{BET} value is observed for x = 0.25; for (Si/Mo) = 5, the maximum is observed for x = 0.75.

Table III.2: Textural properties of some silica-dispersed $Ni_{1-x}Co_xMoO_4$ prepared by sol-gel method, calcined at 773 K.

Composition	Molar Ratio	S_{BET} ($m^2 \cdot g^{-1}$)	V_p ($cm^3 \cdot g^{-1}$)[a]	D_p (nm)[b]
Ni:Mo:Si	1:1:20	327	0.70	7.5
Ni:Mo:Si	1:1:10	307	0.44	5.7
Ni:Mo:Si	1:1:5	216	0.53	8.9
Co:Mo:Si	1:1:20	322	0.56	6.5
Co:Mo:Si	1:1:10	294	0.94	11.0
Co:Mo:Si	1:1:5	217	0.67	10.8
Ni:Co:Mo:Si	0.75:0.25:1:20	441	0.54	4.6
Ni:Co:Mo:Si	0.75:0.25:1:10	324	0.75	8.6
Ni:Co:Mo:Si	0.75:0.25:1:5	241	0.52	8.4
Ni:Co:Mo:Si	0.25:0.75:1:20	352	0.79	8.4
Ni:Co:Mo:Si	0.25:0.75:1:10	298	0.55	6.4
Ni:Co:Mo:Si	0.25:0.75:1:5	254	0.80	11.0
SiO_2 (calc. at 1073 K)	-	215	0.35	5.1

[a] Average pore volume; [b] Average pore diameter

The pore size distribution was determined by means of the BJH (desorption) method, assuming a cylindrical pore model.

As far as porosity is concerned, in the case of $NiMoO_4$ dispersed in different amounts of silica, the catalyst with the intermediate molar ratio (Si/Mo) = 10 is characterized by the lowest values of pore volume and pore diameter. The reverse situation is observed for $CoMoO_4$ for which the intermediate loading corresponds to the highest values of pore volume and pore diameter. It thus appears that the dependence of the textural properties is different for the Ni and Co molybdates. As far as the mixed Ni-Co molybdates are concerned, while the Ni-Co-Mo-Si samples characterized by a (Ni/Co) molar ratio of 0.33 display the same behaviour as pure $NiMoO_4$, those characterized by (Ni/Co) = 3 exhibit the same behaviour as pure $CoMoO_4$. There seems to be only little influence of the Ni/Co composition on the average pore volume and pore size in the catalysts at high loading (Si/Mo = 5); while at lower loading (Si/Mo = 10 or 20), maxima occur but for different compositions.

As mentioned above, a higher loading of active phase leads to lower specific surface area values. It should be noticed that this decrease could be due to the phenomenon of "pore mouth plugging" phenomenon; presumably, the smallest pores are fused together, leaving room to pores characterized by higher Dp, and consequently lowering S_{BET} of the sample.

The textural properties of selected SiO_2-supported samples are described in table III.5 of the Appendix III. As well as for sol-gel prepared samples, the isotherms of all catalysts prepared by impregnation exhibit the same overall shape corresponding to type IV in Brunauer's classification. They are all characterized by similar values of pore diameter and pore volume, with the only exception of $CoMoO_4$, whose Vp is equal to 0.67 cm^3g^{-1} when it is prepared by sol gel method and 0.47 cm^3g^{-1} when prepared by impregnation.

III.1.2.2.3 X-ray photoelectron spectroscopy

The binding energies of the various elements were found in the following ranges: 856.3 ± 0.4 eV for Ni $2p_{3/2}$, 781.4 ± 0.4 eV for Co $2p_{3/2}$ and 103.6 ± 0.1 eV for Si 2p, indicating that all these elements appear only with their normally expected oxidation states: Ni(II) and Co(II). The XPS spectra of oxygen can be resolved into two components corresponding to silica (533 eV) and to the molybdate phase (532 eV), respectively. The XPS spectra of molybdenum are resolved into two components corresponding to molybdenum present in two different oxidation states: 232.7 ± 0.2 eV

for $Mo^{(VI)}3d_{5/2}$ and 231.8 ± 0.2 eV for $Mo^{(V)}3d_{5/2}$ (173). The average value of the experimental ratio (Mo(VI)/Mo) is equal to 0.80.

Table III.3 summarizes the experimental atomic intensity ratios measured by XPS for some sol-gel-prepared catalysts, and the values are compared with the theoretical ones (corresponding to the bulk composition). In both Ni-Mo-Si and Co-Mo-Si samples, the experimental ratios (Ni or Co)/Mo are roughly the same, but significantly lower than the corresponding theoretical ones, indicating a substantial enrichment in Mo on the surface.

In the same way, the experimental (Ni/Si), (Co/Si) and (Mo/Si) ratios are quite different from those expected from the overall composition. The (Ni/Si) ratios in Ni-Mo-Si-samples are the same as the (Co/Si) ratios in Co-Mo-Si. Taking into account the $Ni_{0.25}Co_{0.75}MoO_4$ catalysts, it must be underlined that Ni and Co are characterized by the same dispersion degree in the sample with the higher silicon content (Si/Mo = 20); in the catalyst characterized by (Si/Mo = 10), Ni is better dispersed than Co, and for (Si/Mo = 5), Co appears to be better dispersed than Ni.

The differences between bulk and surface compositions could result from several phenomena: a phase segregation effect related to the preparation or calcination conditions, or partial encapsulation of the active phase in the silica lattice, which is critical from a catalytic point of view because this would restrict the accessibility of these elements.

In order to evaluate the dispersion of Ni, Co and Mo in mixed silica-dispersed catalysts, the coefficients of surface segregation (β) were calculated by a method similar to that proposed by Seah (105,106):

$$(\beta_{Ni}) = \frac{(Ni/Si)_{XPS} - (Ni/Si)_{bulk}}{(Ni/Si)_{bulk}}; \quad (\beta_{Co}) = \frac{(Co/Si)_{XPS} - (Co/Si)_{bulk}}{(Co/Si)_{bulk}};$$

$$(\beta_{Mo}) = \frac{(Mo/Si)_{XPS} - (Mo/Si)_{bulk}}{(Mo/Si)_{bulk}};$$

According to this approach, coefficients of surface segregation close to 0, suggest that the elements are homogeneously distributed, while high segregation coefficients are interpreted as a tendency to surface segregation (segregation normally associated to 2). In our case, β_{Ni} values vary between -0.76 and –0.94, β_{Co} between -0.76 and –0.95 and β_{Mo} between -0.48 and –0.83: therefore, we concluded that Ni, Co and Mo ions are homogeneously distributed in Ni-Co-Mo/SiO_2 catalysts without leading to segregation phenomena.

Table III.3: Relative atomic intensity ratios measured by XPS in the silica dispersed Ni-Co molybdates prepared by the sol-gel method (calcination at 773K).

Composition and Molar ratio	Ni/Mo		Co/Mo		Ni/Co		Ni/Si		Co/Si		Mo/Si	
	Exp.	Th.	Exp.	Th.	Exp.	Th.	Exp.	Th.	Exp.	Th.	Exp.	Th.
Ni:Mo:Si 1:1:20	0.48	1	-	-	-	-	0.007	0.05	-	-	0.016	0.05
Ni:Mo:Si 1:1:10	0.22	1	-	-	-	-	0.006	0.1	-	-	0.027	0.1
Ni:Mo:Si 1:1:5	0.25	1	-	-	-	-	0.012	0.2	-	-	0.051	0.2
Co:Mo:Si 1:1:20	-	-	0.48	1	-	-	-	-	0.007	0.05	0.015	0.05
Co:Mo:Si 1:1:10	-	-	0.21	1	-	-	-	-	0.006	0.1	0.029	0.1
Co:Mo:Si 1:1:5	-	-	0.29	1	-	-	-	-	0.010	0.2	0.035	0.2
Ni:Co:Mo:Si 0.25:0.75:1:20	0.11	0.25	0.36	0.75	0.31	0.33	0.003	0.0125	0.009	0.0375	0.026	0.05
Ni:Co:Mo:Si 0.25:0.75:1:10	0.16	0.25	0.35	0.75	0.46	0.33	0.004	0.025	0.009	0.075	0.026	0.1
Ni:Co:Mo:Si 0.25:0.75:1:5	0.09	0.25	0.43	0.75	0.20	0.33	0.005	0.05	0.026	0.15	0.060	0.2
Ni:Co:Mo:Si 0.5:0.5:1:10	0.28	0.5	0.21	0.5	1.38	1	0.010	0.05	0.007	0.05	0.035	0.1

Table III.7 in Appendix III summarizes the experimental atomic intensity ratios measured by XPS for silica-supported samples prepared by impregnation compared with the theoretical ones. In general, the experimental ratios (Ni or Co/Mo) are very close to the corresponding theoretical ones in the mixed Ni-Co molybdates, but lower in the simple Ni and Co molybdates. The experimental ratio (Ni/Co) is systematically higher. In all samples prepared by impregnation, the experimental ratios Ni/Si, Co/Si, and Mo/Si are much lower than the theoretical ones; however, they are always higher than in the corresponding samples prepared by sol-gel, strengthening the idea that in the latter case, the active phase is partly encapsulated in the silica network.

III.1.2.2.4 Raman spectroscopy

All silica-dispersed $Ni_{1-x}Co_xMoO_4$ samples have been analyzed by Raman spectroscopy (table III.3 and table III.6 in Appendix III) and the spectra were compared with those of the reference materials, listed in table III.1 of Appendix III. Fig. III.6 shows the Raman spectrum of β-$NiMoO_4$ (Si/Mo = 5), characterized by intense peaks at 955-945, 900 and 827 cm^{-1}, a spectral shape which is very different from the one displayed by α'-$NiMoO_4$ obtained by the citrate method.

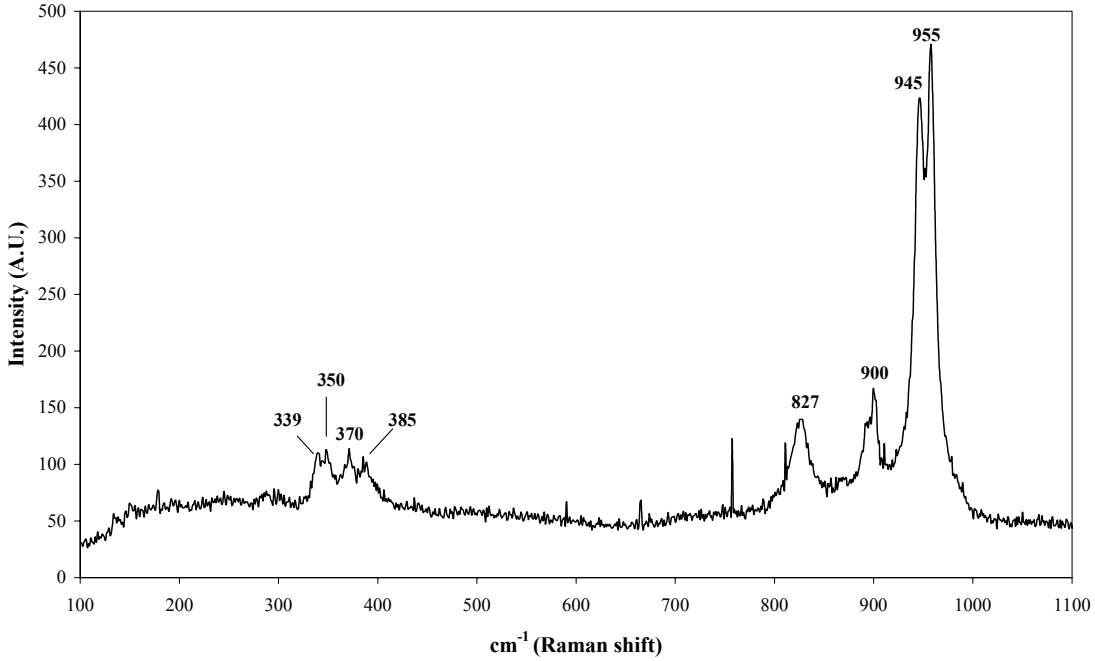

Fig.III.6: Raman spectrum of sol-gel prepared β-$NiMoO_4/SiO_2$ (Si/Mo = 5).

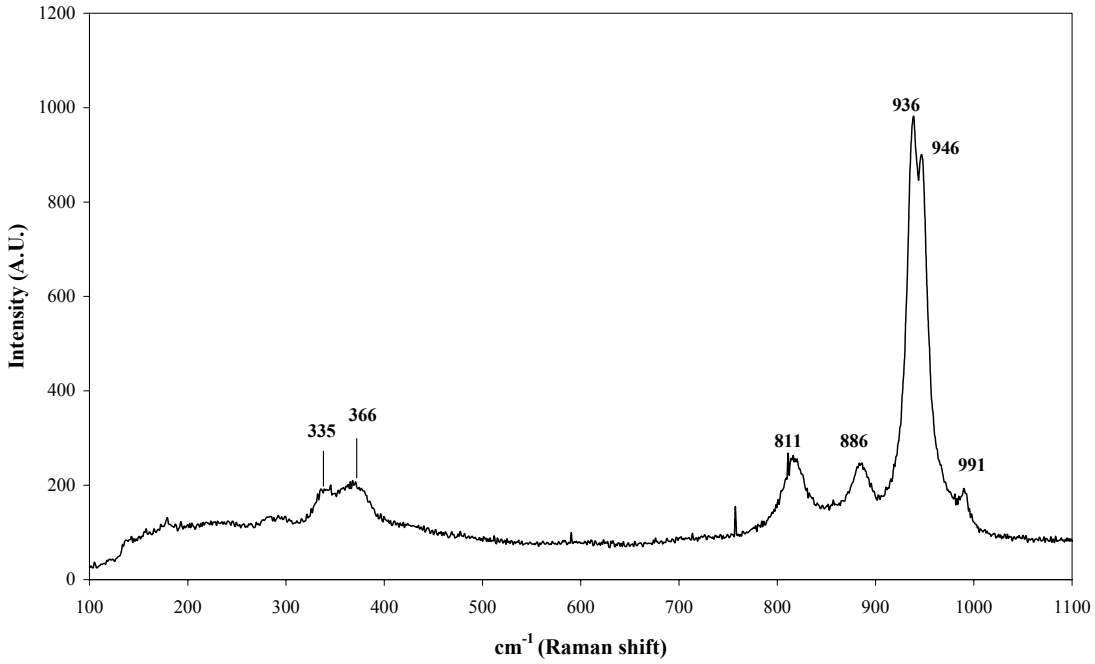

Fig.III.7: Raman spectrum of sol-gel prepared β-$Ni_{0.5}Co_{0.5}MoO_4/SiO_2$ (Si/Mo = 5).

Fig.III.8 shows the Raman spectrum of β-$CoMoO_4$ (Si/Mo = 5) displaying intense peaks at 928, 869 and 811 cm^{-1}. β-$Ni_{0.5}Co_{0.5}MoO_4$ catalyst (Si/Mo = 5) is characterized by a Raman spectrum (see fig. III.7) whose shape is similar to those of both simple Ni or Co molybdates, but with the most intense peaks (946-936 and 886

cm^{-1}) appearing at intermediate Raman shift (cm^{-1}) between those of β-$NiMoO_4$ and β-$CoMoO_4$.

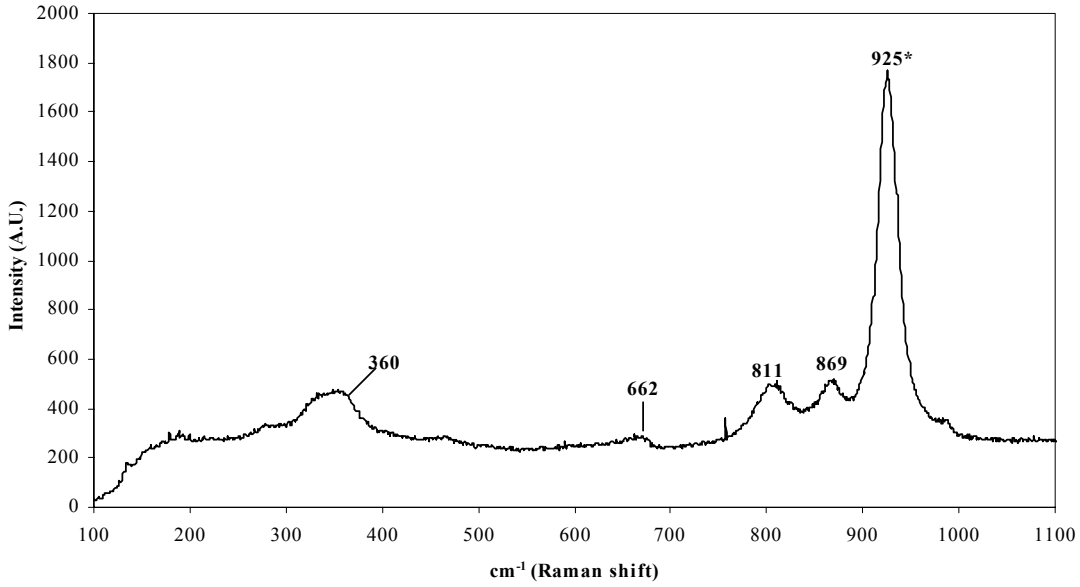

Fig.III.8: Raman spectrum of β-$CoMoO_4/SiO_2$ (Si/Mo = 5).

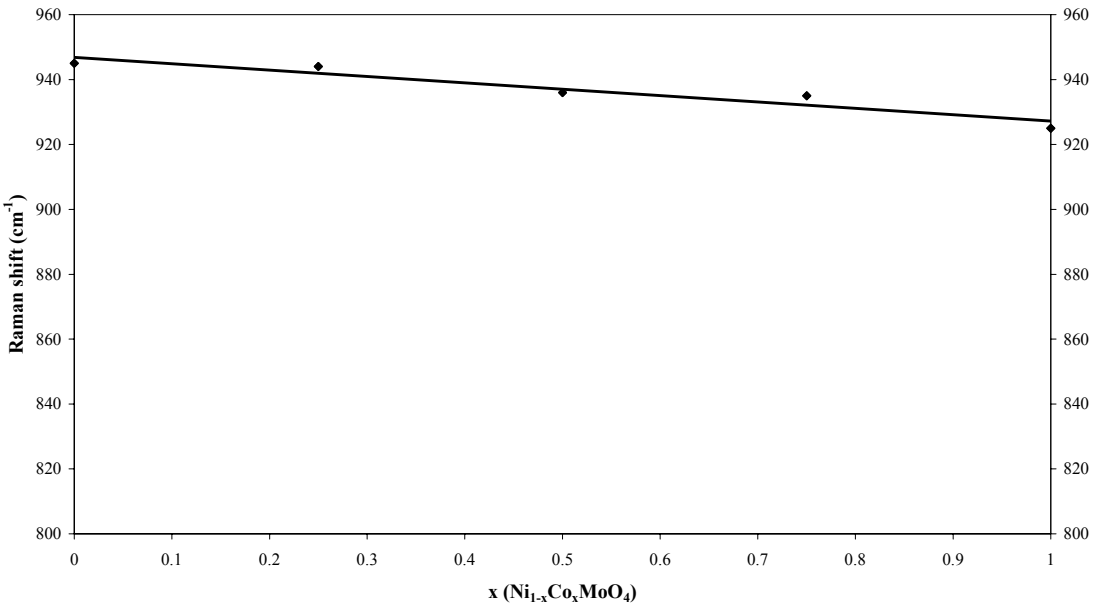

Fig.III.9: Linear decrease of the most intensive peak of SiO_2-dispersed Ni and Co molybdates (Si/Mo = 5), prepared by the sol-gel method.

In the Raman spectra of all mixed Ni-Co molybdates, a linear decrease is observed, as indicated by the Raman shift of the most intense peak (fig.III.9), from 945 cm^{-1} to 925 cm^{-1} (in the case of Si/Mo = 5) when going from β-$NiMoO_4$ to β-$CoMoO_4$.

This could a further assessment that the structures of these mixed Ni-Co molybdates are solid solutions of β-$NiMoO_4$ and β-$CoMoO_4$ in a common molybdate lattice. The same behaviour is observed for all Si/Mo ratios.

Generally speaking, all $Ni_{1-x}Co_xMoO_4$ spectra display two very close bands in the range 940-960 cm^{-1}, leading us to conclude that the Raman spectra of all Ni-Mo, Co-Mo and Ni-Co-Mo samples are in agreement with the XRD results and that the great majority of the bands can be attributed to the β-phase, even if in some cases the presence of MoO_3 can be inferred from the line at 990 cm^{-1}.

III.1.2.2.5 Discussion of the structural and physico-chemical aspects

In this section, attention will be paid to (i) the initial interaction between silica and $[MoO_4]^{2-}$ ions in the starting solution, (ii) the experimental proofs for the interactions between the support between the support and the active phase in the final catalyst and (iii) to the differences between the mechanisms of formation of the active phase in the catalysts prepared by sol-gel method or impregnation. One major question related to the preparation of $Ni_{1-x}Co_xMoO_4/SiO_2$ catalysts, is to understand how molybdate ions interact with silica and are stabilized in a given state. Cauzzi and coworkers (62) reported that the molybdate ions interact strongly with silica oligomers because their presence leads to a strong increase of the gelation rate (and a change in color of the sol).

All the molybdate-based catalysts prepared in this work were obtained from an aqueous solution of ammonium heptamolybdate characterized by a pH = 6-7. In this pH range, the following equilibrium between isolated $[MoO_4]^{2-}$ ions and heteropolyanionic species (essentially heptamolybdate) must be considered: $Mo_7O_{24}^{6-} + 4H_2O \leftrightarrows 7MoO_4^{2-} + 8H^+$ and is shifted towards the production of molybdate ions. When Ni- and/or Co nitrates are added, the pH decreases in the range 4 to 5, allowing the formation of molybdic acid H_2MoO_4 according to the following equations:

$H^+ + MoO_4^{2-} \leftrightarrows HMoO_4^-$ ($K = 10^{3.9}$);

$HMoO_4^- + H^+ \leftrightarrows H_2MoO_4$ ($K = 10^{3.6}$)

According to the literature (107), once TMOS has been added, hydrolysis and condensation processes take place, and the OH groups of silicon react with molybdic acid leading to the stabilization of tetrahedral monomeric molybdate species on the support according to the following scheme:

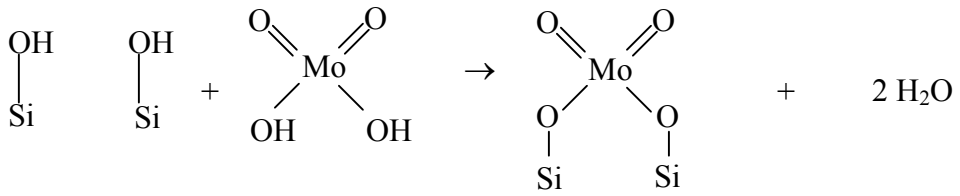

The same process is assumed to occur on the surface of commercial silica used for the impregnation procedures. This model can explain the stabilization of β-$NiMoO_4$ on silica. This would not be the case if a purely electrostatic model is considered, because such a model could not account for the adsorption of anions when the pH of the solution is higher than the corresponding isoelectric point. At pH < 2, where the silica surface is charged positively, the coulombic interactions lead to the adsorption of $[MoO_4]^{2-}$ and $[Mo_7O_{24}]^{6-}$ on the surface of the support; on the contrary at pH > 2, silica results to be negative charged and the repulsive interactions involved would not allow the adsorption of the negatively charged Mo-species.

The precursor-support interaction, and consequently the mechanism of formation of the active phase must be different in the catalysts prepared by impregnation or by the sol-gel method. From the textural point of view, it has been already pointed out that catalysts prepared by the sol-gel method are characterized by higher specific surface areas than those prepared by impregnation, and that the pore volume and pore size of both types of catalysts are very similar. The most important difference between these catalysts is the metal dispersion and accessibility. In the case of the catalysts prepared by impregnation, the active phase is generated from species attached on the surface via reaction between the silanol groups of silica and H_2MoO_4; in catalysts prepared by the sol-gel method, the silica network is formed simultaneously with the active phase.

When observing the XPS results of all $Ni_{1-x}Co_xMoO_4/SiO_2$, the experimental (Mo/Si) ratios are lower than the corresponding theoretical ones, but higher than the experimental (Ni,Co/Si) ratios. At pH > 2, the negatively charged surface silica facilitates the interactions between silica and the cations present in the precursor solution. The resulting positively charged surface layer can thereby interact with the negatively charged $[MoO_4]^{2-}$ and polynuclear moieties such as $[Mo_7O_{24}]^{6-}$, which cover the Ni^{2+} and Co^{2+} ions (fig.III.29) becoming more difficult to detect by XPS. All experimental ratios related to Ni,Co/Si and Mo/Si (much lower than theoretical ones) of sol-gel prepared catalysts, are lower than those of the analogous catalysts prepared by impregnation and that lead us to conclude that all elements (and then the active phase) in sol-gel prepared catalysts could be partially encapsulated in silica matrix.

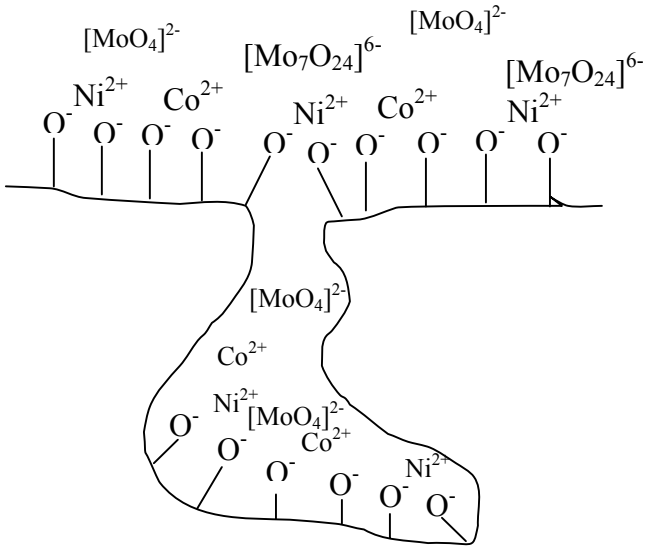

Fig.III.29: Simplified scheme of the interaction between silica, cations and polynuclear moieties at pH = 4-5.

In the citrate-prepared catalysts, the phases observed were quite different, with the α-phase for $NiMoO_4$ and the β-phase for $CoMoO_4$. For the intermediate compositions, α/β mixtures were observed in the Ni-rich region, while only β in the Co-rich region. In this case, the presence of Co seems to be the driving force for stabilizing the β-phase. In the simple $NiMoO_4$, a pure α-phase would then be formed because with the absence of Co the tetrahedral Mo species cannot be stabilized without interaction with a support.

Experimental evidence for interactions between silica and the $[MoO_4]^{2-}$ species can be found in XRD and Raman spectra. When comparing the Raman spectra of pure and silica-supported $NiMoO_4$ and $CoMoO_4$, band shift are always observed: for example in the case of Ni:Mo:Si (1:1:20), the main lines of β-$NiMoO_4$ supported on silica appear at 958-946 and 900 cm^{-1}, while at 945-935 and 896 cm^{-1} for the bulk phases (103). Also in the powder X-Ray diffractograms, slight shifts in the d-spacing values associated with the (220) reflection are observed: from 3.362 Å in bulk $Ni_{0.25}Co_{0.75}MoO_4$, to 3.344 Å when this phase is dispersed on silica (for further examples see table III.4).

Table III.4: Shifts in the d-spacing values associated with the (220) reflection.

	$\Delta d = dNiMoO_4$[a] – $dNiMoO_4/SiO_2$	$\Delta d = dCoMoO_4$[b] – $dCoMoO_4/SiO_2$	$\Delta d = dNi_{0.25}Co_{0.75}MoO_4$[c] – $dNi_{0.25}Co_{0.75}MoO_4/SiO_2$
(Si/Mo)=20	0.0139	0.01	0.018
(Si/Mo)=5	0.0129	0.008	-0.009

a) d-spacing of the (220) reflection of β-$NiMoO_4$ (file 45-0142)

b) d-spacing of the (220) reflection of β-$CoMoO_4$ prepared by citrate method and used as reference

c) d-spacing value of the (220) reflection of β-$Ni_{0.25}Co_{0.75}MoO_4$ prepared by citrate method and used as reference.

Canevali et al. (108) already reported the existence of an interaction between silica and $[MoO_4]^{2-}$ in copper molybdates, showing that $[MoO_4]^{2-}$ species could attack the electrophilic silicon center of TMOS, leading to the formation of a silicomolybdate framework.

III.1.3 Preparation of Ni-Co molybdates supported on alumina, magnesia, titania, zirconia and mixed alumina-magnesia.

III.1.3.1 Alumina-, magnesia- and mixed Al_2O_3-MgO-dispersed catalysts prepared by impregnation and sol-gel methods

Table III.5 lists the main characteristics of all Al_2O_3, MgO and Al_2O_3-MgO-based samples from the point of view of their thermal behaviour, and the crystalline phases identified by means of X-ray diffraction and Raman spectroscopy. The characterizations of the pure support are reported in section V.1.1 of Appendix V.

Table III.5: Main characteristics of Al_2O_3, MgO and Al_2O_3-MgO-based catalysts.

	Al_2O_3	MgO	Al_2O_3-MgO
TGA of sol-gel precursors	3 weight losses: - 303 – 433 K (17%) - 433 – 523 K (15%) - 523 – 773 K (10%)	3 weight losses: - 303 – 413 K (12%) - 413 – 548 K (12%) - 548 – 773 K (22%)	3 weight losses: - 303 – 443 K (17%) - 443 – 523 K (5%) - 523 – 773 K (22%)
XRD	**S-g**: all catalysts are solid sol. of β-$NiMoO_4$ and β-$CoMoO_4$	**S-g**: all catalysts are solid sol. of β-$NiMoO_4$ and β-$CoMoO_4$, MgO present as periclase phase	**S-g**: - for Ni-Mo-O, β-$NiMoO_4$; - for Co-Mo-O, $CoAl_2O_4$; - for Ni-Co-Mo-O (0.25:0.75:1), β solid sol.; -all other catalysts present a poorly resolved spectrum
	Imp: For x = 0: mixt. of α and β-$NiMoO_4$; all other catalysts are solid sol. of β-$NiMoO_4$ and β-$CoMoO_4$	**Imp**: all catalysts are solid sol. of β-$NiMoO_4$ and β-$CoMoO_4$, MgO present as periclase phase	
Raman spectroscopy	**S-g**: confirms XRD	**S-g**: confirms XRD	**S-g**: fluorescence phenomena for all analysed samples
	Imp: For x = 0: only α-phase; confirms XRD for all other catalysts	**Imp**: confirms XRD; *	

By considering that the active phase is made of simple or mixed molybdates with the overall stoichiometry $Ni_{1-x}Co_xMoO_4$ (with $0 \leq x \leq 1$), these compositions correspond to the following mass percentages of active phase in the catalysts, which are all characterized by a Supp./Mo ratio equal to 5: 46 wt. %, 52 wt. % and 48 wt. % for alumina-, magnesia- and Al_2O_3-MgO-dispersed catalysts, respectively.

III.1.3.1.1 X-ray diffraction

In all dispersed Ni-Mo catalysts prepared by impregnation or sol-gel method, XRD revealed the presence of β-$NiMoO_4$: only in the case of alumina-based Ni-Mo prepared by impregnation, α-$NiMoO_4$ (file 33-0948) has been also identified next to β-$NiMoO_4$. β-$CoMoO_4$ was detected in all dispersed catalysts except for Co:Mo:(Al+Mg), in which $CoAl_2O_4$ (38-814) was the only crystalline phase found.

In the case of alumina- or magnesia-dispersed mixed Ni-Co molybdates prepared by sol-gel or impregnation method, the (220) reflection is common to both β-$NiMoO_4$ and β-$CoMoO_4$; a lattice expansion is observed in the $Ni_{1-x}Co_xMoO_4$ series (fig III.9 below, and fig.V.4 in Appendix V), as indicated by the shift in the d-spacing when going from β-$NiMoO_4$ to β-$CoMoO_4$. Application of Vegard's law led us to conclude

that the structures of these mixed Ni-Co molybdates are solid solutions of β-$NiMoO_4$ and β-$CoMoO_4$ in a common molybdate lattice.

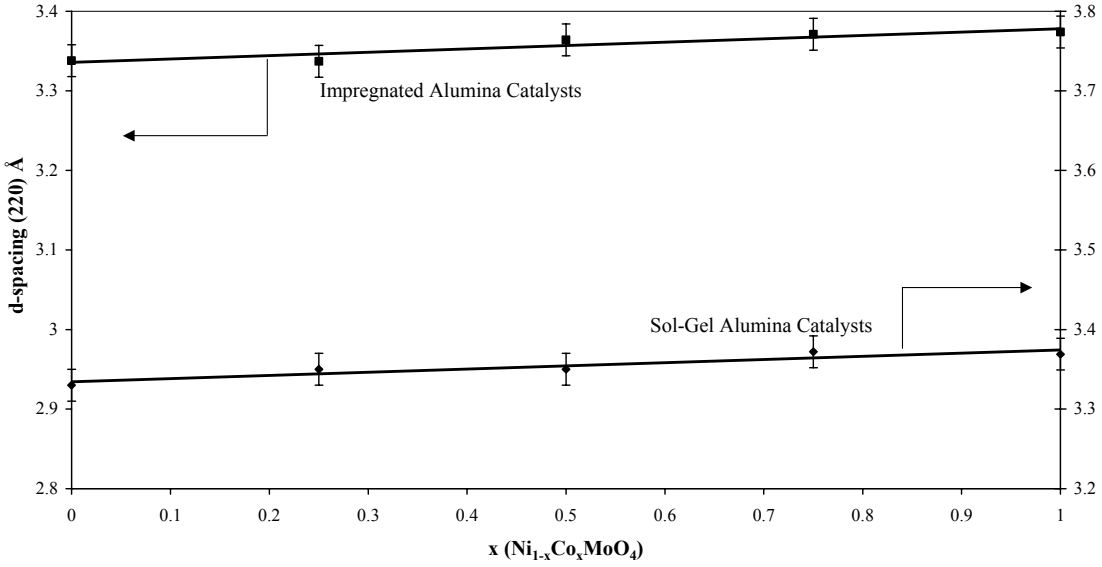

Fig.III.9: Verification of Vegard's law with the interreticular (220) d-spacing in $Ni_{1-x}Co_xMoO_4$ dispersed on alumina (Al/Mo = 5). (♦) β-$Ni_{1-x}Co_xMoO_4$ dispersed on Al_2O_3, prepared by the sol-gel method; (■) β-$Ni_{1-x}Co_xMoO_4$ supported on Al_2O_3, prepared by impregnation.

All Ni-Co-Mo-samples dispersed on the Al_2O_3-MgO support, display an amorphous XRD pattern except the Ni-Co-Mo (0.25:0.75:1) sample, in which the presence of a solid solution of β-$NiMoO_4$ and β-$CoMoO_4$ in a common molybdate lattice is suspected. In all MgO-dispersed catalysts besides Ni-Co-Mo-O based phase, XRD detected also the presence of periclase (file 45-0946).

III.1.3.1.2 General comments on specific surface area and porosity measurements

The main comments on the specific surface areas of alumina-, magnesia- and alumina-magnesia-supported catalysts are the following:

a) Al_2O_3-dispersed Ni-Co molybdates: the surface area values of the samples prepared by impregnation method lie in the range 94-80 $m^2\ g^{-1}$, and those prepared by sol-gel method between 92 and 38 $m^2\ g^{-1}$. In the latter case, they decrease regularly with the Ni content.

b) MgO-dispersed Ni-Co molybdates: the surface area values of the samples prepared by impregnation method lie in the range between 28 and 17 $m^2\ g^{-1}$; those prepared by sol-gel method are in the range between 125 and 78 $m^2\ g^{-1}$.

c) Al_2O_3-MgO-dispersed Ni-Co molybdates: the surface area values of the samples lie in the range between 112 and 50 $m^2\ g^{-1}$.

Table III.6 summarizes the main textural properties of all alumina-, magnesia- and alumina-magnesia-supported catalysts. All isotherms of magnesia- and alumina-magnesia-dispersed catalysts prepared by sol-gel or impregnation methods, and alumina- based catalysts prepared by the sol-gel method exhibit a shape corresponding to type II in Brunauer's classification. Alumina-supported catalysts prepared by impregnation displayed isotherms corresponding to a mixture of types II and IV: in this case, the use of different preparation methods led to catalysts characterized by the same nominal composition but by different textural properties (fig.III.10).

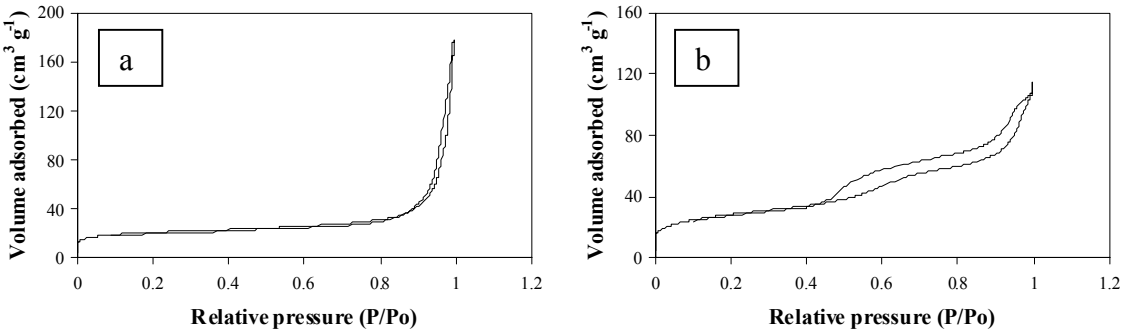

Fig.III.10: Nitrogen adsorption-desorption isotherms of Ni:Co:Mo:Al (0.75:0.25:1:5) prepared by (a) sol-gel method and (b) impregnation.

Usually, isotherms of type II are observed for solids characterized by a pore diameter equal or larger than 50 nm, while isotherms of type IV are typical of samples with pore diameters in the mesoporous range (2.5 and 50 nm). In our case, the samples showing a type II isotherm are characterized by an average Dp value of 28 nm, and those showing a type (II+IV) are characterized by an average Dp equal to 7.6 nm: the size of the pores is directly connected to the type of the isotherm.

Fig. III.10 also shows the kind of hysteresis obtained. In the present case, de Boer's (109) classification does not allow a clear identification of the hysteresis type: in fig.III.10b the observed hysteresis is a combination of two types of hystereses, namely A and B, suggesting that the pores are tubular and characterized by a large diameter and a narrow end; the hysteresis observed in fig.III.10a corresponds to a type E, indicating bottle-shaped pores closed at one end.

For all catalysts, dispersing the active phase leads to a decrease in Vp and in the surface specific surface area values with respect to their pure supports. All catalysts are essentially mesoporous. Generally speaking, for all alumina and alumina-magnesia dispersed catalysts, the pore diameter increases when comparing with the respective pure supports. This is not the case in magnesia-based catalysts, where Dp increases with respect to pure commercial magnesia in the impregnated catalysts, on one hand, while the reverse situation is observed in the magnesia-based catalysts prepared by the sol-gel method.

Table III.6: Textural properties of some alumina-, magnesia- and Al_2O_3-MgO-dispersed $Ni_{1-x}Co_xMoO_4$.

Composition and Molar ratio	Preparation method	Type of isotherm	Vp ($cm^3\ g^{-1}$)	Dp (nm)
Al_2O_3	Sol-gel	IV	0.478	5.41
Al_2O_3	Commercial	II+IV	0.27	5.1
Ni:Mo:Al	*Sol-gel*	*I + II*	-	-
1:1:5	Impregnation	II+IV	0.156	7.20
Ni:Co:Mo:Al	Sol-gel	II	0.256	35.6
0.75:0.25:1:5	Impregnation	II+IV	0.161	7.15
Co:Mo:Al	Sol-gel	II	0.181	33.8
1:1:5	Impregnation	II + IV	0.156	7.14
MgO	Sol-gel	II	0.466	30.9
MgO	Commercial	II	-	20.3
Ni:Mo:Mg	Sol-gel	II	0.385	16.1
1:1:5	Impregnation	II	0.119	28.3
Ni:Co:Mo:Mg	Sol-gel	II	0.305	20.9
0.75:0.25:1:5	Impregnation	II	0.088	17.3
Co:Mo:Mg	Sol-gel	II	0.398	20.8
1:1:5	Impregnation	II	0.143	31.7
Al_2O_3-MgO (Al/Mg = 2)	Sol-gel	IV	0.379	5.4
Ni:Mo:(Al+Mg) 1:1:5	Sol-gel	II	0.251	33.2
Ni:Co:Mo:(Al+Mg) 0.75:0.25:1:5	Sol-gel	II	0.193	34.8
Co:Mo:(Al+Mg) 1:1:5	Sol-gel	IV+II	0.274	8.8

The pore volume of magnesia- and alumina-dispersed samples prepared by sol-gel is higher than in the corresponding impregnated catalysts. In alumina-magnesia-dispersed catalysts, Vp is close to that of alumina-based catalysts.

Alumina-supported catalysts prepared by impregnation are those with the lowest pore diameter (7.14 – 7.20 nm). On the contrary, magnesia-supported catalysts prepared by the sol-gel method display lower Dp than the impregnated samples.

Generally speaking, as already said before for the silica-dispersed catalysts, a decrease in surface areas could be due to a phenomenon of pore mouth plugging; the

pores characterized by lower size are fused together, leaving room to pores characterized by higher Dp, and consequently lowering S_{BET} of the sample.

III.1.3.1.3 X-Ray photoelectron spectroscopy

Table III.7 summarizes the main comment on the XPS results for all Al_2O_3-, MgO and Al_2O_3-MgO-dispersed catalysts.

TableIII.7: Essential trends in XPS results of Al_2O_3-, MgO- and Al_2O_3-MgO dispersed molybdate catalysts.

	Al_2O_3		**MgO**		**Al_2O_3-MgO**
	Sol-Gel	**Impregnation**	**Sol-Gel**	**Impregnation**	**Sol-Gel**
$(Ni/Mo)_{exp}$	$<< (Ni/Mo)_{th}$	$<< (Ni/Mo)_{th}$	$\leq (Ni/Mo)_{th}$	$\leq (Ni/Mo)_{th}$	$< (Ni/Mo)_{th}$
	S-G ≤ Imp		S-G ≈ Imp		
$(Co/Mo)_{exp}$	$<<(Co/Mo)_{th}$	$<< (Co/Mo)_{th}$	$\leq (Co/Mo)_{th}$	$< (Co/Mo)_{th}$	$\leq (Co/Mo)_{th}$
	S-G < Imp		S-G > Imp		
$(Ni/Co)_{exp}$	$\geq (Ni/Co)_{th}$	$< (Ni/Co)_{th}$	$< (Ni/Co)_{th}$	$>> (Ni/Co)_{th}$	$<\approx> (Ni/Co)_{th}$
	S-G > Imp		S-G < Imp		
$(Ni/Supp)_{exp}$	$< (Ni/Al)_{th}$	$> (Ni/Al)_{th}$	$\leq (Ni/Mg)_{th}$	$> (Ni/Mg)_{th}$	$<<(Ni/Al+Mg)_{th}$
	S-G < Imp		S-G < Imp		
$(Co/Supp)_{exp}$	$< (Co/Al)_{th}$	$>> (Co/Al)_{th}$	$\leq (Co/Mg)_{th}$	$> (Co/Mg)_{th}$	$<<(Co/Al+Mg)_{th}$
	S-G << Imp		S-G < Imp		
$(Mo/Supp)_{exp}$	$\geq (Mo/Al)_{th}$	$>> (Mo/Al)_{th}$	$< (Mo/Mg)_{th}$	$>> (Mo/Mg)_{th}$	$< (Mo/Al+Mg)_{th}$
	S-G << Imp		S-G << Imp		
$(Mo^{VI}/Mo_{tot})_{exp}$	0.68	0.74	0.65	0.70	1

Table III.7 suggests the following comments:

- Al_2O_3-dispersed catalysts; all experimental ratios in catalysts prepared by the sol-gel method are lower than those in the impregnated ones, except for the (Ni/Co) ratio.
- MgO-dispersed catalysts; all experimental ratios in the catalysts prepared by sol-gel are lower than those in the impregnated catalysts, except for (Ni,Co/Mo) ratios.
- Whatever the support, the experimental (Ni,Co,Mo/Supp) ratios in all sol-gel prepared catalysts are lower than those in the impregnated catalysts, suggesting in the latter case, a better dispersion and a higher accessibility of the active phase, whereas partial encapsulation of the active phase would occur in the sol-gel catalysts.

It must be also underlined that:

- the main differences between Al_2O_3- and MgO-supported catalysts prepared by impregnation are:
  $(NiMo)_{Al} < (Ni/Mo)_{Mg}$; $(Ni/Co)_{Al} < (Ni/Co)_{Mg}$ and (Ni,Co,Mo/Al) > (Ni,Co,Mo/Mg);
- in Al_2O_3-MgO dispersed catalysts the experimental $(M/Mo)_{Al-Mg}$ ratios (M = Ni or Co) are higher than $(M/Mo)_{Al}$ ratios and lower than $(M/Mo)_{Mg}$; moreover $(Mo/Al+Mg)_{Al-Mg} < (Mo/Mg)_{Mg} < (Mo/Al)_{Al}$;
- in Al_2O_3-MgO dispersed catalysts, the experimental (Al/Mg) ratios are normally equal or very close to theoretical values;
- in order to evaluate the dispersion of Al and Mg in mixed Al_2O_3-MgO-dispersed catalysts, the coefficients of surface segregation (β) were calculated:

$$(\beta_{Al}) = \frac{(Al/Mg)_{XPS} - (Al/Mg)_{bulk}}{(Al/Mg)_{bulk}}; \quad (\beta)_{Mg} = \frac{(Mg/Al)_{XPS} - (Mg/Al)_{bulk}}{(Mg/Al)_{bulk}}$$

  According to this approach, coefficients of surface segregation close to 0, suggest that the elements are homogeneously distributed, while high segregation coefficients are interpreted as a tendency to surface segregation (segregation normally associated to 2). In our case, β_{Al} values vary between 0.36 and –0.11 and β_{Mg} between 0.12 and –0.27: therefore, we concluded that Al and Mg ions are homogeneously distributed in Ni-Co-Mo/Al-Mg catalysts like in a solid solution.

III.1.3.2 Titania- and zirconia-supported catalysts prepared by impregnation

Table III.8 lists the main characteristics of all TiO_2 and ZrO_2-based samples from the point of view of their specific surface areas and crystalline phases identified by means of X-ray diffraction and Raman spectroscopy.

By considering that the active phase is made of simple or mixed molybdates with the overall stoichiometry $Ni_{1-x}Co_xMoO_4$ (with $0 \leq x \leq 1$), these compositions correspond to the following mass percentages of active phase in the catalysts, which are all characterized by a Supp/Mo ratio equal to 5: 35.4 wt. % and 26 wt. % for titania- and zirconia-supported catalysts, respectively.

TableIII.8: Main characteristics of TiO_2 and ZrO_2-supported catalysts prepared by impregnation.

	TiO_2	**ZrO_2**
XRD	all catalysts are solid solutions of β-$NiMoO_4$ and β-$CoMoO_4$, TiO_2 (anatase)	For x = 0: only α-phase is detected; all other catalysts are solid sol. of β-$NiMoO_4$ and β-$CoMoO_4$, ZrO_2 (baddeleyite)
Raman spectroscopy	For x = 0: α'-phase is detected besides the β-phase; For all other catalysts, Raman spectroscopy confirms XRD	For x = 0: α'-phase is detected; For all other catalysts, Raman spectroscopy confirms XRD

III.1.3.2.1 X-ray diffraction, Raman spectroscopy and S_{BET} measurements

In all supported catalysts, XRD detected the presence of anatase or baddeleyite. As for all other supported catalysts, the application of Vegard's law led us to conclude that the structures of these mixed Ni-Co molybdates are solid solutions of β-$NiMoO_4$ and β-$CoMoO_4$ in a common molybdate lattice (fig.III.11). However, it should be noted that in the ZrO_2-supported Ni-Mo sample, only α-$NiMoO_4$ was identified, next to the support.

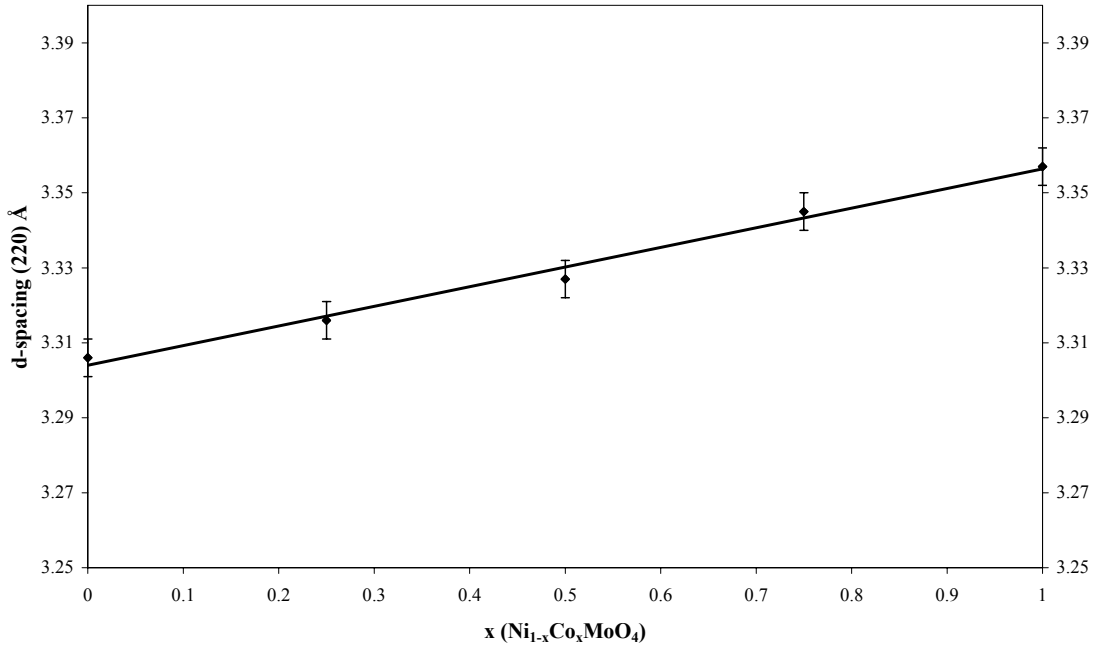

Fig.V.7: Verification of Vegard's law with the interreticular (220) d-spacing in $Ni_{1-x}Co_xMoO_4$ supported on titania (Ti/Mo = 5), prepared by impregnation.

The specific surface areas of titania-supported samples lie in the range 6 – 14 m^2 g^{-1}, whereas those of zirconia-supported catalysts appear in the range 8 – 12 m^2 g^{-1}.

To investigate the way the lattice properties respond to the change in overall composition, we plotted the Raman shift of the most intense line in function of the Co content in all mixed Ni-Co molybdates. As seen in fig.III.12, a linear decrease is observed when going from β-$NiMoO_4$ to β-$CoMoO_4$, from 956 to 930 cm^{-1} in the TiO_2-based catalysts and from 952 to 945 cm^{-1} in the ZrO_2-based catalysts (fig. V.6 in Appendix V). This trend could be considered as a further assessment that the structures of these mixed Ni-Co molybdates are solid solutions of β-$NiMoO_4$ and β-$CoMoO_4$ in a common molybdate lattice.

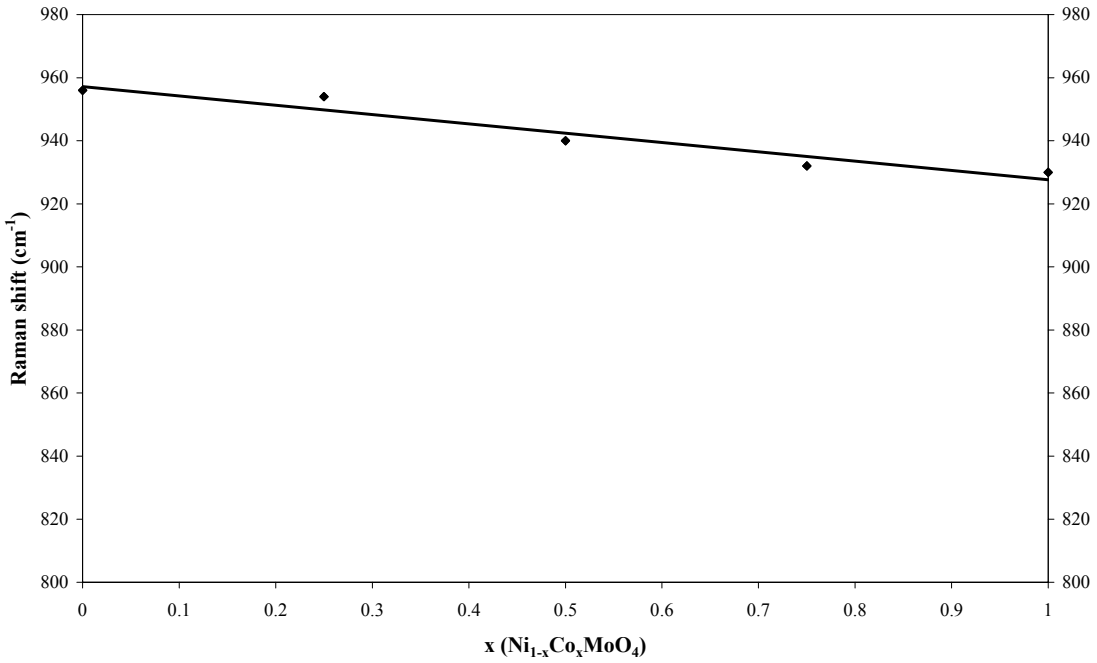

Fig.III.12: Evolution of the Raman shift of the $NiMoO_4$ line at 956 cm^{-1} with respect to the Ni/Co composition in TiO_2-supported $Ni_{1-x}Co_xMoO_4$.

III.1.3.2.2 X-ray photoelectron spectroscopy

Table III.9 summarizes the main comments on the experimental atomic intensity ratios measured by XPS for all TiO_2- and ZrO_2-supported samples (for more details see table V.10 in Appendix V).

The most interesting result worth pointing out is the fact that all experimental (M/Supp) ratios (M = Ni, Co, Mo) are much higher than the corresponding theoretical values: the metals involved in the crystalline active phase cover the surface of the support. Moreover, these experimental ratios are higher in ZrO_2-supported catalysts than in the TiO_2.

TableIII.9: Essential trends in XPS results of all TiO_2- and ZrO_2-supported catalysts.

	TiO_2	**ZrO_2**
	Impregnation	**Impregnation**
$(Ni/Mo)_{exp}$	$< (Ni/Mo)_{th}$	$< (Ni/Mo)_{th}$
	$TiO_2 \approx ZrO_2$	
$(Co/Mo)_{exp}$	$< (Co/Mo)_{th}$	$< (Co/Mo)_{th}$
	$TiO_2 < ZrO_2$	
$(Ni/Co)_{exp}$	$< = > (Ni/Co)_{th}$	$\leq (Ni/Co)_{th}$
	$TiO_2 \geq ZrO_2$	
$(Ni/Supp)_{exp}$	$>> (Ni/Ti)_{th}$	$>>> (Ni/Zr)_{th}$
	$TiO_2 << ZrO_2$	
$(Co/Supp)_{exp}$	$>> (Co/Ti)_{th}$	$>>> (Co/Zr)_{th}$
	$TiO_2 << ZrO_2$	
$(Mo/Supp)_{exp}$	$>> (Mo/Ti)_{th}$	$>>> (Mo/Zr)_{th}$
	$TiO_2 <<< ZrO_2$	
$(Mo^{VI}/Mo_{tot})_{exp}$	0.79	0.75

III.1.4 Ni and/or Co molybdates modified by bismuth and/or lanthanides

III.1.4.1 (Ni,Co)-Ln(Bi)-Mo-catalysts (Ln = La, Ce, Pr, Tb, Sm) prepared by the citrate method

III.1.4.1.1 X-ray diffraction and BET specific surface areas

All Ni(Co)-Ln-Mo samples have been prepared taking into account the stoichiometry 1:1:2.5. This stoichiometry could allow the formation of two Mo-based phases, $Ni(Co)MoO_4$ and $Ln_2Mo_3O_{12}$. Table III.10 lists all the citrate-prepared catalysts with their respective BET specific surface areas and the crystalline phases identified by X-ray diffraction. In the Ce-Mo system, $Ce_2Mo_3O_{12}$ has been identified, a phase already described by Kuang and coworkers (110), who were able to prepare it by sol-gel method. In the Sm-Mo and Tb-Mo systems, considering that the elements were introduced in order to obtain $Ln_2Mo_3O_{12}$ phases and that the diffractograms of the Sm-Mo-O and Tb-Mo-O samples resemble those of $La_2Mo_3O_{12}$ or $Pr_2Mo_3O_{12}$, we concluded that Sm and Tb are present as $Sm_2Mo_3O_{12}$ and $Tb_2Mo_3O_{12}$, although the corresponding JCPDS files are not available.

In most cases, the diffraction lines are slightly shifted with respect to those of the expected $Ni(Co)MoO_4$ or $Ln_2(Bi_2)Mo_3O_{12}$ phases, providing evidence for the formation

of quaternary phases Ni(Co)-Mo-Ln(Bi)-O involving all the elements which are present in the catalyst formulation. In table III.10, all phases labelled with an asterisk are supposed to be quaternary phases in which Ln^{3+}(Bi^{3+}) ions are included in the Ni(Co)-Mo-O-lattice, while the phases labelled with "+" are assumed to be quaternary phases in which Ni^{2+}(Co^{2+}) ions are included in the Ln(Bi)-Mo-O-lattice.

In most Ni-based samples XRD identifies the β-$NiMoO_4$ phase with a tetrahedral coordination of molybdenum, which appears to be stabilized by the inclusion of a rare-earth element in the lattice. α-$NiMoO_4$ is detected only twice, namely in the Ni-Bi-Mo and Ni-Sm-Mo systems. It is worth reminding that when simple Ni molybdates were prepared by the same citrate method, only the α-phase was obtained. In all $Ln(Bi)_2Mo_3O_{12}$-phases except La, Ni^{2+} is probably included in the lattice, because the peaks of the "$Ln_2Mo_3O_{12}$" are shifted with respect to the diffraction lines of the corresponding JCPDS file.

Table III.10: Composition, specific surface area and crystalline phases detected in modified Ni or Co molybdates prepared by the citrate method.

Composition	S_{BET} ($m^2\ g^{-1}$)	Detected crystalline phases (XRD)
Ni-La-Mo	3.6	β-$NiMoO_4$* – $La_2Mo_3O_{12}$
Ni-Ce-Mo	3.9	β-$NiMoO_4$* – $Ce_2Mo_3O_{12}^+$
Ni-Pr-Mo	3.9	β-$NiMoO_4$* - $Pr_2Mo_3O_{12}^+$
Ni-Sm-Mo	-	α-$NiMoO_4$* – **$Sm_2Mo_3O_{12}^+$**
Ni-Tb-Mo	-	β-$NiMoO_4$* – **$Tb_2Mo_3O_{12}^+$**
Ni-Bi-Mo	2.5	α-$NiMoO_4$* - $Bi_2Mo_3O_{12}^+$
Co-La-Mo	2.3	β-$CoMoO_4$ – $La_2Mo_3O_{12}$
Co-Ce-Mo	1.8	β-$CoMoO_4$* – $Ce_2Mo_3O_{12}^+$
Co-Pr-Mo	2.8	β-$CoMoO_4$* - $Pr_2Mo_3O_{12}^+$
Co-Sm-Mo	-	β-$CoMoO_4$* – **$Sm_2Mo_3O_{12}^+$**
Co-Tb-Mo	-	β-$CoMoO_4$* – **$Tb_2Mo_3O_{12}^+$**
Co-Bi-Mo	2.4	β-$CoMoO_4$*- $Bi_2Mo_3O_{12}^+$

All M-Ln(Bi)-Mo-catalysts are characterized by the molar ratio: 1:1:2.5

All catalysts have been calcined at 923 K, except M-Bi-Mo-catalysts (M = Ni, Co), which were calcined at 823 K.

*, + = the experimental diffraction lines are slightly shifted with respect to those of the reference phases.

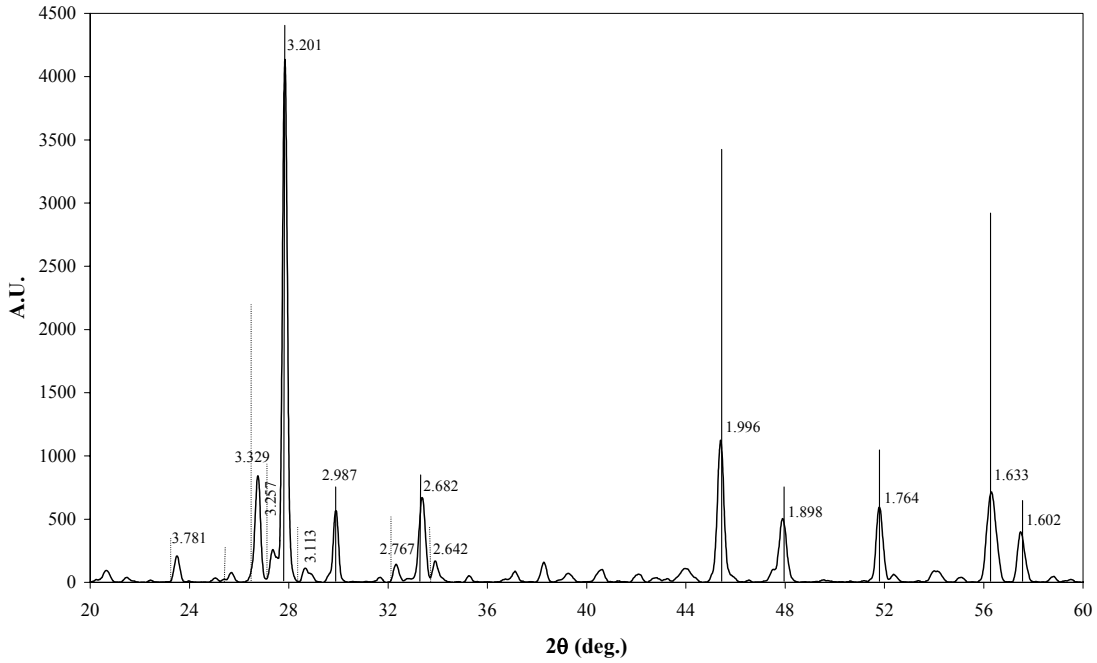

Fig.III.13: Diffractogram of Ni-La-Mo: (---) β-$NiMoO_4$ (JCPDS file n° 45-0142); (—) $La_2Mo_3O_{12}$ (JCPDS file n° 45-0407).

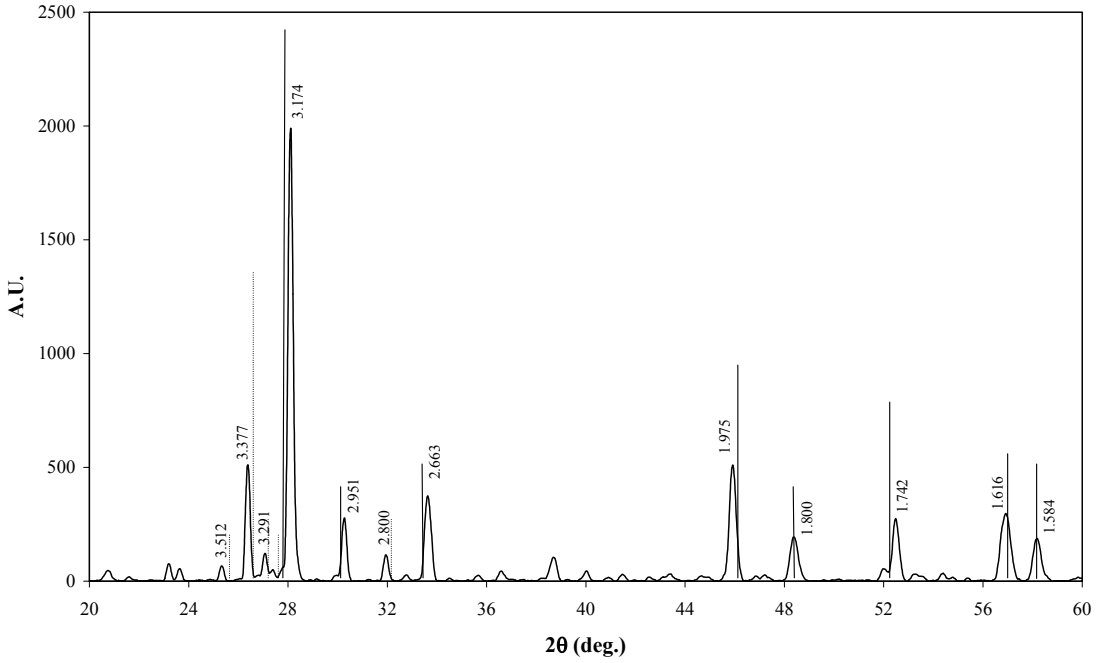

Fig.III.14: Diffractogram of Co-Pr-Mo: (---) β-$CoMoO_4$ (21-0868); (—) $Pr_2Mo_3O_{12}$ (24-0911).

Fig. III.13 shows the diffractogram of the Ni-La-Mo catalyst: the peaks corresponding to β-$NiMoO_4$ are shifted with respect to those of the reference file (45-0142), but those of $La_2Mo_3O_{12}$ match exactly to those of the file 45-0407; this overall picture leads us to conclude that some La^{3+} could be included in the β-$NiMoO_4$ lattice;

the catalyst would therefore correspond to an intimate mixture of a quaternary and a ternary phase.

Fig. III.14 displays the diffractogram of the Co-Pr-Mo sample, where the peaks corresponding to β-$CoMoO_4$ and $Pr_2Mo_3O_{12}$ are both shifted with respect to their reference data (files 21-0868 and 24-0911, respectively). This leads us to conclude that some Pr^{3+} could be included in β-$CoMoO_4$ and also that some Ni^{2+} could be included in $Pr_2Mo_3O_{12}$; these catalysts would therefore correspond to a mixture of two quaternary phases. The same general behaviour is assumed in the case of M-Sm(Tb)-Mo (M = Ni or Co) samples, with M^{2+} ions partly included in the $(Sm,Tb)_2Mo_3O_{12}$-lattice.

Generally, two quaternary phases are supposed to be formed in the catalysts due to the incorporation of the various elements in different lattices. The incorporation of lanthanides except Sm in the formulation of the catalysts is consequently found to stabilize β-$NiMoO_4$, while bismuth does not play that role. The same conclusions also hold for Co-molybdate catalysts, in which the β-$CoMoO_4$ phase is always detected, as it was already the case when pure Co molybdate was prepared by the same method. This means that in this case the incorporation of lanthanides or bismuth in the Co-Mo-O-lattice does not change molybdenum coordination. Furthermore, in all $Ln(Bi)_2Mo_3O_{12}$-phases but La, the incorporation of Co^{2+} in the host lattice is not excluded.
As indicated in table III.10, the BET specific surface areas lie in the range 1.8-3.9 m^2/g.

III.1.4.1.2 Raman spectroscopy

In the Ni-based samples, evidence for the presence of a distorted form of α-$NiMoO_4$, called the α'-phase (104), was provided, and this is assumed to be the consequence of sampling conditions, as already mentioned in the literature (111). In almost all cases, β-$NiMoO_4$ has been identified next to the α'-$NiMoO_4$. Only in the Ni-Bi-Mo sample, α'-$NiMoO_4$ is present next to $Bi_2Mo_3O_{12}$. The Raman spectra of the Ni-La-Mo and Ni-Pr-Mo samples show peaks, which are clearly assigned to β-$NiMoO_4$ and to $La_2Mo_3O_{12}$ (see fig.III.15) or $Pr_2Mo_3O_{12}$.

In the case of the Ni-Sm-Mo system, α'-$NiMoO_4$ and $Sm_2Mo_3O_{12}$ are identified; this is the only case in which the presence of a lanthanide does not stabilize β-$NiMoO_4$. The Raman spectra of the (Ni,Co)-Ce-Mo systems exhibit the same profile as those of (Ni,Co)-La-Mo and (Ni,Co)-Pr-Mo, therefore we concluded that besides the usual β-$(Ni,Co)MoO_4$ clearly identified, $Ce_2Mo_3O_{12}$ is present because of the peaks at 915-905,

817 and 768 cm^{-1} (see fig.III.16). In the case of (Ni,Co)-Tb-Mo catalyst, β-(Ni,Co)MoO_4 is once again identified next to a $Tb_2Mo_3O_{12}$ phase.

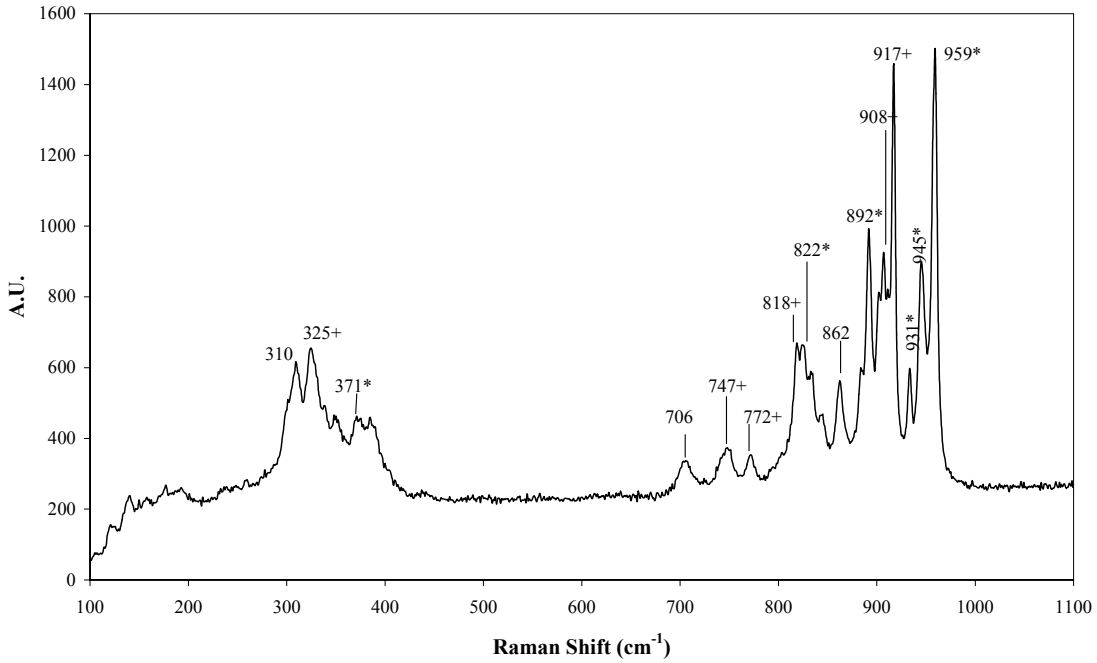

Fig.III.15: Raman spectrum of Ni-La-Mo prepared by the citrate method: (*, +) main lines of β-$NiMoO_4$ and $La_2Mo_3O_{12}$, respectively.

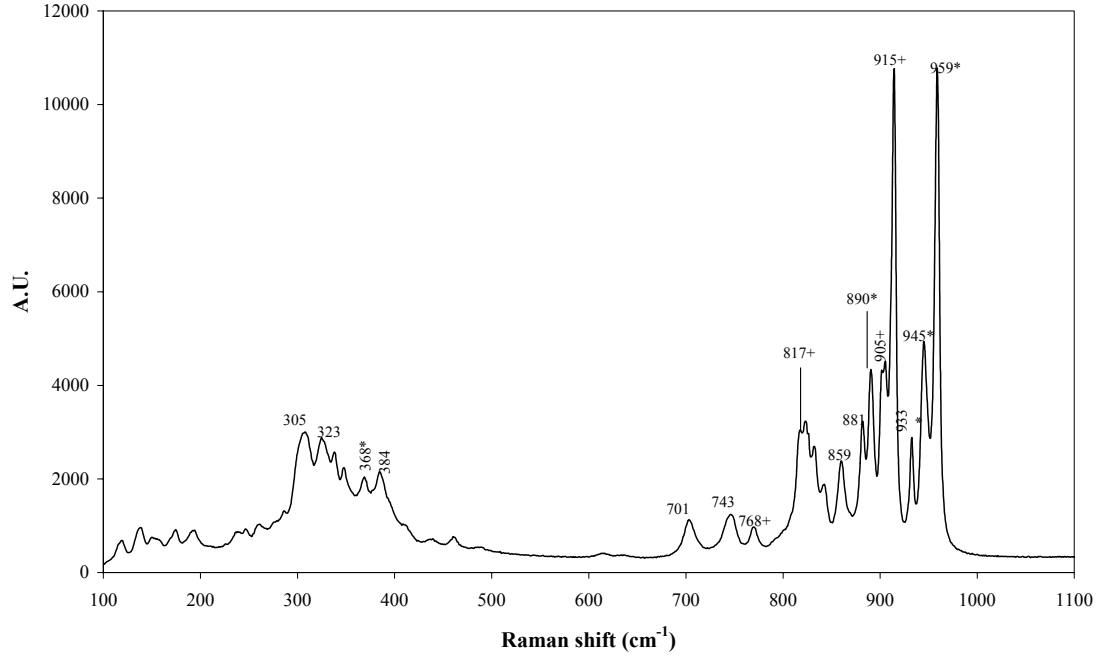

Fig.III.16: Raman spectrum of Ni-Ce-Mo prepared by the citrate method: (*,+) main lines of β-$NiMoO_4$ and $Ce_2Mo_3O_{12}$, respectively.

III.1.4.2 (Ni,Co)-Ln(Bi)-Mo-Si (1:1:2.5:20) catalysts prepared by the sol-gel method

III.1.4.2.1 X-ray diffraction and BET specific surface areas

In the M-Ln(Bi)-Mo-Si systems, the main difference between the samples calcined at 773 K or 1073 K is the presence of residual MoO_3 at the lowest calcination temperature: it is assumed that heating at 1073 K allows MoO_3 to sublime. The other phases detected are $Bi_2Mo_3O_{12}$ (at 773 K), CeO_2 (at 1073 K) and Sm_2O_3 (in Co-Sm-Mo-Si at 1073 K). In Ni(Co)-Bi-Mo-Si catalysts calcined at 1073 K, the β-phase $Bi_2Mo_2O_9$ is also detected (for major details see table IV.5 in Appendix IV).

In general, the diffraction lines of Ni or Co molybdates, CeO_2, $Bi_2Mo_3O_{12}$ and $Bi_2Mo_2O_9$ are slightly shifted with respect to their normal position in pure phases suggesting again partial incorporation of Ln or Bi ions in the Ni or Co molybdate lattices; in the same way, the Ni or Co ions are assumed to be included in cerium oxide and in both bismuth molybdate lattices, resulting in "Ni(Co)-Ln(Bi)-Mo-O" quaternary phases.

The specific surface area measurements of all modified catalysts calcined at 773 K lie in the range 83 – 378 $m^2\ g^{-1}$. Those related to the samples calcined at 1073 K are significantly lower (6.6 – 56 $m^2\ g^{-1}$).

III.1.4.2.2 X-ray photoelectron spectroscopy

Tables IV.6 and 7 in Appendix IV summarize the XPS results of the sol-gel catalysts calcined at 773 and 1073 K, respectively. In almost all cases the experimental atomic ratios are lower than the corresponding theoretical ones. As evidenced by (Ni,Co/Ln,Bi) ratios, the surface of these compounds seems to be richer in rare earth or bismuth than in Ni or Co. Generally speaking the coefficients of surface segregation of Ni, Co and Ln, calculated in the same way of those described in section III.1.2.2.3, are higher than –1. The experimental (M,Ln/Si) ratios clearly indicate that lanthanides are better dispersed than Ni or Co.

However, observing the experimental (Ni,Co/Ln,Bi) ratios, Bi and Ln are more easily detected in the catalysts calcined at 1073 K rather than in those catalysts calcined at 773 K. This phenomenon can be explained by taking into account the fact that at higher calcination temperature a certain amount of MoO_3, which could in principle cover the rare earth elements present in the samples, sublimes, resulting in a higher (Ni,Co/Ln) ratio. The experimental atomic ratio (M/Si) values (M = Ni, Co) of samples

calcined at 773 K are higher than those calcined at 1073 K: Ni and Co are better dispersed when the precursors are calcined at 773 K.

III.1.4.2.3 Raman spectroscopy

All sol-gel catalysts calcined at 1073 K have been analyzed by Raman spectroscopy (table IV.8 Appendix IV). The presence of silica makes however the interpretation of the Raman spectra quite difficult, particularly at active phase low loading. In the Ni(Co)-La-Si catalyst, the presence of bands close to those of $La_2Mo_3O_{12}$ (at 913, 904, 841 cm^{-1}) and the shift of (Ni,Co)MoO_4 peaks towards higher wavelength values, lead us to suppose the incorporation of La^{3+} in Ni(Co)-Mo-O lattice. It is also the case of Ce-, Sm-, Tb- and Bi-modified catalysts in which the shift of (Ni,Co)MoO_4 led us to suppose the formation of quaternary phases. The Ni(Co)-Pr-Mo-Si systems represent the only cases in which we did not observe any formation of quaternary phases by Raman spectroscopy, but α'-$NiMoO_4$ was clearly detected.

III.1.4.3 Characterization of Ni-Co-Ln(Bi)-Mo-Si (1:1:1:2.5:20) and Ni-Co-Ln-Ln'(Bi)-Mo-Si (1:1:1:1:2.5:20) prepared by the sol-gel method

In contrast with the catalysts described in the previous section, those described here correspond to Ni-Co-Ln(Bi)-Mo-Si (1:1:1:2.5:20) and Ni-Co-Ln-Ln'(Bi)-Mo-Si (1:1:1:1:2.5:20) non-stoichiometric compositions. There is less Mo with the respect to the total amount of transition metal and lanthanide elements than in the first class of catalysts. While, in the (Ni,Co)-Ln-Mo-Si samples, two quaternary mixed molybdate-type phases were detected, a more complex situation is expected in the non-stoichiometric catalysts; although it will be difficult to get a clear picture of these multicomponent systems, some hypotheses will be put forward.

III.1.4.3.1 X-ray diffraction and BET specific surface area

Table IV.9 in Appendix IV summarizes the detected crystalline phases and the specific surface area values of Ni-Co-Ln(Bi)-Mo-Si (1:1:1:2.5:20) and Ni-Co-Ln-Ln'(Bi)-Mo-Si (1:1:1:1:2.5:20).

In the first class of catalysts, the formation of a solid solution of β-$NiMoO_4$ and β-$CoMoO_4$ is always observed; moreover, when bismuth or cerium are involved in the

formulation of the catalyst, two other phases are identified, namely $Bi_2Mo_3O_{12}$ and CeO_2.

In all modified catalysts, adding Bi or Ln results in an increase of the specific surface area values compared to that of Ni:Co:Mo:Si (1:1:2.5:20) sample. When samarium or bismuth are added the highest and lowest specific surface area values, respectively, are observed. In general the specific surface areas of all these modified catalysts lie in the range 288 – 349 $m^2\ g^{-1}$.

When two lanthanides or one rare earth element and bismuth are involved in the formulation of the catalyst, XRD revealed only the presence of a solid solution of β-$NiMoO_4$ and β-$CoMoO_4$. The SBET values of these catalysts lie in the range 222 – 339 m^2g^{-1}.

III.1.4.4 Discussion

III.1.4.4.1 Stabilization of the β-$MMoO_4$ (M = Ni or Co) by incorporation of lanthanide ions and formation of quaternary phases

As already discussed in section III.1.2.2.5, also in the case of Ln-modified nickel or cobalt molybdates prepared by sol-gel method, an interaction of ($[MoO_4]^{2-}$)species with silica is supposed to take place.

A shift of the Raman lines of the supported catalysts from those of the bulk ones prepared by citrate method is observed; this shift could reflect an interaction with the support, but could also be due to the inclusion of the lanthanide element in the Ni(Co)-Mo-lattice. For example, comparing the Raman peaks of citrate Ln-modified catalyst (Ni-La-Mo: 959-945 cm^{-1}) in which the formation of a quaternary Ni(Co)-Ln(Bi)-Mo-O-phase is observed, and the analogous one prepared by sol-gel method, the same values are found (Ni-La-Mo-Si: 959-946 cm^{-1}). All these observations allow us to conclude that if the formation of a quaternary phase in citrate-compounds is certain, the formation of a quaternary phase in analogous sol-gel compounds is strongly suspected. The β-phase of Ni-molybdate could be stabilized not only by the interaction with silica but also by including a lanthanide element in the lattice or as reported in section III.1.2.1.1 by including a certain amount of Co in the lattice.

III.1.4.4.2 Overall picture of the multiphase catalysts

The three types of catalysts prepared by the sol-gel method are characterized by different phases. Due to the high complexity of these systems, it was not possible to

deliver a non-equivocal picture of the real catalyst. However, some hypotheses can be put forward on the basis of the physico-chemical characterization.

Stoichiometric M-Ln(Bi)-Mo-Si (M= Ni, Co) (1:1:2.5:20)

In the case of "stoichiometric" catalysts like (Ni,Co)-Ln(Bi)-Mo-Si (1:1:2.5:20) calcined at 1073 K, two phases are dispersed in the silica network according to the following scheme:

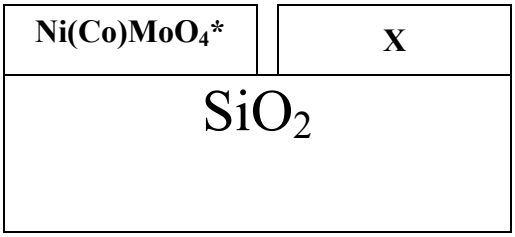

$Ni(Co)MoO_4^*$ is a quaternary phase in the way it has incorporated Ln/Bi ions as suggested by XRD and Raman spectroscopy. The second phase (X) is much more difficult to identify and only some hypotheses can be formulated. In the case of Ce-modified catalysts, a ternary phase based on CeO_2 in which some Ni^{2+} or Co^{2+} could be incorporated, is supposed. Because molybdenum oxide detected at 773 K sublimes at higher temperatures, the corresponding amount of MoO_3 would not be observed at 1073 K.

In the presence of Bi, X must be a quaternary phase in the way that Co^{2+} or Ni^{2+} can be incorporated in the $Bi_2Mo_2O_9$ lattice. The latter phase is assumed to be produced from the decomposition of $Bi_2Mo_3O_{12}$ into $Bi_2Mo_2O_9$ and MoO_3, which normally sublimes at 1073 K; moreover the shift of the XRD lines with respect to those of the corresponding JCPDS file led us to assume that some other ions are included in the Bi-based phase.

Concerning Pr-, Sm-, Tb-modified catalysts, X could in principle be a $Ln_2Mo_3O_{12}$ phase (which should be well identified by XRD because of its very characteristic crystalline pattern, but this is not the case). However, considering that MoO_3 is volatile at 1073 K and sublimes, the X phase could be the corresponding Ln-oxide, namely Pr_2O_3, TbO_2 or Sm_2O_3; however there is no evidence of the formation of those oxides.

Another possibility would be that the actual X phase is a ternary phase in which Ni^{2+} or Co^{2+} ions are incorporated in the Ln-based oxide lattice.

Non stoichiometric Ni-Co-Ln(Bi)-Mo-Si (1 :1 :1 :2.5 :20) catalysts

In the case of "non stoichiometric" Ni-Co-Ln(Bi)-Mo-Si catalysts, the situation is different because neither XRD nor Raman spectroscopy could help us in the identification of the phases present in the catalysts. Nevertheless, the following scheme can give an approximate idea of the picture of this kind of catalysts:

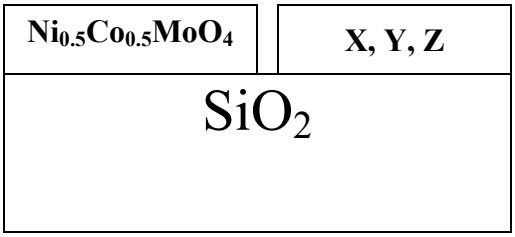

In the case of Ce-modified catalyst, XRD detected the presence of CeO_2 and MoO_3, corresponding possibly to the X and Y phases. In the Bi-modified catalyst, X is $Bi_2Mo_3O_{12}$ as revealed by XRD, and we can also expect NiO and CoO as additional Y- and Z-phases.

In the case of Ni-Co-Ln-Mo-Si catalysts (Ln = Sm, Pr, La), there are two possible hypotheses: (i) besides the normal $Ni_{0.5}Co_{0.5}MoO_4$ phase, there could be the corresponding $Ln_2Mo_3O_{12}$-phases (as X-phase) and NiO and CoO as Y- and Z-phases; (ii) the Ln_2O_3-phase could also exist with some MoO_3 as phases X and Y, respectively: however the latter hypothesis does not convince us at all because crystalline MoO_3 is in principle very easily detected by XRD or Raman spectroscopy. Furthermore, in the case of Pr, the more mixed valency oxide Pr_6O_{11} cannot be excluded.

In the presence of Tb, we have assumed it in its tetravalent oxidation state and we think it could behave in the same way as the other tetravalent ion Ce^{4+}, leading then to phases X and Y, which could be TbO_2 and MoO_3. However, the mixed valency oxide Tb_4O_7 cannot be excluded.

To conclude this section, although the picture of this type of catalysts is quite complicated and uncertain, we can suspect a mixture of at least three phases; moreover, the so-called X-, Y-, Z-phases could also incorporate additional ions coming from the other phases.

Non stoichiometric Ni-Co-Ln-Ln'(Bi)-Mo-Si (1 :1 :1 :1:2.5 :20) catalysts

Of course, the case of "non stoichiometric" multimodified Ni-Co-Ln-Ln'(Bi)-Mo-Si catalysts, is the most complicated. The presence of a mixed Ni-Co molybdate phase is obvious, but some other phases are also present. There are three different hypotheses that must be taken into account:

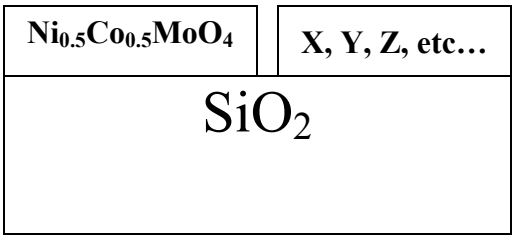

1) MoO_3 and the two Ln-oxides (Ln_2O_3 or LnO_2, depending on the oxidation state of the additional elements); 2) a Ln-oxide (LnO_2 or Ln_2O_3), a molybdate-type phase ($Ln_2Mo_3O_{12}$ or $Bi_2Mo_3O_{12}$), NiO and CoO; or 3) two molybdate-type phases, two Ln-oxides, NiO and CoO.

We actually think that the most realistic hypothesis is the first one, because we never observed the formation of Ln-molybdate phases in any catalyst prepared by the sol-gel method, even if we did not find any MoO_3 that would normally be easy to detect. The last hypothesis seems quite unrealistic because it would involve the existence of six different phases. Moreover in all phases, the incorporation of ions coming from the other phases cannot be excluded. To summarize, we expect four different phases at least in this type of catalysts.

Generally speaking, the highly complex nature of our catalysts does not allow us to make credible any hypotheses on the distribution and the dispersion of the phases, and on which phases are in contact with each other.

III.1.5 Conclusions

The sol-gel method has been successfully applied to the synthesis of solid solutions of $NiMoO_4$ and $CoMoO_4$. The main difference between the bulk and silica-dispersed Ni-Co-Mo catalysts prepared by citrate or sol-gel methods as well as impregnation, is related to the fact that it is possible to stabilize the β-$Ni_{1-x}Co_xMoO_4$ phase throughout the whole composition range in the dispersed catalysts, whereas this was not the case at low Co content in the bulk catalysts, because a mixture of α and β-phase is observed. This result completes the observations by other authors showing that the pure β-$NiMoO_4$ phase can be stabilized on supports like SiO_2 or TiO_2 when prepared by impregnation or precipitation, or when it is encapsulated in a silica matrix following the sol-gel method (62,66,69). According to the literature, the β-phase is normally generated in situ by increasing the temperature to 973 K and could be also stabilized at room temperature in the presence of an excess of Ni (64). The stabilization of the β-phase at low temperature throughout the Ni-Co composition range, presumably due to the interactions between the surface silanol groups and the $[MoO_4]^{2-}$ species,

leading to Si-O-Mo(=O)$_2$-O-Si moieties with tetrahedrally coordinated molybdenum, is therefore very important, because this phase, which is normally metastable at room temperature, is known to display better catalytic performances in alkane ODH. From a structural point of view, these experiments demonstrate that supporting or dispersing the mixed $Ni_{1-x}Co_xMoO_4$ phase on any kind of support leads to the preferential stabilization of the β-phase. When the sol-gel method is used for the preparation of the samples, the β-phase is always identified. In impregnated catalysts, when simple $NiMoO_4$ is supported on alumina, on titania, the β-phase is partly stabilized but coexists with the α-phase, while the latter appears alone in the ZrO_2-supported catalyst. We can conclude that the sol-gel method can definitely ensure the purity of the β-phase.

The incorporation of a lanthanide in Ni and/or Co molybdate stabilizes the β-phase for citrate-prepared catalysts except in the case of Sm- and Bi-modified Ni molybdates in which only the α-phase was detected. It has been observed that in the case of sol-gel modified Ni molybdates, the β-phase could be stabilized not only because of the interaction with silica but also by including a lanthanide element in the lattice. Quaternary phases have been identified in citrate as well as in sol-gel prepared catalysts characterized by the formulation (Ni,Co):Ln(Bi):Mo (1:1:2.5). In the case of "non stoichiometric" Ni-Co-Ln(Bi)-Mo-Si and Ni:Co:Ln(Bi):Ln':Mo:Si catalysts, the situation is complicated. Nevertheless, in order to have an approximate idea of the picture of this kind of catalysts, some hypotheses have been put forward. For the first class of catalysts there are two possibilities: (i) next to the normal $Ni_{0.5}Co_{0.5}MoO_4$ phase, there could be the corresponding $Ln_2Mo_3O_{12}$-phases, NiO and CoO; or (ii) the Ln_2O_3-phases could also exist with some MoO_3. For the second class of catalysts, we actually think that the most realistic hypothesis is the one related to the formation of MoO_3 and the two Ln-oxides (Ln_2O_3 or LnO_2, depending on the major oxidation state of the additional elements).

III.2 Overview of the catalytic results

III.2.1 Introduction

The purpose of the second part of this chapter is to present the main catalytic results of the catalysts that were characterized in the first part, and to discuss and give

tools for the interpretation of their catalytic performances in propane ODH. The discussion will be subdivided into three different parts.

In the first part, the catalytic behaviour of the SiO_2-based catalysts will be investigated in propane ODH and their catalytic performances will be also compared with those reported for bulk or supported catalysts from the literature. The results will demonstrate (i) the importance of dispersing the active phase on a support, as well as (ii) the importance of solid solutions of Ni and Co molybdates, which are more active than the corresponding simple molybdates. Finally, correlations between the catalytic performances of silica-supported "Ni(Co)Mo"catalysts and their textural properties will be put forward.

The second part will be devoted to the presentation and discussion of the catalytic performances of the analogous catalysts dispersed on various supports characterized by different acidities: Al_2O_3, MgO, TiO_2, ZrO_2 and also a mixed Al_2O_3-MgO support. It is worth reminding that alumina- and magnesia-based catalysts were prepared by impregnation and sol-gel methods, in order to evidence the influence of the preparation method on the textural properties and the resulting catalytic behaviour. These data will be analyzed not only with respect to the different support acidities (Al_2O_3 is a very acidic support which could facilitate the adsorption of the alkane and MgO is a basic support which could facilitate the desorption the alkene), but also in relationship with the used preparation method, leading to different dispersion degrees of the active phase and textural properties.

The last part will deal with the catalytic properties of Ni(Co)-Ln(Bi)-Mo-Si catalysts, whose performances will be explained by assuming the presence of a single multicomponent phase, and by taking into account the mobility of the oxygen of the lattice. We will also, at the same time, look at the catalytic activity of Ni-Co-Ln(Bi)-Mo-Si and Ni-Co-Ln-Ln'(Bi)-Mo-Si, by trying to evidence the effect that the additional elements can exert in the catalytic behaviour of the mixed nickel and cobalt molybdates in which they are incorporated. The ultimate goal will be to correlate some parameters related to the catalytic behaviour of the catalysts with some fundamental physico-chemical properties such as ionisation energy, absolute hardness and the standard redox potential, which are described in the section I.3 of Appendix I.

III.2.2 Silica-dispersed Solid Solutions of Ni and Co Molybdates

The catalytic performances of the silica dispersed Ni(Co)Mo-catalysts are presented in tables III.8-10 in Appendix III according to their loading of active phase (5,10 or 20 mol Si/mol Mo). By considering that the active phase is made of simple or mixed molybdates with the overall stoichiometry $Ni_{1-x}Co_xMoO_4$ (with $0 \leq x \leq 1$), these compositions correspond to the following mass percentages of active phase in the catalysts: 15 wt. % for Si/Mo = 20, 27 wt. % for Si/Mo = 10 and 42 wt % for Si/Mo = 5.

III.2.2.1 Influence of Ni/Co composition

Particular attention must be paid to the Ni/Co stoichiometry involved in the formulation of the catalysts because it seems to strongly influence the catalytic performances of Ni-Co-Mo-Si catalysts.

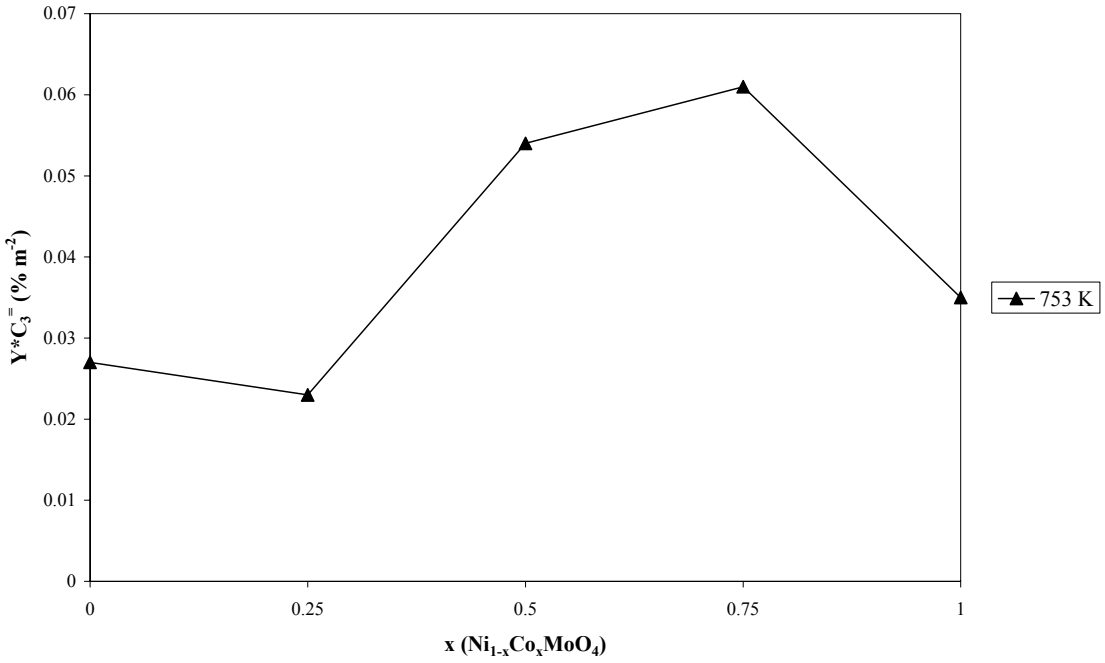

Fig.III.17: Evolution of the intrinsic propene yield ($Y^*C_3^=$) in $Ni_{1-x}Co_xMoO_4/SiO_2$ (Si/Mo = 20), prepared by the sol-gel method.

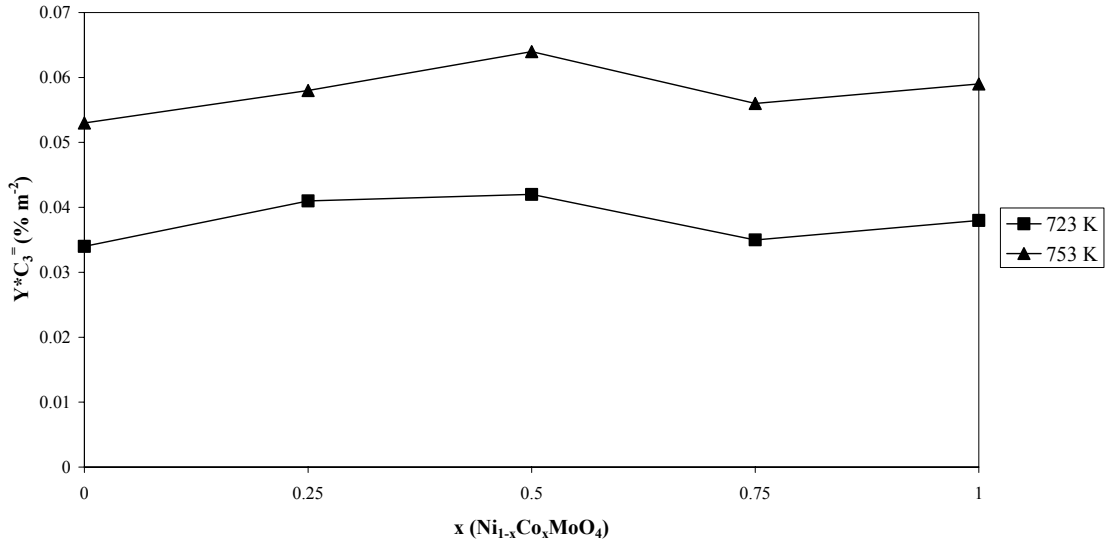

Fig.III.18: Evolution of the intrinsic propene yield ($Y^*C_3^=$) in $Ni_{1-x}Co_xMoO_4/SiO_2$ (Si/Mo = 10), prepared by the sol-gel method.

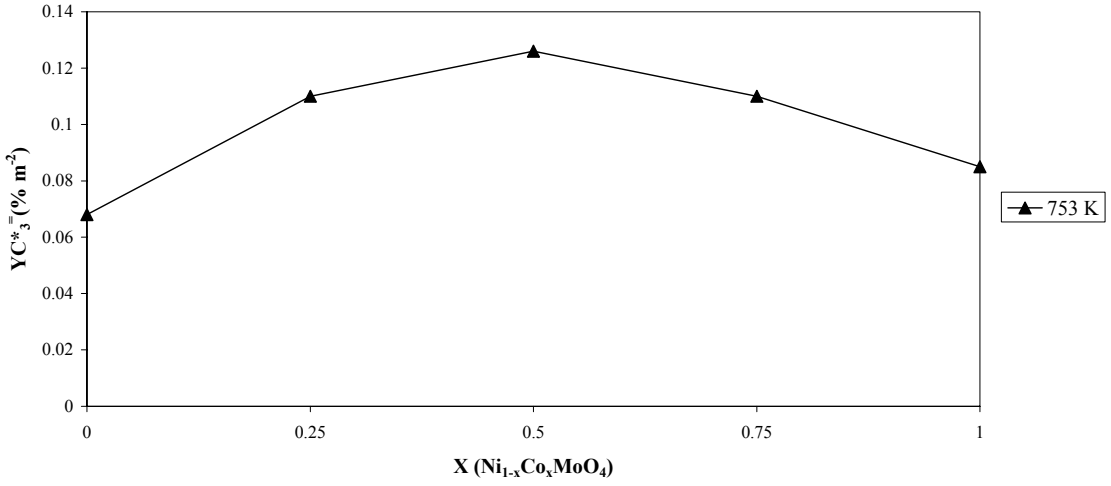

Fig.III.19: Evolution of the intrinsic propene yield ($Y^*C_3^=$) in $Ni_{1-x}Co_xMoO_4/SiO_2$ (Si/Mo = 5), prepared by the sol-gel method.

By observing the evolution of intrinsic propene yields with respect to the Ni/Co composition (figures III.17-20), it must be underlined that, in general, mixed Ni and Co molybdates display a better catalytic behaviour than simple Ni or Co molybdates, or there is at least one mixed Ni-Co molybdate showing a higher activity in comparison with those of the simple molybdates.

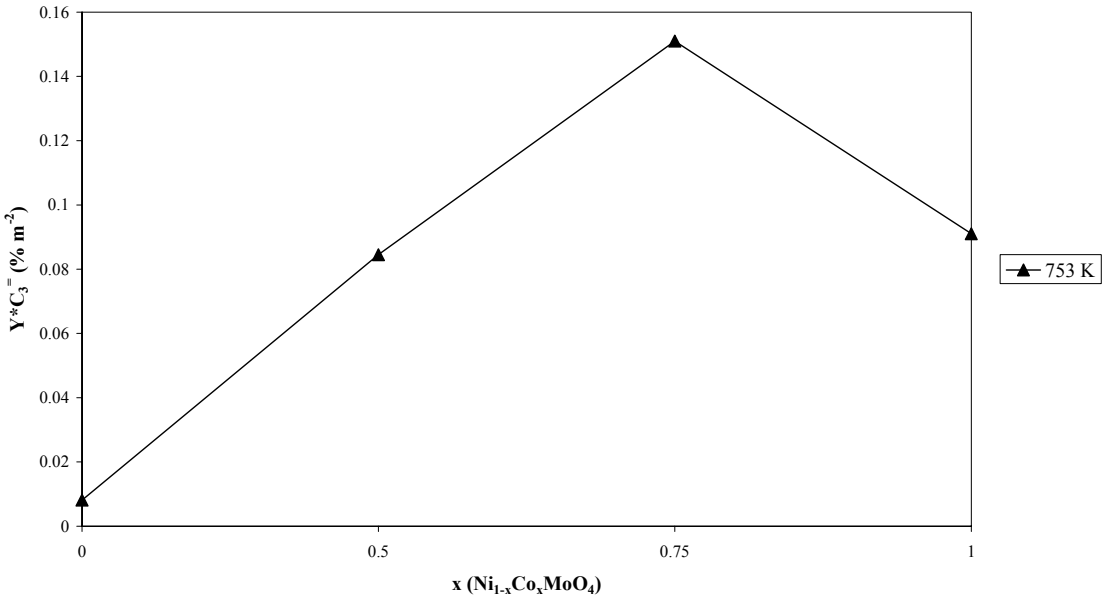

Fig.III.20: Evolution of the intrinsic propene yield ($Y^*C_3^=$) in $Ni_{1-x}Co_xMoO_4/SiO_2$ (Si/Mo = 5), prepared by impregnation.

III.2.2.2 Influence of silica loading

Fig.III.21 illustrates the influence of active phase loading on silica on the intrinsic propene yields, for all $Ni_{1-x}Co_xMoO_4$. Generally speaking, the higher the active phase loading (i.e. the lower the silica loading), the higher the intrinsic yields in propene (fig. III.21) and also CO_2 (for major details see section III.4.3 in Appendix III). Departure from this general trend is observed only when comparing the solid solutions x = 0.75 for Si/Mo = 20 which presents an intrinsic propene yield a little bit higher than the analogous one characterized by a Si/Mo = 10. In all cases, the catalysts with the highest loading in active phase are those producing the highest amounts of propene and CO_2.

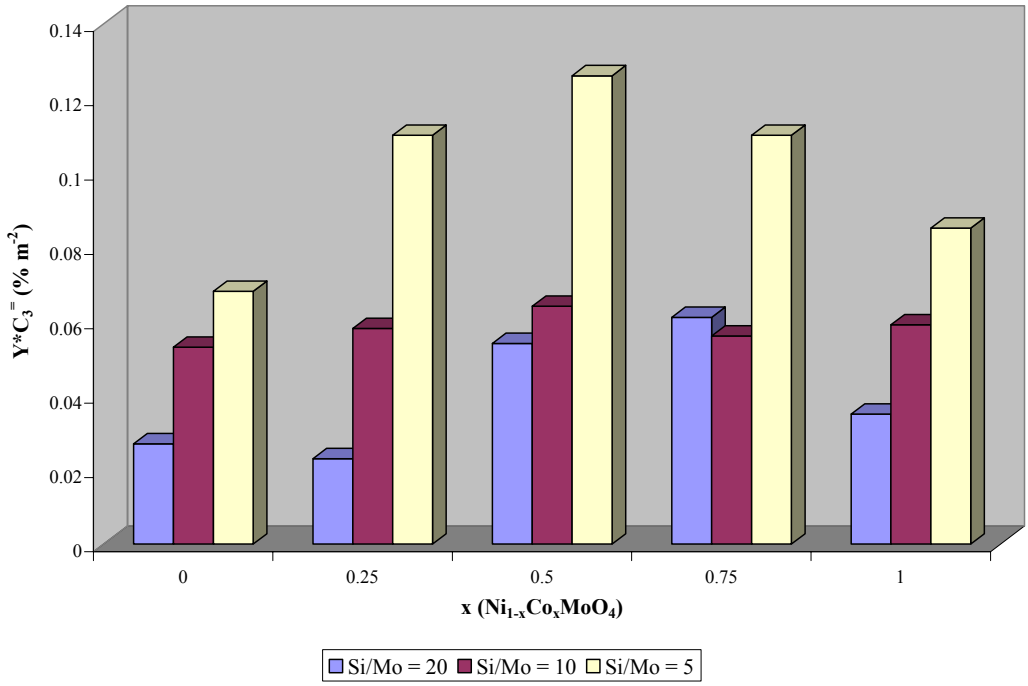

Fig.III.21: Effect of the silica loading in the evolution of the intrinsic propene yield ($Y^*C_3^=$) in SiO_2-dispersed $Ni_{1-x}Co_xMoO_4$ (at 753 K).

III.2.2.3 Comparison between catalysts prepared by impregnation and sol-gel method

When comparing $Ni_{1-x}Co_xMoO_4/SiO_2$ (Si/Mo = 5) prepared by sol-gel method with the those prepared by impregnation (fig. III.22), no general trend appears: sometimes, samples prepared by sol-gel method are more active than those prepared by impregnation and sometimes not. Catalysts prepared by sol-gel method convert more propane and more oxygen than the analogous ones prepared by impregnation, except Ni-Mo-Si. But if we consider the intrinsic propane or O_2 conversion, no significant difference is observed between the two series of catalysts, except in the case of Ni-Mo-Si, catalyst prepared by impregnation

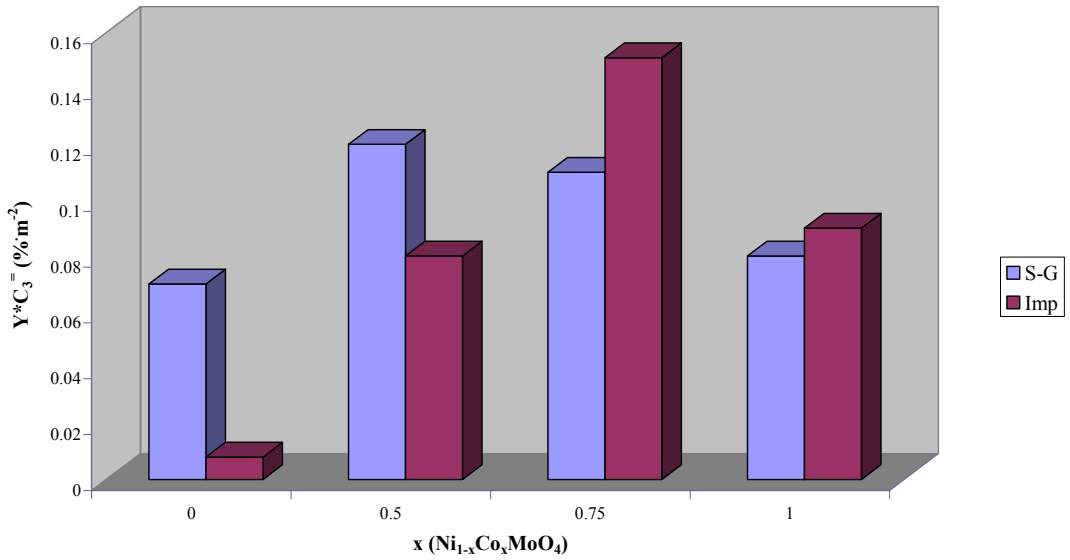

Fig.III.22: Comparison between the intrinsic propene yields of $Ni_{1-x}Co_xMoO_4/SiO_2$ (Si/Mo = 5) prepared by sol-gel method and impregnation (at 753 K).

III.2.2.4 Comparison with catalysts from the literature

Table III.11 lists the performances of $Ni_{1-x}Co_xMoO_4/SiO_2$ catalysts prepared by sol-gel and impregnation method, together with some relevant data from the literature. Quite generally, at the same reaction temperature (T = 753 K), the sol-gel prepared catalysts behave equally or better in terms of propene productivity than those prepared by impregnation. All propene productivity values of molybdate catalysts prepared by sol-gel are higher than those of the catalysts prepared by impregnation: this is due to the fact that the propene productivity does not take into account the difference in specific surface areas of the sol-gel samples which are higher and consequently give higher propene productivity results. Among all our sol-gel prepared Ni and Co molybdates, those characterized by a (Si/Mo) equal to 20, display the highest propene productivity values: it seems the higher the dilution of the active phase on the silica matrix, the higher the propene productivity.

Barsan et al. (61) measured the catalytic performances in propane ODH of β-$Ni_{0.5}Co_{0.5}MoO_4$ prepared by coprecipitation at different pH values. While all those catalysts display a higher intrinsic propene activity (10-60 μmol $h^{-1}m^{-2}$), they show a lower propene productivity (≤ 2.31 mmol $h^{-1}g_{ph}^{-1}$). Because the active phase is the same in both cases (β), this is assumed to reflect the advantage of dispersing the active phase in the silica matrix.

Table III.11: Catalytic performances of bulk and silica-dispersed Ni, Co and Ni-Co molybdate catalysts in propane ODH: comparison with literature data.

Composition and molar ratio	Preparation method	Temperature (K)	Intrinsic propene activity ($\mu mol\ h^{-1}m^{-2}$)	Propene productivity ($mmol\ h^{-1}g_{ph}^{-1}$)
Ni:Mo:Si 1:1:20	Sol-gel	753	1.98	4.21
Ni:Co:Mo:Si 0.75:0.25:1:20	Sol-gel	753	1.69	4.85
Ni :Co :Mo :Si 0.5:0.5:1:20	Sol-gel	753	3.98	8.58
Ni :Co :Mo :Si 0.25:0.75:1:20	Sol-gel	753	4.50	10.3
Co:Mo:Si 1:1:20	Sol-gel	753	2.56	5.36
Ni:Mo:Si 1:1:10	Sol-gel	753	3.91	4.48
Ni:Co:Mo:Si 0.75:0.25:1:10	Sol-gel	753	4.28	5.17
Ni :Co :Mo :Si 0.5:0.5:1:10	Sol-gel	753	4.72	5.20
Ni :Co :Mo :Si 0.25:0.75:1:10	Sol-gel	753	4.13	4.59
Co:Mo:Si 1:1:10	Sol-gel	753	4.31	4.73
Ni:Mo:Si 1:1:5	Sol-gel	753	4.94	2.57
Ni:Co:Mo:Si 0.75:0.25:1:5	Sol-gel	753	8.69	4.56
Ni :Co :Mo :Si 0.5:0.5:1:5	Sol-gel	753	10.5	5.06
Ni :Co :Mo :Si 0.25:0.75:1:5	Sol-gel	753	8.27	4.85
Co:Mo:Si 1:1:5	Sol-gel	753	6.23	3.23
Ni:Mo:Si 1:1:5	Impregnation	753	0.6	0.28
Ni :Co :Mo :Si 0.5:0.5:1:5	Impregnation	753	6.24	2.88
Ni :Co :Mo :Si 0.25:0.75:1:5	Impregnation	753	11.1	4.78
Co :Mo :Si 1:1:5	Impregnation	753	6.73	2.74
Ni:Co:Mo 0.5:0.5:1	Coprecip. (pH = 6.0) (61)	723	58.8	1.35
Ni:Co:Mo 0.5:0.5:1	Coprecip. (pH = 7.5) (61)	723	11.3	0.68
Ni:Co:Mo 0.5:0.5:1	Coprecip. (pH = 8.5) (61)	723	22.5	2.31
Ni:Mo:Si 1:1:1.1	Impregnation (70)	833	124	4.45
Ni:Co:Mo:Si 0.75:0.25:1:1.1	Impregnation (70)	833	120	3.95
Ni :Co :Mo :Si 0.5:0.5:1:1.1	Impregnation (70)	833	72.3	2.38
Ni :Co :Mo :Si 0.25:0.75:1:1.1	Impregnation (70)	833	29.6	0.71
Co :Mo :Si 1:1:1.1	Impregnation (70)	833	36.1	0.79

The results obtained by Stern et al. (70) with silica-supported mixed Ni-Co molybdates prepared by impregnation (80 wt. % of active phase) are also given for comparison but it has to be underlined that these data refer to a much higher reaction

temperature (T = 833 K). First, these solid solutions are characterized by lower values of intrinsic propene activity and propene productivity in comparison with simple $NiMoO_4$, while in our case, all solid solutions, prepared either by sol-gel method or by impregnation, display better catalytic performances than simple Ni or Co molybdates. Second, in spite of the much higher temperature, their propene productivity, expressed per unit weight of active phase, remains in most cases lower than that of our sol-gel or impregnated catalysts. This is particularly marked for the Co-rich composition ($x \geq 0.5$).

III.2.2.5 On the catalytic performances of solid solutions of Ni and Co molybdates supported on silica

$NiMoO_4$ and $CoMoO_4$ dispersed on SiO_2

In the case of silica-supported $NiMoO_4$ prepared by sol-gel method, it has been observed that at 753 K (see fig.III.23), increasing the loading of the active phase, the propane conversion increases as well as the propene intrinsic yield, but propene selectivity decreases.

In the analogous sol-gel $CoMoO_4/SiO_2$ catalysts an opposite behaviour is observed: increasing the active phase loading results in a decrease of propane conversion, and increase of propene selectivity (fig.III.24).

If we calculate the P.P. (propene productivity) of these catalysts by taking into account the actual amount of the active phase (depending in the Si amount), higher values are observed for lower active phase loading. This indicates that a high dilution of the active phase in the silica matrix leads to a better-dispersed and consequently more active catalyst.

However, for both molybdates, a high amount of active phase leads to a lower specific surface area. Observing the evolution of I.PA. (intrinsic propene activity), a parameter which takes into account the different specific surface areas of SiO_2-dispersed $NiMoO_4$ and $CoMoO_4$, it can be noticed that the molybdates characterized by higher active phase loading also have the higher I.P.A. values.

Neither the average pore volume nor the average pore diameter are able to explain the differences of catalytic behaviour observed between these two sets of catalysts. Moreover, in Ni(Co):Mo:Si (1:1:20,10 or 5) catalysts, XPS analysis revealed that for the same amount of silica, the degree of dispersion of Ni in $NiMoO_4/SiO_2$ and Co in $CoMoO_4/SiO_2$ are almost the same.

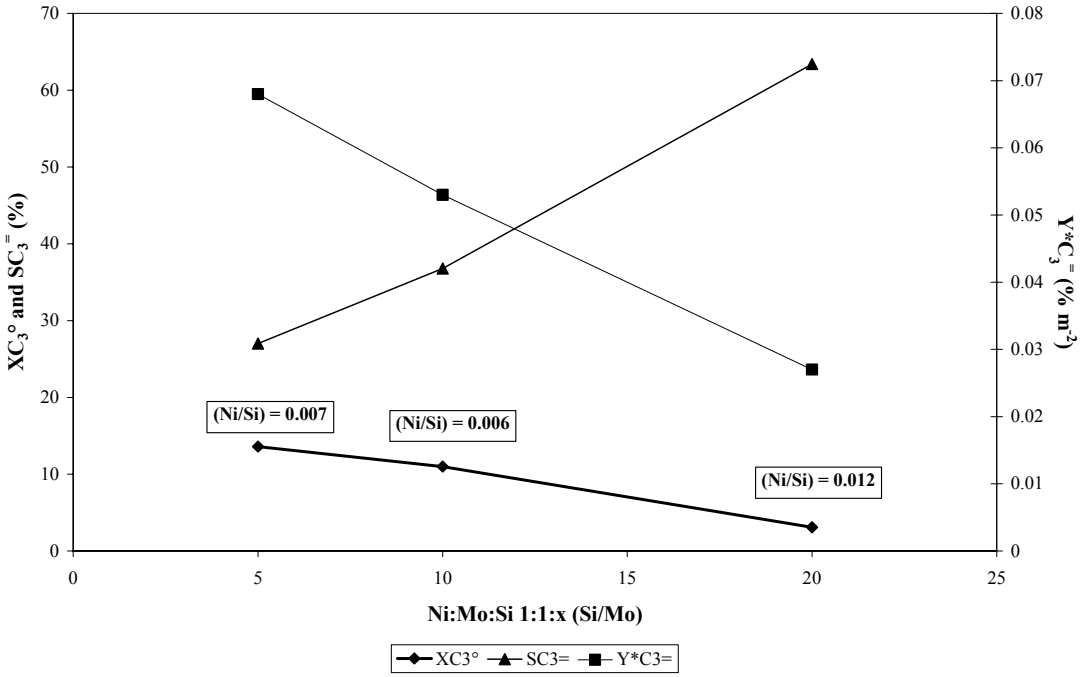

Fig.III.23: Evolution of the catalytic performances at 753 K of Ni:Mo:Si (1:1:5, 1:1:10 and 1:1:20) prepared by sol-gel method with respect to the silica loading. The corresponding XPS (Ni/Si) ratios are also given.

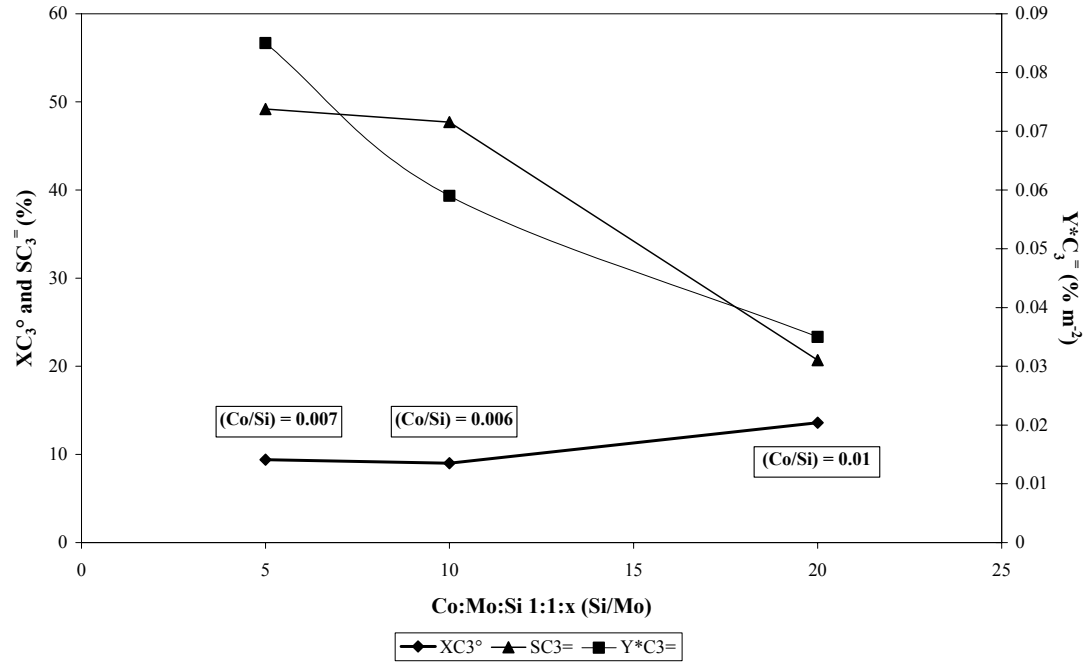

Fig.III.24: Evolution of the catalytic performances at 753 K of Co:Mo:Si (1:1:5, 1:1:10 and 1:1:20) prepared by sol-gel method with respect to the silica loading. The corresponding XPS (Co/Si) ratios are also given.

Table III.12: Intrinsic propene activity, propene productivity and pore diameter in silica- dispersed Ni and Co molybdates, prepared by sol-gel method. a) Intrinsic propene yield; b) Propene productivity at 753 K.

$Ni_{1-x}Co_xMoO_4$	Si/Mo = 20			Si/Mo = 10			Si/Mo = 5		
	I.P.A.[a] ($\mu mol\ h^{-1}\ m^{-2}$)	P.P.[b] ($mmol\ h^{-1}\ g_{ph}^{-1}$)	Dp (nm)	I.P.A.[a] ($\mu mol\ h^{-1}\ m^{-2}$)	P.P.[b] ($mmol\ h^{-1}\ g_{ph}^{-1}$)	Dp (nm)	I.P.A[a] ($\mu mol\ h^{-1}\ m^{-2}$)	P.P.[b] ($mmol\ h^{-1}\ g_{ph}^{-1}$)	Dp (nm)
x = 0	1.98	4.21	7.5	3.91	4.48	5.7	4.94	2.57	8.9
x = 0.25	1.69	4.85	4.6	4.28	5.17	8.6	8.69	4.56	8.4
x = 0.5	3.98	8.58	-	4.72	5.20	-	10.5	5.06	-
x = 0.75	4.50	10.3	8.4	4.13	4.59	6.4	8.27	4.85	11.0
x = 1	2.56	5.36	6.5	4.31	4.73	11	6.23	3.23	10.8

Mixed Ni-Co molybdates dispersed on SiO_2

When considering the evolution of both I.P.A (intrinsic propene activity) and P.P. (propene productivity) values with respect to the active phase loading, in the case of solid solutions of $NiMoO_4$ and $CoMoO_4$, it can be generally observed that the higher the active phase loading, the higher the I.P.A. and the lower the P.P. values.

According to Stern and Grasselli (70), an excess of Ni and consequent high CO_2 production, could be related to the formation of surface A-O-A moieties (in our case Ni-O-Ni) or to the formation of surface AO (NiO) that would lead to high non-selective propane conversions, resulting in waste products. Surface A-O-A moieties would attack and combust the formed propene. The mixed Ni and Co molybdates displayed good catalytic performances, because of the formation of mixed Ni-O-Co-O moieties, which are assumed to be responsible for a little decrease of the catalytic activity of the solid solutions, but at the same time also responsible for an enhanced selectivity towards propene and intrinsic propene yield.

Effect of textural properties of SiO_2 sol-gel prepared catalysts on their catalytic activity

In the case of $NiMoO_4$ and $CoMoO_4$, we observed an increasing intrinsic propene activity (I.P.A.) with the increasing loading of active phase on one hand and a decreasing propene productivity (P.P.) (see the table III.12, for I.P.A. and P.P. values) with increasing loading of the active phase; in the case of the mixed Ni and Co molybdates there is no correlation between the amount of the active phase present in the catalyst and I.P.A or P.P. values.

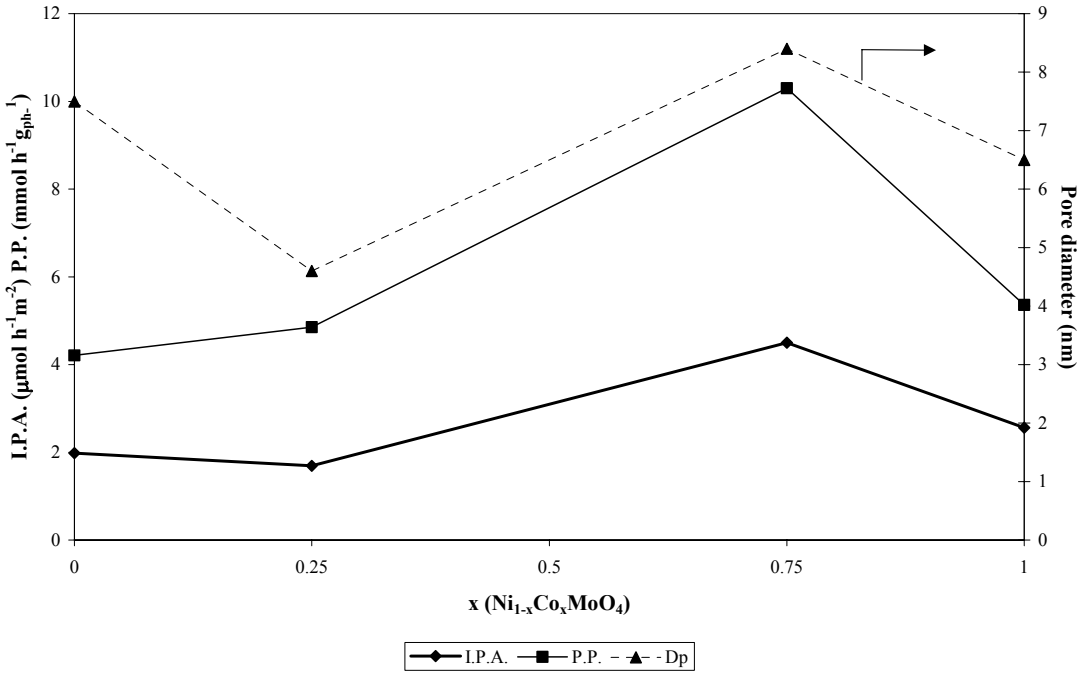

Fig.III.25: Evolution of the intrinsic propene activity and propene productivity with respect to the composition and pore diameter (dashed line) of Ni:Co:Mo:Si (1-x:x:1:20) (at 753 K).

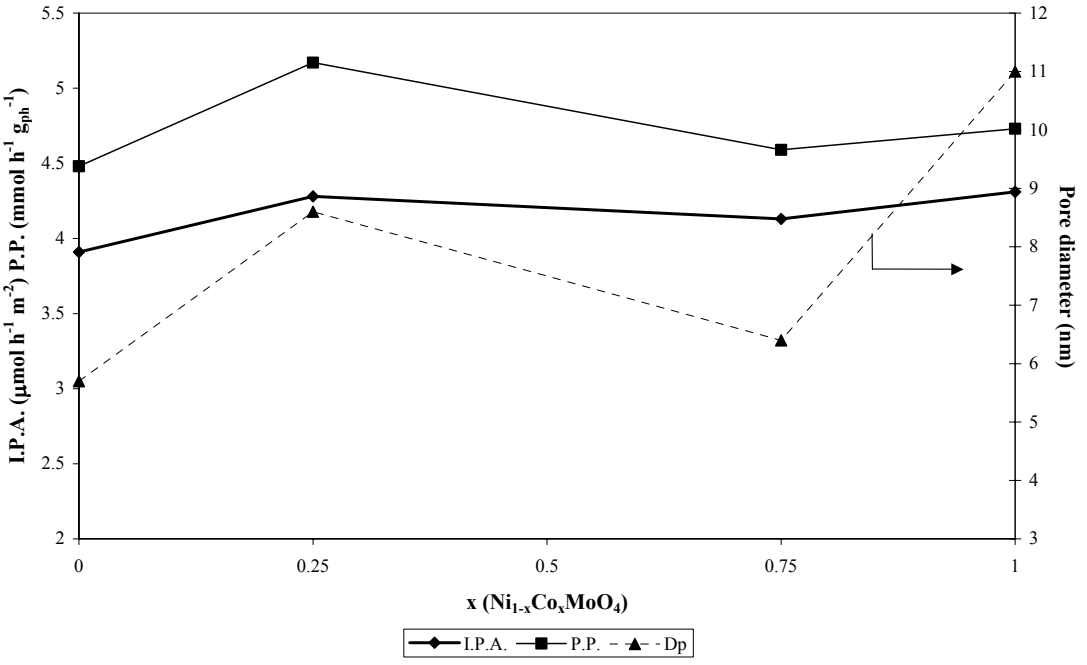

Fig.III.26: Evolution of the intrinsic propene activity and propene productivity with respect to the composition and pore diameter (dashed line) of Ni:Co:Mo:Si (1-x:x:1:10) (at 753 K).

Considering the catalysts characterized by (Si/Mo) equal to 20 or 10 (fig. III.25 - 26, data at 753 K) the pore diameter (Dp) of the samples seems to play an important

role on the I.P.A. and P.P., which both increase with Dp. This kind of correlation does not seem to work well with molybdate catalysts characterized by a (Si/Mo) equal to 5.

From a general point of view, the catalysts with lower pore diameter are characterized by a lower catalytic activity and those characterized by higher pore diameter display a higher catalytic activity: low diameters can restrict the access to the active sites located in the pores leading to a lower catalytic activity.

$NiMoO_4$ and $CoMoO_4$ supported on SiO_2 prepared by impregnation method

Concerning the silica-supported $NiMoO_4$ prepared by impregnation, it must be said that its very low intrinsic propene yield could be due to the fact that $(Ni/Mo)_{imp}$ is higher than $(Ni/Mo)_{S\text{-}g}$ (0.44 and 0.25, respectively) with consequent higher formation of surface Ni-O-Ni moieties which normally favour the formation of overoxidation product: $YCO_2/3$ of the sample prepared by impregnation is 11.4 % at 753 K and that of the sol-gel-prepared sample is 7 % only.

In $CoMoO_4$ prepared by impregnation method, the (Co/Mo) ratio is also higher than in the corresponding sol-gel catalyst (0.42 and 0.29, respectively), but we observe that $YCO_2/3$ and the intrinsic propene activity (I.P.A.) values are very similar close in the two types of catalysts. A possible explanation could be found in the fact that even if both catalysts are characterized by Co-O-Co moieties, the one prepared by impregnation shows a (Mo/Si) ratio much higher than $(Mo/Si)_{S\text{-}g}$ (0.084 and 0.035, respectively) with a consequent formation of Mo-O-Mo moieties which are responsible of an improvement of catalytic activity towards the formation of propene, lowering CO_2 yield (70): this could explain why in the case of the impregnated catalyst we do not observe a high $YCO_2/3$ (which would be normal, because of the formation of Co-O-Co moieties) nor a low $YC_3^=$.

Considering that the difference between $(Mo/Si)_{imp}$ and $(Mo/Si)_{S\text{-}g}$ in the case of $CoMoO_4$ (0.049) is higher than that between $(Mo/Si)_{imp}$ and $(Mo/Si)_{S\text{-}g}$ (0.025) in the case of $NiMoO_4$, this could be a reason for which the formation of Mo-O-Mo moieties in $NiMoO_4$ does not influence its catalytic activity in comparison to Ni-O-Ni moieties.

III.2.3 Catalytic behavior of alumina-supported Ni and Co molybdates

See tables V.12 and 13 in Appendix V for the catalytic performances of alumina-supported Ni and Co molybdates.

Ni-Mo-O / Co-Mo-O

- *Sol-gel prepared catalysts:*

  $CoMoO_4$ displays a higher values of $XC_3°$, $YC_3^=$, XO_2 and $YCO_2/3$ than $NiMoO_4$.

- *Catalysts prepared by impregnation:*

  $CoMoO_4$ shows a lower XO_2 and consequently lower $YCO_2/3$ than $NiMoO_4$; both catalysts are characterized by the same $XC_3°$ and $YC_3^=$ values.

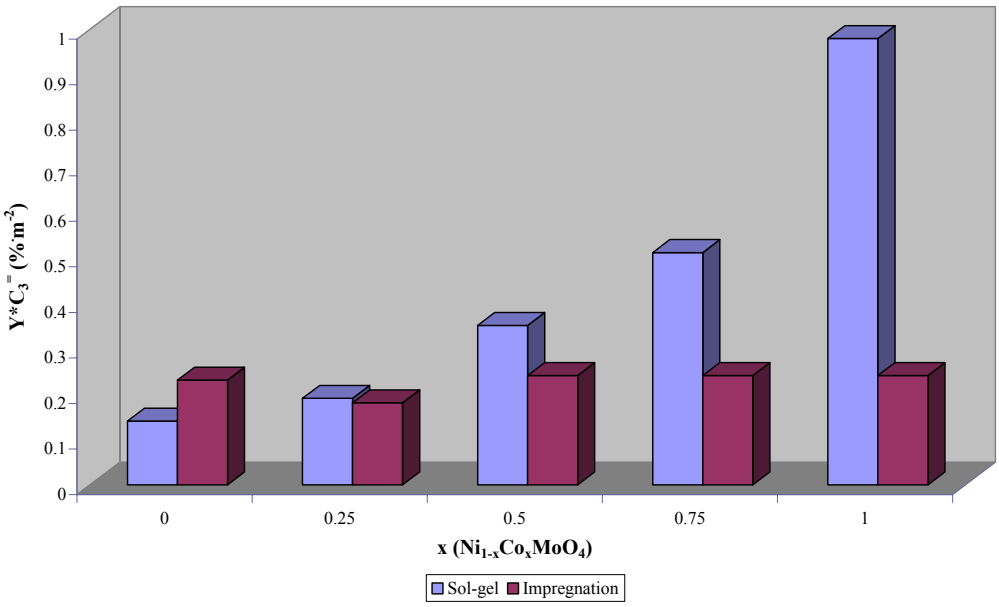

Fig.III.27: Evolution of the intrinsic propene yield ($Y*C_3^=$) of alumina-dispersed catalysts with respect to the Co content (at 753 K).

Sol-gel vs Impregnation

- Ni-Mo-O and Co-Mo-O:

$NiMoO_4$ and $CoMoO_4$ prepared by the sol-gel method present higher values of $XC_3°$, XO_2, $YCO_2/3$ than the impregnated catalysts.

- Ni-Co-Mo-O:

Mixed Ni and Co molybdates prepared by impregnation or sol-gel give the same values of propene yield.

When intrinsic propene yields are considered ($Y*C_3^=$), (fig.III.27) it comes that the alumina-supported $Ni_{1-x}Co_xMoO_4$ prepared by sol-gel are characterized by higher values than those prepared by impregnation. Among all alumina-dispersed catalysts, the

most active one is a supported-$CoMoO_4$ prepared by sol-gel method ($Y^*C_3^= = 0.98\%\ m^{-2}$ at 753 K).

Ni-Mo-O and Co-Mo-O vs Ni-Co-Mo-O

- Sol-gel prepared catalysts:

Mixed Ni and Co molybdates show lower values of $XC_3°$, XO_2 and $YCO_2/3$ than the simple Ni and Co molybdates; they are also characterized by propene yields that are intermediate between that of $NiMoO_4$ and that of $CoMoO_4$.

- Catalysts prepared by impregnation:

Generally speaking, all $XC_3°$, $YC_3^=$, XO_2 and $YCO_2/3$ values of mixed Ni-Co molybdates are the same as those of simple Ni and Co molybdates.

Effect of the Co content in mixed Ni-Co molybdates

- Sol-gel prepared catalysts:

Increasing the loading of Co does not affect neither propane conversion nor propene yield.

On the other hand, XO_2 and $YCO_2/3$ values reach a maximum in correspondence of Ni:Co:Mo :Al (0.5:0.5:1:5).

- Catalysts prepared by impregnation:

Increasing the loading of Co leads to decreasing values of $XC_3°$, XO_2 and $YCO_2/3$.

$YC_3^=$ reaches a maximum in correspondence of Ni:Co:Mo:Al (0.5:0.5:1:5).

III.2.4 Catalytic behavior of magnesia-supported Ni and Co molybdates

See tables V.14 and 15 in Appendix V for all catalytic performances of magnesia-supported Ni and Co molybdates.

Ni-Mo-O / Co-Mo-O

- Sol-gel prepared catalysts:

$NiMoO_4$ shows higher values of $XC_3°$ and $YCO_2/3$ than $CoMoO_4$, but a lower $YC_3^=$.

- Catalysts prepared by impregnation:

$NiMoO_4$ displays a lower value of $XC_3°$ than $CoMoO_4$.

Sol-gel vs Impregnation

- Ni-Mo-O and Co-Mo-O :

Magnesia-dispersed $NiMoO_4$ prepared by the sol-gel method shows a higher $XC_3°$ than the impregnated catalyst. $CoMoO_4$ prepared by sol-gel displays lower values of $XC_3°$ and $YC_3^=$ than the impregnated catalyst.

- Ni-Co-Mo-O:

The propene yields of mixed Ni -Co molybdates prepared by the sol-gel method are lower than in the impregnated catalysts.

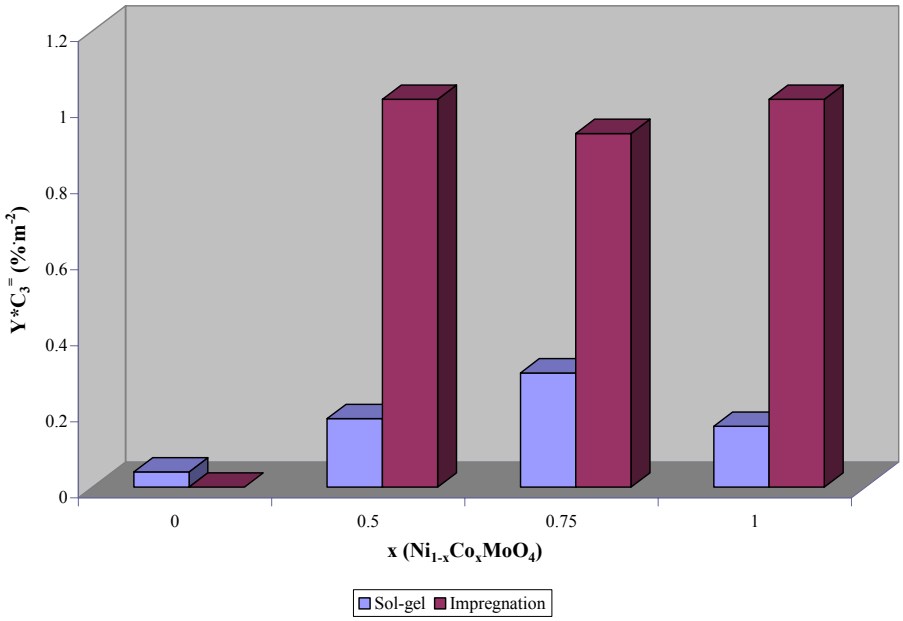

Fig.III.28: Evolution of the intrinsic propene yield ($Y^*C_3^=$) of MgO-dispersed catalysts with respect to the Co content (at 753 K).

When intrinsic propene yields are taken into account, fig.III.28 shows that all magnesia-supported $Ni_{1-x}Co_xMoO_4$ prepared by impregnation are generally characterized by higher $Y^*C_3^=$ values than those of the sol-gel method.

Ni-Mo-O and Co-Mo-O vs Ni-Co-Mo-O

- Sol-gel prepared catalysts:

Mixed Ni and Co molybdates show higher values of $XC_3°$ than simple Ni and Co molybdates, except for Ni:Co:Mo:Mg (0.75:0.25:1:5).

- Catalysts prepared by impregnation:

Mixed Ni-Co molybdates display intermediate values of $XC_3°$ values between those of Ni molybdate and Co molybdate and are also characterized by lower values of $YC_3^{=}$, XO_2 and $YCO_2/3$ than Co molybdate.

Effect of the Co content in mixed Ni-Co molybdates

- Sol-gel prepared catalysts:

Increasing the Co loading leads to increasing propane conversion ($XC_3°$).

- Catalysts prepared by impregnation:

Increasing the Co loading leads to larger values of $XC_3°$, XO_2 and $YCO_2/3$.

III.2.5 Catalytic behavior of Al_2O_3-MgO-supported Ni and Co molybdates

See table V.16 in Appendix V for the catalytic performances of Al_2O_3-MgO supported Ni and Co molybdates.

Ni-Mo-O / Co-Mo-O

Ni-Mo-O displays lower values of $XC_3°$, $YC_3^{=}$, XO_2 and $YCO_2/3$ than Co-Mo-O.

Among all catalysts, Co-Mo-O is the one consuming the highest amount of oxygen (XO_2 = 65.1 % at 753 K) and the one producing the highest amount of CO_2 ($YCO_2/3$ = 12.3 % at 753 K).

Ni-Mo-O and Co-Mo-O vs Ni-Co-Mo-O

Ni-Co-Mo-O catalysts show higher $XC_3°$, $YC_3^{=}$, $YCO_2/3$ values than Ni-Mo-O and lower than those displayed by Co-Mo-O.

Effect of the content of Co in mixed Ni and Co molybdates

Taking into account the $XC_3°$ values, it is observed that an increasing content of Co leads to higher propane conversion: all mixed Ni-Co-Mo-O are in fact characterized by higher $XC_3°$ values than Ni-Mo-O and lower than those of Co-Mo-O ($XC_3°$ = 22.2 % at 753 K).

XO_2 and $YCO_2/3$ show a maximum in correspondence of Ni:Co:Mo:(Al+Mg) (0.5:0.5:1:5).

Fig.III.29 shows the intrinsic propene yield ($Y^*C_3^=$) of all Al_2O_3-MgO-supported Ni-Co-Mo prepared by sol-gel method. Mixed Ni and Co molybdates are characterized by $Y^*C_3^=$ values higher than Ni-Mo-O. The catalyst which displays the highest $Y^*C_3^=$ is Ni-Co-Mo (0.25:0.75:1) followed by Co-Mo-O. It must be underlined that the $Y^*C_3^=$ of all Al_2O_3-MgO-dispersed catalysts are lower than the corresponding ones supported on alumina and higher than those supported on magnesia.

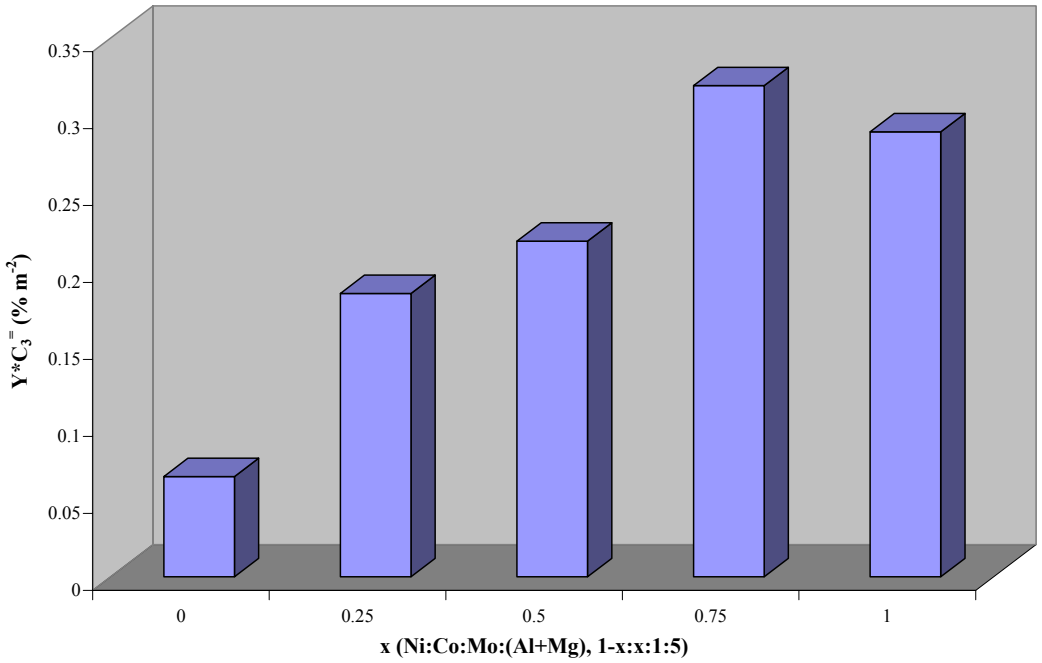

Fig.III.29: Evolution of the intrinsic propene yield ($Y^*C_3^=$) of Al_2O_3-MgO-dispersed catalysts with respect to the Co content (at 753 K).

III.2.6 Catalytic behavior of TiO_2-supported Ni and Co molybdates

See table V.17 in Appendix V for the catalytic performances of titania supported Ni and Co molybdates

Ni-Mo-O / Co-Mo-O

$NiMoO_4$ shows higher values of $XC_3°$, $YC_3^=$, XO_2 and $YCO_2/3$ than $CoMoO_4$.

Ni-Mo-O and Co-Mo-O vs Ni-Co-Mo-O

Concerning mixed Ni-Co molybdates, they generally convert less propane ($XC_3° = 2.0 – 3.8$ %, at 753 K) than $NiMoO_4$ ($XC_3° = 3.8$ %), but more than $CoMoO_4$ ($XC_3° = 1.4$ %). $NiMoO_4$ also displays the highest $YC_3^=$ value ($YC_3^= = 3.3$ %), followed by the mixed Ni-Co molybdates ($YC_3^= = 1.4 – 2.3$ %) and then by $CoMoO_4$ ($YC_3^= = 1.2$ %).

Effect of the Co content in mixed Ni-Co molybdates

Increasing the Co content leads to higher propene yields. Propane and oxygen conversions are both characterized by a minimum in correspondence of $Ni_{0.5}Co_{0.5}MoO_4$.

III.2.7 Catalytic behavior of ZrO_2-supported Ni and Co molybdates

See table V.18 in Appendix V for the catalytic performances of zirconia supported Ni and Co molybdates

Ni-Mo-O / Co-Mo-O

$NiMoO_4$ shows higher values of $XC_3°$, $YC_3^=$, XO_2 and $YCO_2/3$ than $CoMoO_4$, as already observed for TiO_2-supported catalysts.

Ni-Mo-O and Co-Mo-O vs Ni-Co-Mo-O

At 753 K, mixed Ni-Co molybdates show lower $XC_3°$ values (5.4 – 10.4 %) than $NiMoO_4$ (11.9 %), but higher than $CoMoO_4$. The same behaviour is observed for $YC_3^=$, XO_2 and $YCO_2/3$.

Effect of the Co content in mixed Ni-Co molybdates

It seems that increasing the Co content leads to lower $XC_3°$ values. Concerning the oxygen consumption (XO_2), it follows the same behaviour as the propane conversion: a higher Co content in the catalyst leads to lower oxygen conversion.

III.2.8 Selectivity – conversion relationships

Fig.III.30 displays the selectivity to propene as function of the hydrocarbon conversion for all sol-gel prepared catalysts characterized by a (Supp./Mo) ratio equal to 5. The catalysts displaying the highest selectivities to propene are those dispersed in silica; the catalysts dispersed on Al_2O_3 and Al_2O_3-MgO show performances that are a good compromise between propene selectivity and propane conversion.

Fig.III.31 shows the same relationship for all catalysts prepared by impregnation. Among all impregnated catalysts, TiO_2- and ZrO_2-supported ones display the highest propene selectivities but also the lowest propane conversion, the latter being directly affected by the specific surface areas, which are very low in the case of TiO_2 and ZrO_2-based catalysts.

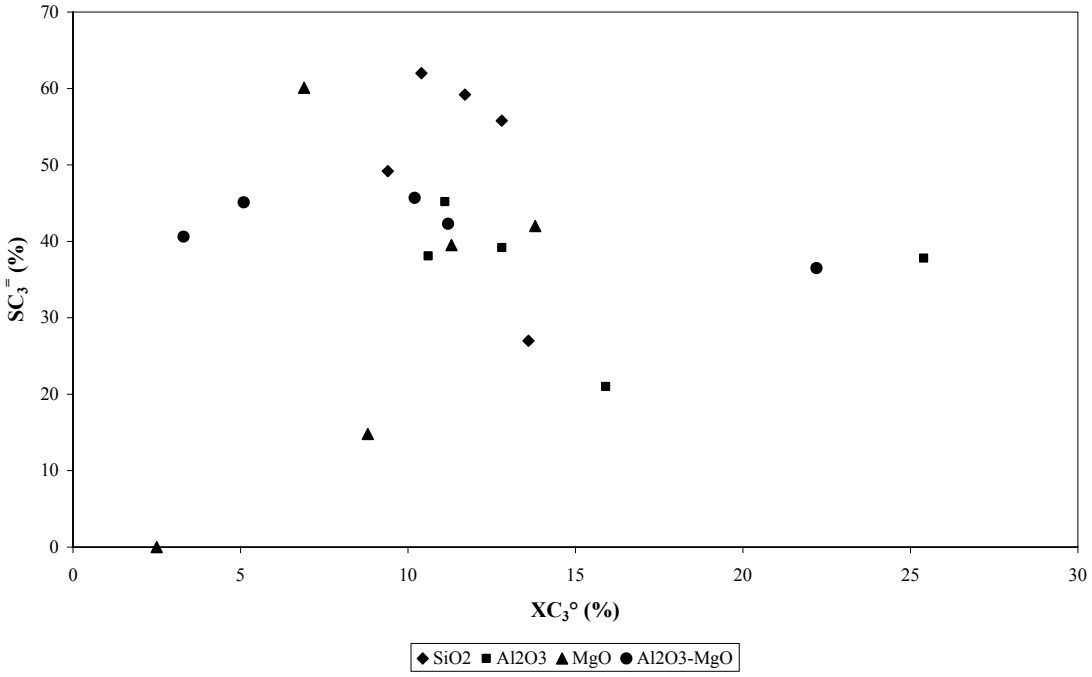

Fig.III.30: Selectivity to propene from propane with respect to the hydrocarbon conversion for all sol-gel prepared catalysts characterized by a (Supp./Mo) ratio equal to 5 (T = 753 K).

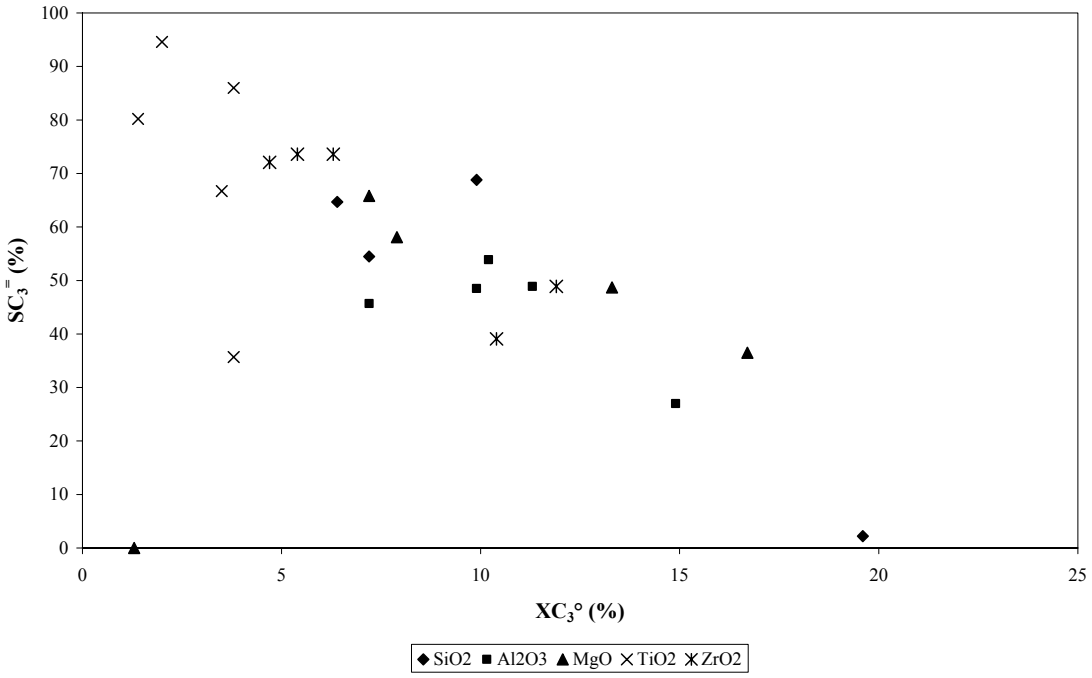

Fig.III.31: Selectivity to propene from propane as a function of hydrocarbon conversion for all catalysts prepared by impregnation and characterized by a (Supp./Mo) ratio equal to 5 (T = 753 K).

III.2.9 General comments and remarks on the role of support

Blank experiments, carried out under the same experimental conditions with the pure supports, showed that, in all cases, but silica, the intrinsic contribution of the support itself could be not negligible at all. Even if an additivity relationship for both contributions of the active phase and the support cannot be strictly applied, we used this assumption to evaluate the "possible" contribution. In most cases, the main product of the catalytic activity of the support alone is CO_2, but besides this product, propene appears even if in small amount.

For example, the mixed support Al_2O_3-MgO is responsible for a propane conversion of 12 % at 753 K: it is curious to remark that some Al_2O_3-MgO-dispersed catalysts do not reach this $XC_3°$ value, even if they display a better global catalytic activity in terms of propene yield or propene selectivity than the support.

Table III.13: Relative contribution of the supports to the global propene yield ($YC_3^=$) of the catalysts.

Catalysts Support – Prep. method	**Wt. % of the active phase**	**$YC_3^=$ (%) of the support at 753 K**	**Relative contribution (%) of the support to the global activity ($YC_3^=$) of the catalysts, at 753 K**
Al_2O_3 - Sol-gel	46	1.9	11 – 31
MgO - Sol-gel	52	0.7	5.8 – 25
Al_2O_3-MgO - Sol-gel	48	0.4	2.5 – 16
TiO_2 - Impregnation	35	0.2	4 – 11
ZrO_2 - Impregnation	26	1.7	22 – 37

Table III.13 lists the contribution of the different supports to the global activity, expressed in terms of $YC_3^=$ (%) of the tested catalysts.ZrO_2 is clearly the support that contributes most to the global catalytic activity, followed by Al_2O_3. Titania and mixed Al_2O_3-MgO support seem to be those exerting the lowest influence. In our case, the role of the support is therefore twofold: it allows to increase the dispersion of the active phase through its surface area, but also plays a direct role in the catalytic activity.

III.2.10 Influence of the acid-base properties

Table III.14 lists the catalytic performances in propane ODH at 753 K of supported-$NiMoO_4$ or $CoMoO_4$ prepared by the sol-gel method on different supports of various acidities. The intrinsic propene yields can be evaluated with respect to the

acidity the used supports (112). For both $NiMoO_4$ and $CoMoO_4$ it seems that a lower acidity of the support leads to lower intrinsic propene activity, with a much more pronounced effect in the case of $CoMoO_4$: the same effect is also observed if the propene productivity values are taken into account.

Table III.14: Intrinsic propene activity and propene productivity of all catalysts prepared by sol-gel method and tested at 753 K.

Composition and molar ratio	Intrinsic propene activity ($\mu mol\ h^{-1}m^{-2}$)	Propene productivity ($mmol\ h^{-1}g_{ph}^{-1}$)
Ni:Mo:Al 1:1:5	10.6	2.12
Ni:Co:Mo:Al 0.75:0.25:1:5	14.3	2.57
Ni :Co :Mo :Al 0.5:0.5:1:5	26.0	3.21
Ni :Co :Mo :Al 0.25:0.75:1:5	38.0	3.21
Co:Mo:Al 1:1:5	74.8	6.16
Ni:Mo:Al + Mg 1:1:5	4.81	0.80
Ni:Co:Mo:Al + Mg 0.75:0.25:1:5	13.6	1.41
Ni :Co :Mo :Al + Mg 0.5:0.5:1:5	16.1	2.89
Ni :Co :Mo :Al + Mg 0.25:0.75:1:5	23.6	2.89
Co:Mo:Al + Mg 1:1:5	21.4	4.98
Ni:Mo:Mg 1:1:5	3.20	0.74
Ni:Co:Mo:Mg 0.75:0.25:1:5	-	-
Ni :Co :Mo :Mg 0.5:0.5:1:5	13.6	2.55
Ni :Co :Mo :Mg 0.25:0.75:1:5	22.0	3.29
Co:Mo:Mg 1:1:5	12.0	2.33

The behaviour of $MMoO_4$ (M = Ni or Co) changes strongly when the impregnated catalysts are considered (table III.15): they show particularly good catalytic performances when they are supported especially on zirconia.

Generally speaking, considering the mixed Ni-Co molybdates prepared by the sol-gel method, we observe once again that the higher the basicity of the support, the lower the intrinsic propene activity and propene productivity: among the sol-gel prepared catalysts, those supported on alumina display the highest catalytic activity.

Table III.15: Intrinsic propene activity and propene productivity of all catalysts prepared by impregnation and tested at 753 K.

Composition and molar ratio	Intrinsic propene activity ($\mu mol\ h^{-1}m^{-2}$)	Propene productivity ($mmol\ h^{-1}g_{ph}^{-1}$)
Ni:Mo:Al 1:1:5	17.3	3.53
Ni:Co:Mo:Al 0.75:0.25:1:5	13.6	2.56
Ni :Co :Mo :Al 0.5:0.5:1:5	17.6	3.53
Ni :Co :Mo :Al 0.25:0.75:1:5	17.7	3.08
Co:Mo:Al 1:1:5	17.7	3.4
Ni:Mo:Ti 1:1:5	69.7	2.78
Ni:Co:Mo:Ti 0.75:0.25:1:5	34.5	1.18
Ni :Co :Mo :Ti 0.5:0.5:1:5	46.9	1.6
Ni :Co :Mo :Ti 0.25:0.75:1:5	75.6	1.93
Co:Mo:Ti 1:1:5	59.2	1.01
Ni:Mo:Zr 1:1:5	143	6.58
Ni:Co:Mo:Zr 0.75:0.25:1:5	135	4.65
Ni :Co :Mo :Zr 0.5:0.5:1:5	170	5.22
Ni :Co :Mo :Zr 0.25:0.75:1:5	132	4.54
Co:Mo:Zr 1:1:5	126	3.85
Ni:Mo:Mg 1:1:5	-	-
Ni:Co:Mo:Mg 0.75:0.25:1:5	77.3	2.67
Ni :Co :Mo :Mg 0.5:0.5:1:5	75.6	2.61
Ni :Co :Mo :Mg 0.25:0.75:1:5	107	3.69
Co:Mo:Mg 1:1:5	75.2	3.46

In the case of the catalysts prepared by the impregnation method, those supported on zirconia show the best catalytic behaviour, while the alumina-supported mixed Ni-Co molybdates are characterized by the lowest intrinsic propene activity and those supported on TiO_2, the lowest propene productivity.

In terms of intrinsic propene activity (I.P.A.), the various catalysts appear in the following order according to the support: $Al_2O_3 > Al_2O_3$-MgO > MgO for the sol-gel catalysts, and $ZrO_2 >$ MgO $\geq TiO_2 > Al_2O_3$ for the catalysts prepared by impregnation. In terms of propene productivity (P.P.) the sequence is: $Al_2O_3 > Al_2O_3$-MgO > MgO for

the sol-gel catalysts, and ZrO_2>Al_2O_3 ≈ MgO > TiO_2 for the catalysts prepared by impregnation.

III.2.11 Discussion of the catalytic results of Al_2O_3-, MgO- and Al_2O_3-MgO-supported Ni and Co molybdates prepared by impregnation and sol-gel method

Correlation between catalytic activity and XPS analyses in alumina-dispersed catalysts

Fig.III.27 shows that the alumina-supported $Ni_{1-x}Co_xMoO_4$ prepared by sol-gel are characterized by higher $Y^*C_3^=$ values than those prepared by impregnation. The most active catalyst is a supported-$CoMoO_4$ prepared by sol-gel method ($Y^*C_3^=$ = 0.98% m^{-2} at 753 K).

When referring to the XPS atomic ratios on alumina-dispersed catalysts, it comes out that the impregnation method leads to a better dispersion of all elements, all (Ni, Co, Mo/Al) atomic ratios being higher than in the corresponding samples prepared by the sol-gel method (table V.5 in Appendix V). The difference in the catalytic behaviour could be due to the fact that the impregnated catalysts are characterized by very high (Mo/Al) atomic ratios (between 0.73 and 2), higher than the theoretical value (equal to 0.2) (fig.III.32). We can suppose the formation of some surface MoO_3 next to the molybdate phase, which can lead to a low catalytic activity. Nevertheless, Raman spectroscopy and X-ray diffraction did not reveal any traces of MoO_3.

The Al-dispersed catalyst prepared by the sol-gel method is, on the other hand, characterized by a (Mo/Al) atomic ratio very close to the theoretical one (fig.III.32): Stern and Grasselli (70) already underlined that the catalyst surface characterized by a stoichiometric Mo composition favors the formation of non-CO_x products.

Another factor that could play an important role in the catalytic activity of these catalysts is the presence of Co on the surface. For Al_2O_3-sol-gel catalysts, experimental (Ni/Co) atomic ratios are higher than the corresponding samples prepared by impregnation characterized by lower catalytic activity: generally speaking, the lower the Co content on the surface, the higher the yields towards propene (table III.15).

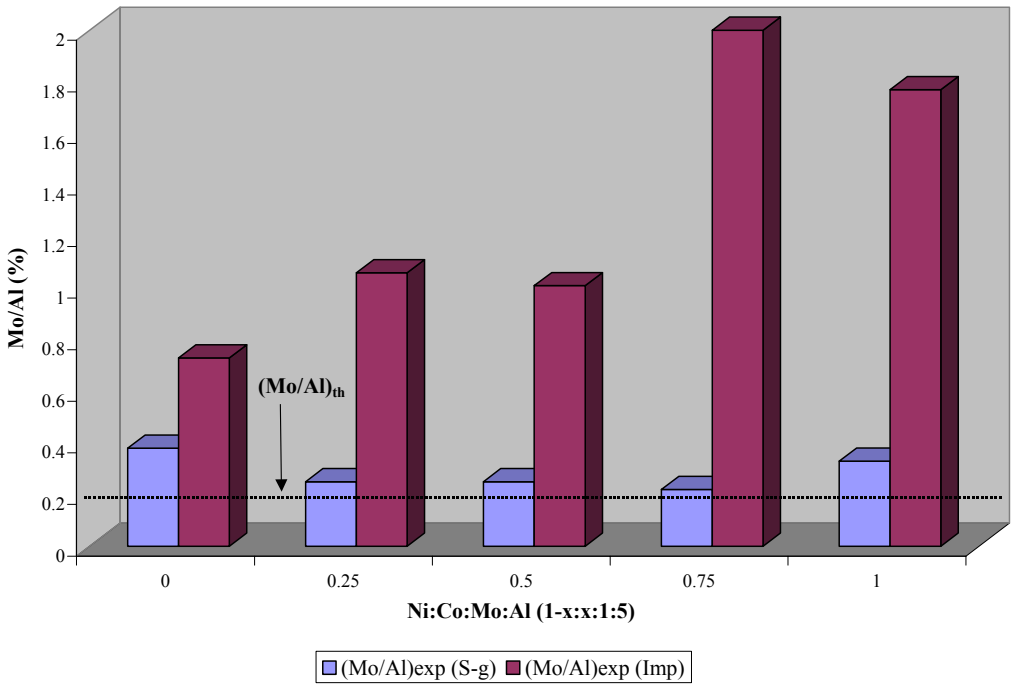

Fig.III.32: Experimental (Mo/Al) atomic ratio in alumina dispersed catalysts prepared by sol-gel and impregnation methods with respect to their composition.

Table III.15: Relative atomic ratios measured by XPS and $YC_3^=$ values of Ni:Co:Mo:Al at 753 K.

Composition and Molar Ratio	Ni/Co			$Y^*C_3^=$ (% m^{-2})	
	Exp (S-g)	Exp (Imp)	Theoretical	S-g	Imp
Ni:Co:Mo:Al 0.75:0.25:1:5	3	2.53	3	0.19	0.18
Ni:Co:Mo:Al 0.5:0.5:1:5	1.08	0.85	1	0.35	0.24
Ni:Co:Mo:Al 0.25:0.75:1:5	0.45	0.29	0.33	0.51	0.24

Correlation between catalytic activity and XPS analyses in magnesia-dispersed catalysts

Fig.III.28 shows that all magnesia-supported $Ni_{1-x}Co_xMoO_4$ prepared by impregnation are much more active than the corresponding ones prepared by sol-gel method, except for $NiMoO_4$.

The XPS results (table V.6 in Appendix V) seem to corroborate the hypothesis that a better dispersion of Ni, Co and Mo is normally reached when preparing the catalysts by impregnation rather than by sol-gel. We can also suppose the formation of surface MoO_3 in impregnated catalysts because the (Mo/Mg) ratios are higher than the

theoretical ones (fig.V.11 in Appendix V) and higher than those prepared by sol-gel method. According to what we said previously for alumina-based catalysts, this would lead to a decrease of the catalytic activity. However, we observe better catalytic performances for impregnated catalysts than sol-gel catalysts. The hypothesis of surface MoO_3 cannot be invoked in this case. However, a major difference can be found in the absolute values of the experimental (Mo/Mg) ratios: in MgO impregnated catalysts, this ratio (range 0.4 - 0.72) is lower than the experimental (Mo/Al) ratios observed for alumina-impregnated catalysts (range 0.73 - 2). In MgO-supported catalysts prepared by impregnation, the amount of Mo present on the surface does not inhibit the catalytic activity of such catalysts in the same way it does in Al_2O_3-impregnated catalysts.

For MgO-impregnated catalysts (Ni/Co) experimental atomic ratios are higher than the theoretical ones and higher than in the corresponding samples prepared by sol-gel method and that are characterized by a lower catalytic activity: once again, the lower the Co content on the surface, the higher the yields towards propene (table III.16).

Table III.16: Relative atomic ratios measured by XPS and $YC_3^=$ values of Ni:Co:Mo:Mg at 753 K.

Composition and Molar Ratio	Ni/Co			$Y^*C_3^=$ (% m^{-2})	
	Exp (S-g)	Exp (Imp)	Theoretical	S-g	Imp
Ni:Co:Mo:Mg 0.75:0.25:1:5	2.23	3.2	3	Nd	1.04
Ni:Co:Mo:Mg 0.5:0.5:1:5	0.83	1.83	1	0.18	1.02
Ni:Co:Mo:Mg 0.25:0.75:1:5	0.48	0.76	0.33	0.3	0.93

Correlation between catalytic activity and XPS analyses in mixed alumina-magnesia-dispersed catalysts

As already seen in MgO-dispersed catalysts, the differences in catalytic behaviour of mixed alumina-magnesia-dispersed catalysts cannot be explained by taking into account the experimental (Mo/(Al+Mg)) ratios: in fact the (Mo/Al) ratio is somewhat higher than the theoretical one, and the (Mo/Mg) and (Mo/(Al+Mg)) ratios (fig.V.12 in Appendix V) are very close to the corresponding theoretical ratios: the hypothesis of surface MoO_3 formation cannot be invoked.

But, if we compare the experimental atomic (Ni/Co) ratios of Al_2O_3-MgO-dispersed catalysts to the analogous ones Al_2O_3- and MgO-dispersed prepared by the sol-gel method (table III.17), it is also observed in this case that the higher the experimental (Ni/Co) atomic ratio, the higher the propene yield.

Table III.17: Relative atomic ratios measured by XPS and $YC_3^=$ values of Ni:Co:Mo:Al+Mg prepared by sol-gel method at 753 K.

Composition and Molar Ratio	Ni/Co		$Y^*C_3^=$ (% m^{-2})
	Experimental	Theoretical	
Ni:Co:Mo:Al+Mg 0.75:0.25:1:5	1.51	3	0.184
Ni:Co:Mo:Al+Mg 0.5:0.5:1:5	0.94	1	0.218
Ni:Co:Mo:Al+Mg 0.25:0.75:1:5	0.43	0.33	0.319

III.2.12 Discussion of the catalytic results of TiO_2 and ZrO_2-supported Ni and Co molybdates prepared by impregnation

We have already mentioned that TiO_2- and ZrO_2-dispersed Ni and Co molybdates are the most active catalysts in propane ODH among all the catalysts tested in this work.

If we take into account the $YC_3^=$ (%) and $Y^*C_3^=$ (% m^{-2}) values (it must be reminded that both kind of catalysts are characterized by very little specific surface areas), those of zirconia-supported catalysts are higher than those of the titania-supported ones. In this case the reason for a better catalytic activity of ZrO_2-based catalysts cannot be found, neither in the experimental (Ni/Co) ratios, nor in the experimental (Ni,Co/Mo) ratios, because they are very close to each other; but, the difference can be related to the fact that the experimental (Ni,Co and Mo/Ti,Zr) ratios are very high (figs.V.13 and V.14 in Appendix V), much higher than the theoretical values.

All metals constituting the active phase completely cover the surface of the catalysts, leading to a high catalytic activity. The additional differences in the catalytic behavior between TiO_2- and ZrO_2-based catalysts can also be explained by referring to the fact that all experimental (Ni,Co and Mo/Zr) ratios are much higher than the experimental (Ni,Co and Mo/Ti) ratios.

The experimental (Ni,Co and Mo/Ti,Zr) ratios are also higher than those in the analogous impregnated catalysts supported on alumina and magnesia which show lower activity than those supported on TiO_2 or ZrO_2.

III.2.13 Catalytic performances of Ni and cobalt molybdates modified by lanthanides

III.2.13.1 Catalytic performances of "non-stoichiometric" Ni-Co-Ln(Bi)-Mo-Si (1:1:1:2.5:20)

Table IV.14 in Appendix IV lists the catalytic performances of all Ni-Co-Ln(Bi)-Mo-Si-catalysts at 723 and 753 K. The incorporation of La, Ce, Pr and Tb in the catalyst formulation results in improving the catalytic performances of the Ni-Co molybdate catalyst used as reference, by enhancing the overall activity towards partial and total oxidation, and more particularly the propene yield up to a factor 2 (from 5.4% for a simple Ni:Co:Mo:Si-sample to 10% for a Tb-modified catalyst). In all these cases, the carbon balance is very close to 100 % with propene and CO_2 as only products, whereas it amounts to about 75 % only in non modified or Bi-promoted catalysts.

The maximum propene productivity is observed at 753 K with the Tb-modified catalyst and corresponds to 0.12 $g_{propene}$ $(h\ g_{cat})^{-1}$. La-, Pr- and Ce-modified catalysts present high propene productivities (between 0.11 and 0.1 $g_{propene}$ $(h\ g_{cat})^{-1}$) close to that of Tb-modified catalyst. Sm- and Bi-based catalysts showed the same propene productivity (0.05 $g_{propene}$ $(h\ g_{cat})^{-1}$) but lower than that displayed by Ni-Co-Mo-Si-sample (0.067 $g_{propene}$ $(h\ g_{cat})^{-1}$).

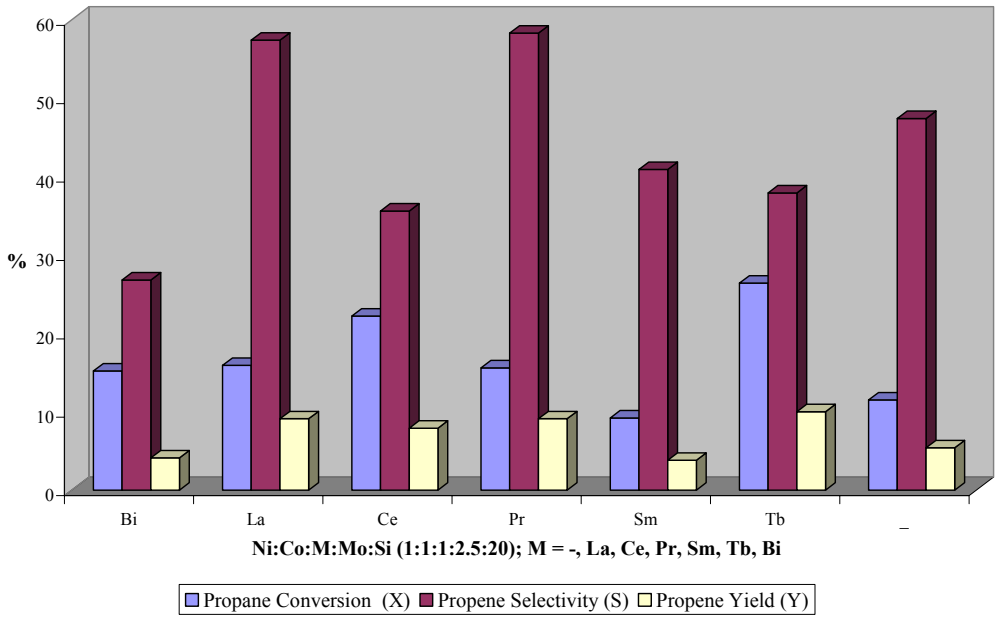

Fig.III.33: Propane conversion, propene selectivity and propene yield of Ni-Co-M-Mo-Si (1:1:1:2.5:20) catalysts, at 753 K.

Fig.III.33 displays $XC_3°$, $SC_3^=$ and $YC_3^=$ of all modified mixed Ni and Co molybdates, at 753 K. The catalysts containing Ce or Tb display the highest propane

conversions but also the highest selectivity to CO_2; this is consistent with the very high oxygen consumption displayed by those two catalysts (96 and 74.5%, respectively at 753 K). The Bi- and Sm-based catalysts are the least productive systems with respect to propene: the Sm-based catalyst is the least active and the Bi-based catalyst the least selective towards propene. The highest selectivities to propene are obtained in the case of La- and Pr-based catalysts (50 to 63%).

III.2.13.2 Catalytic performances of "non-stoichiometric" Ni-Co-M-M'(Bi)-Mo-Si (1:1:1:1:2.5:20)

Table IV.15 in Appendix IV lists the catalytic performances of multimodified Ni and Co molybdates. The main comments on the catalytic data are reported in the section IV.4.3 of Appendix IV. We will report hereafter some comments related to the comparison of selectivities at isoconversion and the evaluation of the synergetic effects.

Comparison at isoconversion

In order to make comparisons between all tested catalysts it is important to focus on catalysts characterized by the same propane conversion values at the same temperature.

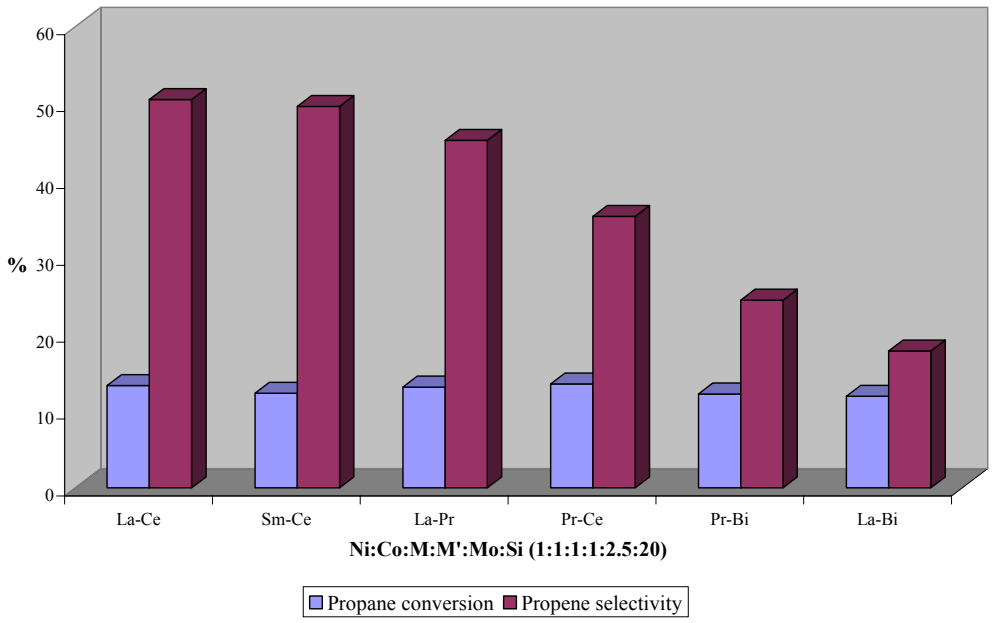

Fig.III.34: Propane conversion and propene selectivity of some Ni:Co:Ln:Ln'(Bi):Mo:Si, at 753 K.

Fig.IV.14 in Appendix IV and fig.III.34 show how the selectivity to propene depends on the nature of the additional elements, for two series of catalysts characterized by the same propane conversion at 723 and 753 K, respectively. It appears

clearly that the La-Ce, Sm-Ce and La-Sm combinations provide the most selective catalysts, whereas all Bi-based formulations (La-Bi, Pr-Bi,) result in low selectivities.

Evaluation of the synergetic effects

In order to evidence synergetic effects between the two additional elements incorporated in the multimodified catalysts, we compared selectivities and yields of catalysts containing two elements with those of the catalysts containing only one element.

For each multimodified catalyst, a "theoretical" value of yield or selectivity ($Y_{th}C_3^=$ and $S_{th}C_3^=$) was also calculated as the average of the two individual experimental values obtained with the corresponding monomodified catalysts. Moreover, the synergy on propene yield and propene selectivity were calculated, defined by the following expressions:

$$\Delta YC_3^= = \frac{YC_{3\,exp}^= - YC_{3\,th}^=}{YC_{3\,th}^=} \text{ ; and } \Delta SC_3^= = \frac{SC_{3\,exp}^= - SC_{3\,th}^=}{SC_{3\,th}^=}$$

The calculated values are listed in table III.18. According to these calculations, the catalytic data of table IV.15 in Appendix IV could be divided into four groups showing different behaviours.

Table III.18: Theoretical value of yield or selectivity ($Y_{th}C_3^=$ and $S_{th}C_3^=$) and synergy on yield and selectivity ($\Delta YC_3^=$ and $\Delta SC_3^=$) for multimodified Ni:Co:M:M':Mo:Si (1:1:1:1:2.5:20).

Catalysts	$Y_{th}C_3^=$ (%)	$S_{th}C_3^=$ (%)	$\Delta YC_3^=$ (%)	$\Delta SC_3^=$ (%)
La-Ce	8.5	46.5	-0.21	0.09
La-Pr	9.1	57.9	-0.35	-0.21
Ce-Pr	8.5	46.9	-0.43	-0.25
La-Bi	6.6	42.1	-0.68	-0.59
Pr-Bi	6.6	42.6	-0.55	-0.43
Ce-Bi	6.0	31.2	-0.23	-0.18
Sm-La	6.5	49.2	-0.12	0.34
Sm-Pr	6.5	49.6	-0.26	0.32
Sm-Bi	4.0	33.9	-0.55	-0.44
Sm-Ce	5.9	38.3	0.03	0.29
Tb-Ce	9.0	36.8	0.27	-0.13
Tb-La	9.6	47.7	0.17	-0.16
Tb-Pr	9.6	48.1	0.19	-0.08
Tb-Bi	7.1	32.4	-0.81	-0.16
Tb-Sm	6.9	39.4	0.72	-0.08

The results are described schematically, in table III.19. Behaviour I refers to catalysts for which selectivity and yield are both improved or close to the average calculated values. Behaviour II refers to situations where one property is negatively affected, while the other one is equal to the average calculated value (cfr. fig.III.36). In behaviour III: both selectivity and yield are worse than the calculated values (cfr. fig.III.37), and in behaviour IV: one property is improved while the other one is reduced (cfr. fig.III.38). Type I behaviour corresponds to a true synergetic effect, the values of selectivity or yield obtained with the catalysts containing both elements being higher or close than the average value calculated from the corresponding monomodified. This behaviour was observed in five cases (cfr. fig. III.35). For some bimetallic combinations, the effect was negative or non existent (i.e. equal to the calculated value).

Table III.19: Different types of catalytic behaviour observed in Ni-Co-Ln-Ln'(Bi)-Mo-Si catalysts.

Behaviour type	Effect on		Additional elements in multimodified catalysts
	Propane selectivity ($SC_3^=$)	Propene yield ($YC_3^=$)	
Behaviour I	↑	≈	Sm-Ce ; Sm-La
	≈	↑	Tb-Pr; Tb-Sm; Tb-Ce
Behaviour II	≈	↓	La-Ce
	↓	≈	
Behaviour III	↓	↓	La-Pr; Ce-Pr; La-Bi; Pr-Bi ; Sm-Bi ; Tb-Bi; Ce-Bi
Behaviour IV	↑	↓	Sm-Pr
	↓	↑	Tb-La

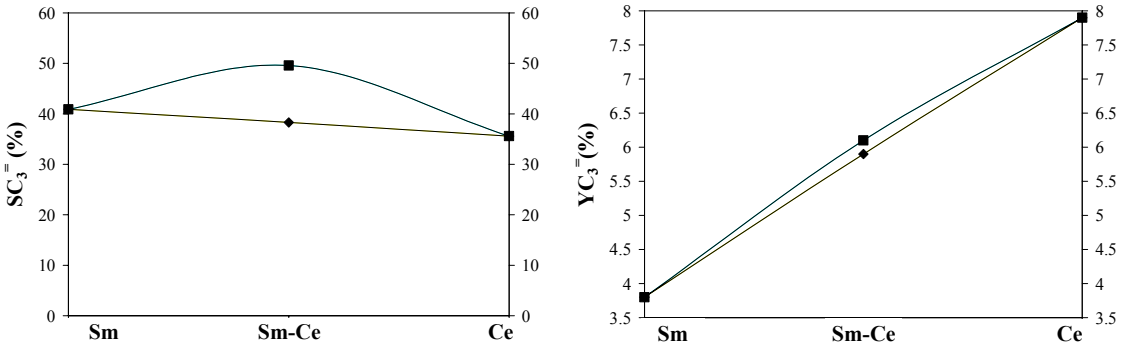

Fig.III.35: Behaviour-type I displayed by Ni-Co-Sm-Ce-Mo-Si catalyst.

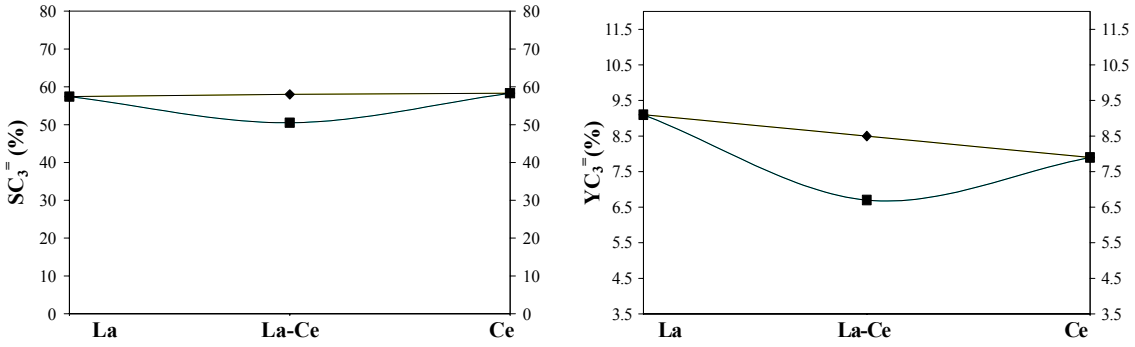

Fig.III.36: Behaviour-type II displayed by Ni-Co-La-Ce-Mo-Si catalyst.

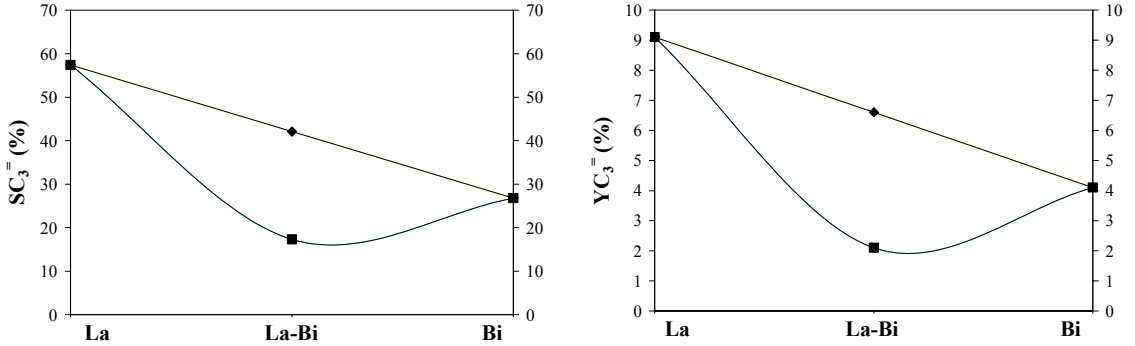

Fig.III.37: Behaviour-type III displayed by Ni-Co-La-Bi-Mo-Si catalyst.

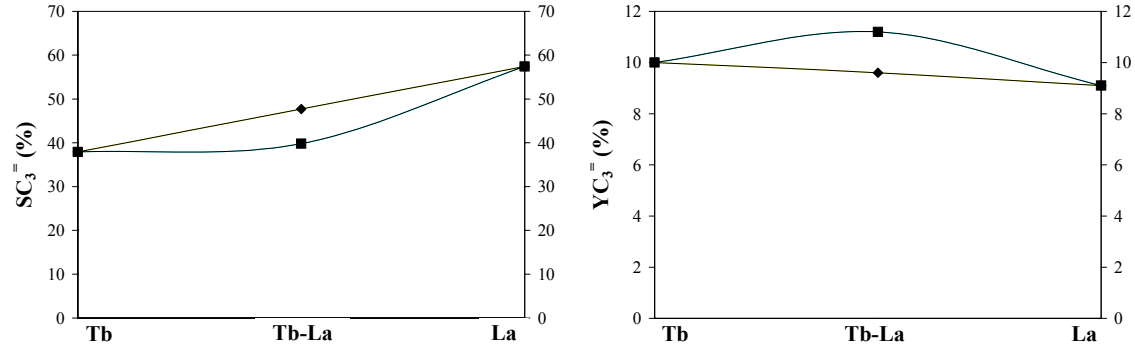

Fig.III.38: Behaviour-type IV displayed by Ni-Co-Tb-La-Mo-Si catalyst.

The seven catalysts listed in behaviour-type III all display lower selectivities and yields than the average of the two individual experimental values obtained with the corresponding monomodified catalysts. In these cases, the inhibiting effect exerted by

bismuth, which lowers both propene yield and selectivity, is quite evident and allows us to conclude that there is no advantage in incorporating Bi as additional element in such catalysts.

The substantial synergetic effects to be noticed (described in table III.18) are obtained with Tb, which leads to an increase of propene yield and for Sm, which leads to an increase of propene selectivity.

III.2.14 On the catalytic behaviour of modified mixed Ni and Co molybdates (Ni:Co:Ln(Bi):Mo:Si, 1:1:1:2.5:20)

By referring to a previous approach aimed at rationalizing the role of lanthanides in multiphase catalysts for isobutene oxidation (113), we will present and discuss here three types of correlations based on the concepts of ionization energy, absolute hardness and redox potential (values taken from (114), table VI.18 in Appendix IV). Although these parameters are interrelated with each other, they reflect different facets of the Lewis acido-basicity and redox character.

While redox potential essentially describes the ability to transfer electrons from the catalyst to molecular oxygen, the ionization energy is more specifically involved in the M-O bond polarization in the lattice and affects the nucleophilicity of lattice oxygen. The third parameter, absolute hardness, which is a combination of IE and electron affinity, is involved in the overall catalytic process, by allowing to describe the interactions between catalyst, substrate and intermediate products on the basis of preferential hard-hard interactions.

However, during our attempts to deduce correlations between the physico-chemical parameters and the activity-selectivity, we faced a difficulty. In several cases, the yields to propene ($YC_3^=$) were found to vary in a very erratic way, whereas the CO_2 yields changed regularly. For these reasons, the following discussion will focus mainly on the CO_2 production ($YCO_2/3$ or $Y^*CO_2/3$), and propane conversion ($XC_3°$).

III.2.14.1 Ionization energy

Fig. III.39 shows the evolution of CO_2 yields (%) with respect to the ionization energy (IE); considering the major oxidation state identified by XPS or assumed (Tb^{4+}) at the catalyst surface, this graph refers to the 4th IE ($Ln^{3+} \rightarrow Ln^{4+}$) for Bi, La, Pr and Sm, whereas the 5th IE ($Ln^{4+} \rightarrow Ln^{5+}$) is used for Ce and Tb.

Fig.III.39 shows that the most active catalysts towards total oxidation are those characterized by an additional element with the highest IE. Even if we consider the evolution of the intrinsic CO_2 yield ($Y*CO_2/3$) with respect to the ionization energy, we observe the same behavior. This trend is actually the opposite of that found previously, on the basis of the 4th IE values only, when binary oxides Ln_xO_y were used in total or selective oxidation of butane (115) or isobutene (113). In those two cases, the tendency to total oxidation was higher with oxides containing elements with low 4th IE values, in line with the fact that this would facilitate the formation and increase the concentration of surface electrophilic oxygen species resulting from electron transfers between M^{n+} cations and adsorbed molecular oxygen (O^{2-}, O_2^{2-}, O^-).

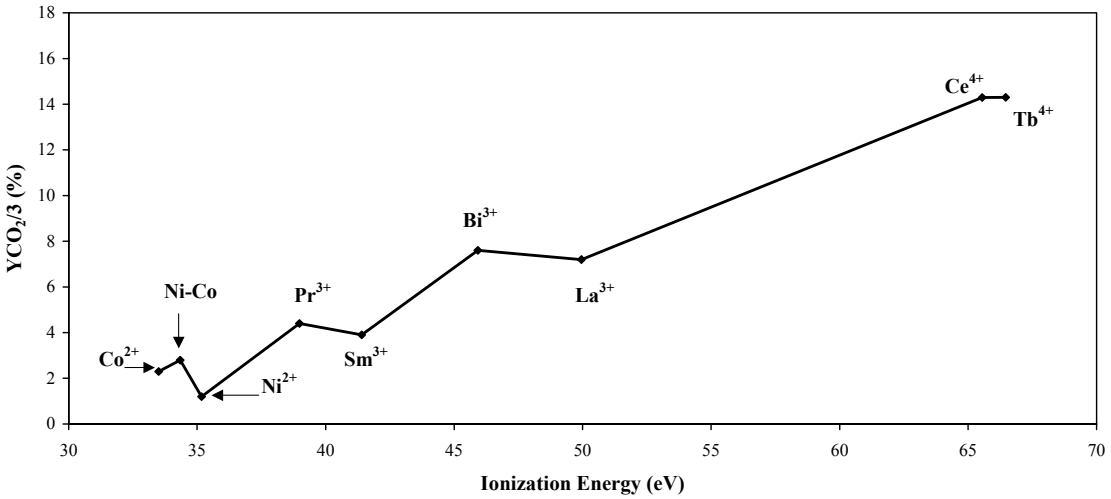

Fig.III.39: Evolution of the CO_2 yield of Ni:Co:Ln:Mo:Si catalysts with respect to the ionization energy of the additional elements.

The fact that reverse behaviors are observed suggests that, even if a Mars and van Krevelen-type mechanism is accepted with the first hydrogen-abstraction from the secondary C-H bond being the rate-determining step (74), some key mechanistic features could actually differ. The fact that low CO_2 yields are observed in the presence of elements with low IE values suggests that in this case the metal cation is involved through its neighbourhood with lattice oxygens whose nucleophilicity increases when the metal IE decreases.

In comparison with the non modified Ni, Co or Ni-Co molybdate catalysts used as references, the incorporation of Bi^{3+} or $Ln^{3+/4+}$ in the molybdate lattice affects the

polarization of the M^{n+}-O^{2-} and consequently the electron density on the lattice O^{2-} anions. Different properties can therefore be expected according to the way these elements are distributed in the lattice, namely the various possible arrangements like the $Ni^{2+}(Co^{2+})$-O^{2-}-Mo^{VI} and $Ln^{3+/4+}(Bi^{3+})$-O^{2-}-Mo^{VI} moieties. In the presence of additional elements with low IE, the average nucleophilicity of lattice oxygen will increase and lower CO_2 yields result. In this way, the global evolution of the CO_2 yield with respect to the IE values seems to account quite satisfactorily for the influence of the additional elements.

III.2.14.2 Absolute hardness

A second correlation can be described between the catalytic performances and the Lewis acid-base properties of the cations involved, which can be represented by their absolute hardness. While coordinatively unsaturated metallic ions in a high oxidation state can be considered as acidic centers, oxygenated ions and organic substrates constitute basic centers. For propane ODH, it is usually claimed that the catalysts have to display a certain hard acid character to activate propane, which is assimilated to a poorly polarizable, hard base, due to the presence of strong σ bonds.

In fig.III.40, propane conversion, CO_2 yields and selectivity to propene at 753 K are plotted against the absolute hardness of the concerned ions, calculated according to Pearson's definition. A similar bell-shaped relationship appears for the propane conversion and the yield in CO_2 (and also for $Y*CO_2/3$), with a maximum occurring for Ce^{4+} and Tb^{4+}. On one hand, the initial increase of propane conversion and CO_2 yield with increasing hardness reflects the importance of strong interactions between the alkane and the metal cation to activate the substrate (rate-determining step) and convert it into total oxidation products. If we plot the evolution of SCO_2 (CO_2 production) with respect to the absolute hardness of the modifying elements involved in the formulation of the catalyst, we observe a maximum for Ce^{4+} and a strong decrease of SCO_2 in the case of La-modified catalyst (see fig.IV.18 in Appendix IV). This fact is in line with HSAB concepts, on the basis that the oxidation of an alkane would be more selective if it involves a soft cation rather than a hard one, because the interaction with the catalyst would be weaker. On the other hand, decrease of these parameters at high hardness values reflects the necessity to have well-adapted properties between the alkane and the catalyst. For very hard cations (La^{3+}), the increase in selectivity to partial oxidation

could also be the consequence of much weaker interactions between the catalyst and the formed propene, which would desorb more easily from the surface.

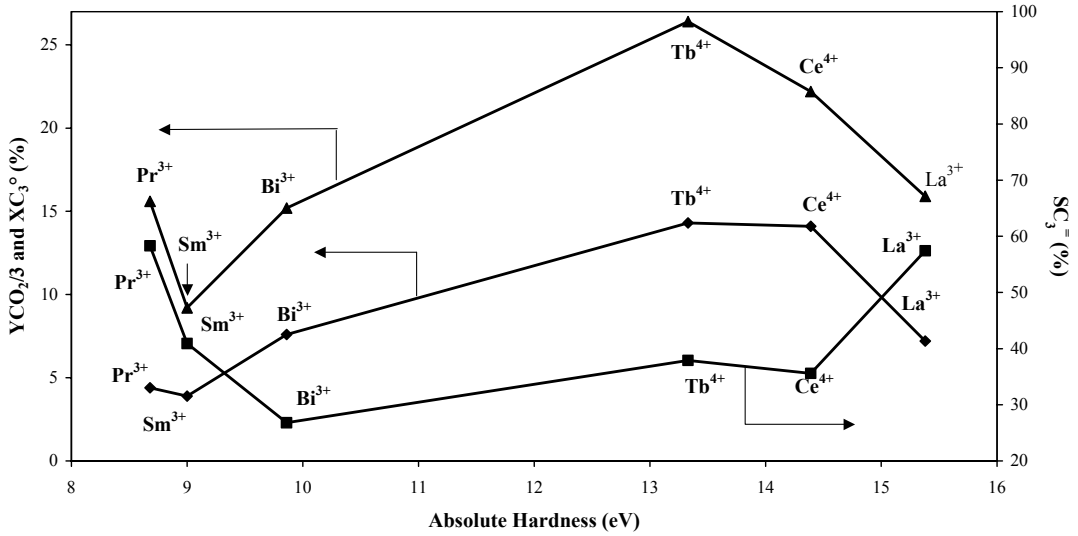

Fig.III.40: Evolution of the CO_2 yield (♦), propane conversion (▲) and the selectivity to propene (■) with respect to the absolute hardness of the additional elements.

III.2.14.3 Redox potential

The ease of removal of lattice oxygen, which determines the selectivity towards partial or total oxidation products, can be measured in two different ways; by referring to the metal-oxygen bond strength or to the ease of reduction of the cation in the solid. The metal-oxygen bond strength could be evaluated via measurements of the differential heats of reoxidation of the reduced catalysts. Because the removal of lattice oxygen from the active site is accompanied by the reduction of the neighboring cation, another way to evaluate the feasibility of this process is to look at the reduction potential of the cations at the active site.

Figure III.41 illustrates such a correlation between selectivity to propene and the standard redox potential of the additional elements. The most selective catalysts are characterized by the lowest redox potentials. In this case, the low reducibility of the M^{n+} cation diminishes the availability of lattice oxygen (O^{2-}) as electrophilic species (like O^-), promoting thereby partial oxidation. On the other hand, the relatively higher selectivities reached in the case of Ce^{4+} and Tb^{4+} could be explained by the involvement of Ln^{4+}/Ln^{3+} redox couples: on one hand, the high reducibility of Ln^{4+} species would in

principle favour total oxidation (the absolute CO_2 yields are high) by facilitating the conversion of O^{2-} to O^-, but on the other hand, the resulting steady-state concentrations of reduced Ln^{3+} species could be involved in the reoxidation mechanism of the reduced catalyst and permit fast replenishment of the lattice oxygen vacancies by helping to convert molecular oxygen to O^{2-} species.

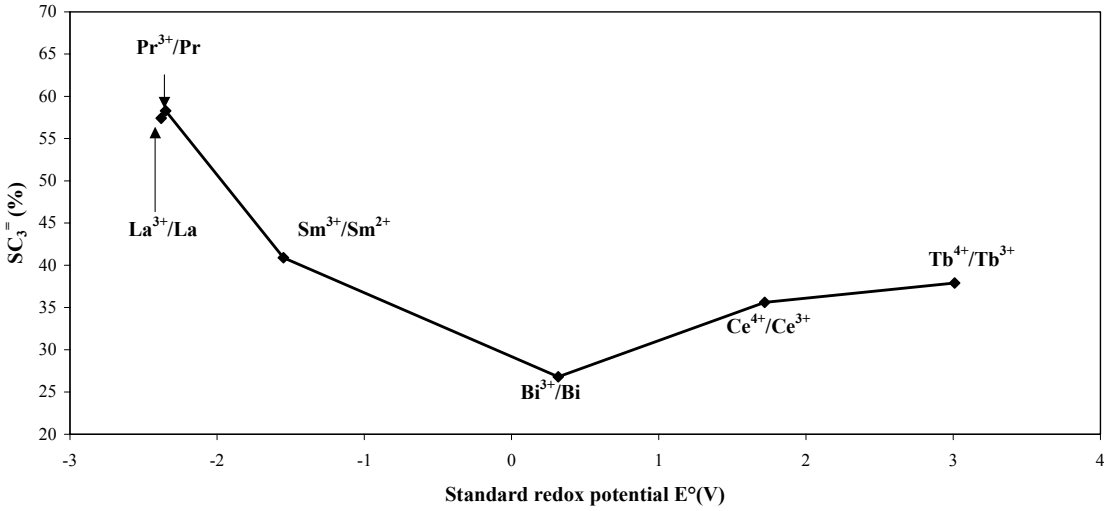

Fig.III.41: Evolution of the selectivity to propene with respect to the standard redox potential of the additional elements (at 753 K).

Fig.IV.19 in Appendix IV shows how the catalytic activity (expressed in terms of $YCO_2/3$) depends on the redox potential: the catalysts involving additional elements characterized by higher redox potential (Ce^{4+}, Tb^{4+}) display higher catalytic activity, due to the fact that they can easily change their oxidation state: a higher redox potential leads to higher selectivities towards overoxidation products. The same behaviour is observed when considering the intrinsic CO_2 yield.

III.2.15 On the catalytic behaviour of multi-modified mixed Ni and Co molybdates (Ni:Co:Ln:Ln':Mo:Si, 1:1:1:1:2.5:20)

The correlations described between the catalytic activity of Ni:Co:Ln(Bi)Mo:Si catalysts and some fundamental properties of the additional elements, like ionization energy, absolute hardness and redox potential, suggest that these parameters are useful theoretical tools to account for the global properties of multicomponent oxidation catalysts involving several active elements. By starting with a similar approach we will try to rationalize the catalytic performances of multimodified mixed Ni and Co molybdates by correlating them to the same physico-chemical properties.

Admitting that oxygen is mobile in and on the crystalline network of oxides active in catalytic oxidation, it can be assumed that the reactive oxygen ions are statistically present with similar probabilities in the vicinity of the two modifying elements. We define consequently an average ionization energy and an average absolute hardness by taking into account the proportions of their respective cations in the catalyst. Taking into account the generic formula Ni:Co:Ln:Ln':Mo:Si (1:1:1:1:2.5:20), the average physico chemical parameter (A.P.) was calculated as follows: A.P. = (P_{Ln} +$P_{Ln'}$)/2; where P_{Ln} and $P_{Ln'}$ refer to values of the chosen physico-chemical parameter of the two different lanthanides. Table IV.20 in Appendix IV summarizes these average parameters calculated for all Ni:Co:Ln:Ln':Mo:Si catalysts.

III.2.15.1 Ionization energy

Fig.III.42 shows the evolution of intrinsic CO_2 yields (% m^{-2}) with respect to the ionization energy (IE) of the Ln ions involved in the formulation of the catalyst; this graph refers to the 4th IE ($Ln^{3+} \rightarrow Ln^{4+}$) for La, Pr and Sm, whereas the 5th IE ($Ln^{4+} \rightarrow Ln^{5+}$) is used for Ce and Tb. What can be remarked first is that the graph could be split up into two different parts: an upper part in which Tb-Ln modified catalysts are present displaying higher CO_2 yield values than all other multimodified catalysts, and a lower part in which, for all catalysts the higher the average ionization energy of the modifying elements, the higher the observed intrinsic CO_2 yield (fig.III.43). This last correlation is respected in Ln-Ln' modified catalysts also at lower temperature (723 K).

The conclusion already mentioned in the Ni-Co-Mo-Si catalysts modified by only one lanthanide element can therefore be extended to the catalysts in which two different lanthanides have been incorporated; the low intrinsic CO_2 yields are observed in the presence of elements with low I.E. values, suggesting that the metal cation is

involved through its neighborhood with lattice oxygens whose nucleophilicity increases when the metal IE decreases.

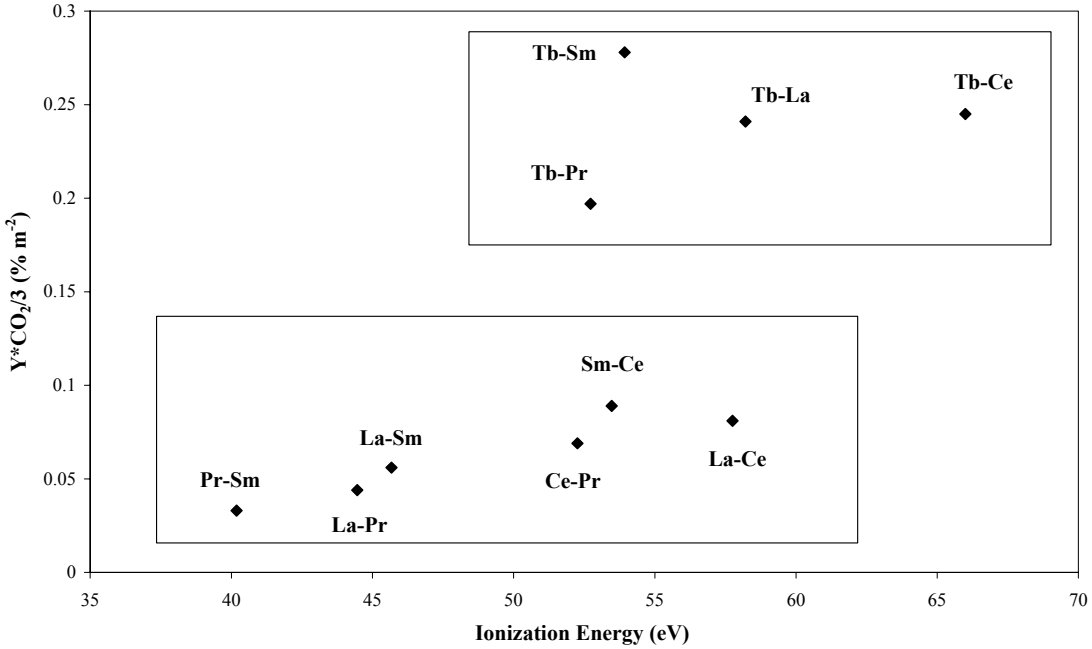

Fig.III.42: Evolution of the intrinsic CO_2 yield of Ni:Co:Ln:Ln':Mo:Si (Ln, Ln' = La, Ce, Pr, Sm, Tb) catalysts with respect to the ionization energy of the additional elements (at 753 K).

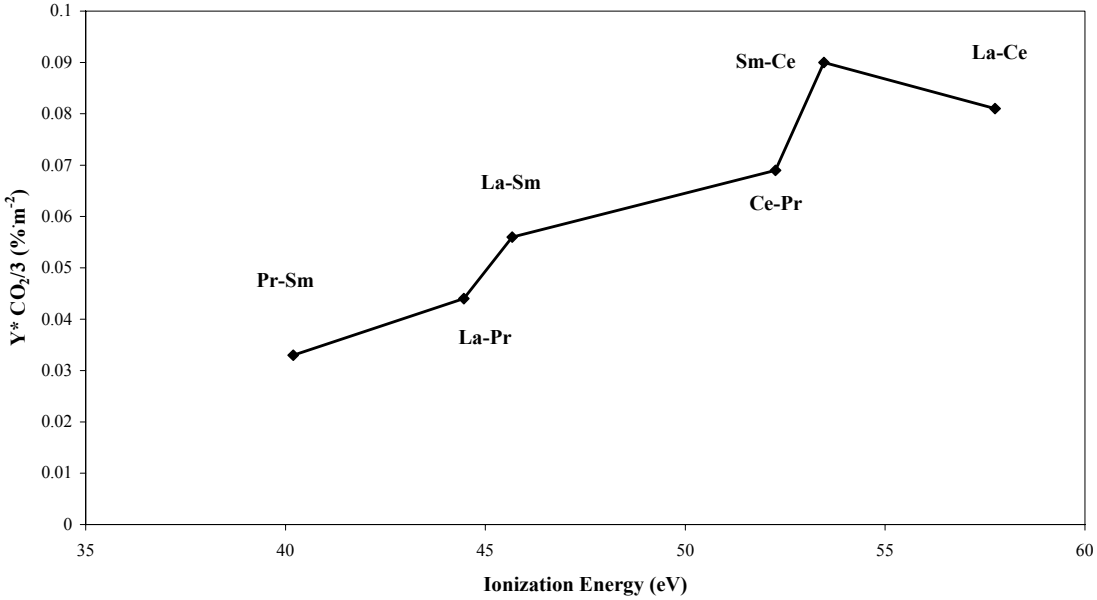

Fig.III.43: Evolution of the intrinsic CO_2 yield of Tb-free Ni:Co:Ln:Ln':Mo:Si catalysts with respect to the ionization energy of the additional elements (at 753 K).

Whenever Tb is present, the catalyst behaves differently, even if their global average IE (in Tb-Ln modified catalysts) is sometimes lower than that of some Ln-Ln' modified ones (average $I_{(La-Ce)}$ and $I_{(Sm-Ce)} > I_{(Tb-Sm)}$ and $I_{(Tb-Pr)}$), it could be that Tb^{IV} plays the main role in the catalytic performances when present. Due to the fact that Tb^{IV} is the most easily reducible species, the reactive oxygen ions could be more numerous in its vicinity, rather than statistically distributed in the lattice. This fact could explain the extremely high catalytic activity of all Tb-Ln modified catalysts, even if they have an average IE lower than that of some other Ln-Ln' modified catalysts. In other words, the concept of statistical distribution of active oxygen species would not be valid anymore.

Fig.III.44 displays the evolution of the propane conversion with respect to the average IE of the modifying elements. The evolution of propane conversion globally reflects the evolution of the intrinsic CO_2 yield: the lower the average IE, the lower the propane conversion. Again this graph could be split up into two different parts, the upper part with Tb-Ln modified catalysts and the lower part with Tb-free modified catalysts.

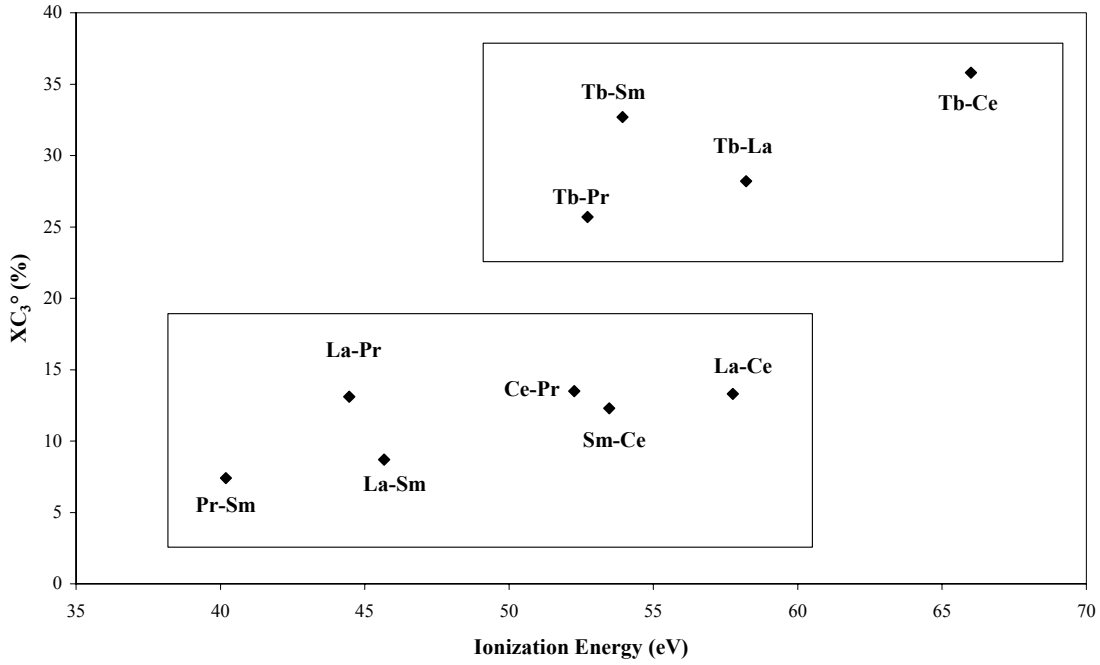

Fig.III.44: Evolution of propane conversion of Ni:Co:Ln:Ln':Mo:Si (Ln, Ln' = La, Ce, Pr, Sm, Tb) catalysts with respect to the ionization energy of the additional elements (at 753 K).

III.2.15.2 Absolute hardness

Fig. III.45 and fig. III.46 show the evolution of the catalytic behaviour of multimodified Ni-Co molybdate catalysts expressed in terms of intrinsic CO_2 yield (% m^{-2}) and propane conversion (%) with respect to the average absolute hardness of the modifying elements. At first view, a bimodal distribution appears in both graphs, with two maxima and a minimum. However, at a closest analysis this behaviour once again reflects the presence of two series of catalysts corresponding to a splitting of this graph into two different parts, the upper part with the Tb-Ln modified catalysts and the lower part with the Tb-free catalysts (fig.III.47).

Generally speaking, the catalytic behaviour of Tb-based catalysts do not show a clear dependence on the average absolute hardness. In the upper part of figures III.45 and 46 we observe an initial increase of both intrinsic CO_2 yield and propane conversion going from the Tb-Pr to the Tb-Sm associations, probably due to a strong interaction between the alkane (considered as a hard base) and the metal cations: this strong interaction leads to increasing amounts of total oxidation products. However, the decrease in intrinsic CO_2 yield and propane conversion that we observe in the case of the most hard lanthanides present in Tb-Ln catalysts could be due to the weak interactions between the very hard cations and the formed propene, making the propene desorption from the surface easier.

In the second series of catalysts (fig.III.47), free of Tb, there is a general trend of increasing CO_2 when the average absolute hardness is higher (and this is confirmed also for the catalytic data at 723 K). The higher production of CO_2 depends on the degree of interaction between the metal cation and the reactant: for Tb-free catalysts we observe increasing intrinsic CO_2 yield values due to increasing strong interactions between the substrate and the reactant. For any Tb-free catalyst (even if we consider those with the highest A.H. values), we observe a decrease in total oxidation products which could be due to weaker interaction between too hard cations and the formed propene. However, it must be pointed out once again that close absolute hardness values do not allow a satisfactory qualitative discrimination between the catalysts.

The differences in catalytic behaviour between Tb-Ln- and Tb-free Ni and Co molybdates can again be attributed to the fact that Tb plays the main role in the catalytic reaction. Even if it is associated with lanthanides with lower absolute hardness, Tb^{4+} (which is a very hard cation) is thought to interact strongly with the reactant, leading to very high intrinsic CO_2 values.

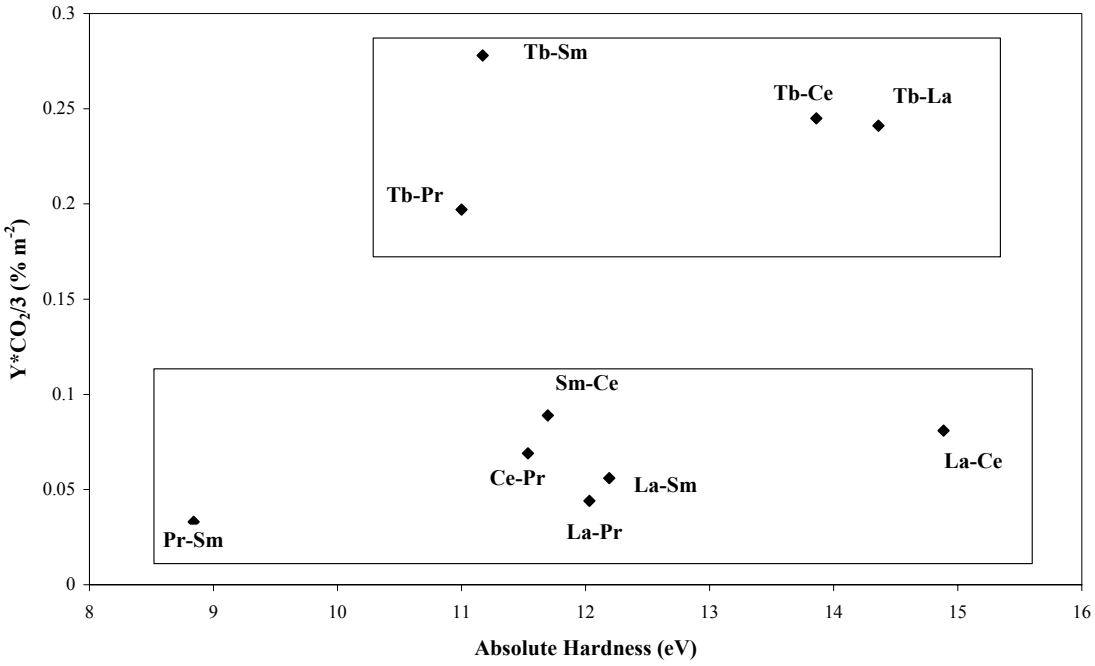

Fig.III.45: Evolution of intrinsic CO_2 yield of Ni:Co:Ln:Ln':Mo:Si (Ln, Ln' = La, Ce, Pr, Sm, Tb) catalysts with respect to the absolute hardness of the additional elements (at 753 K).

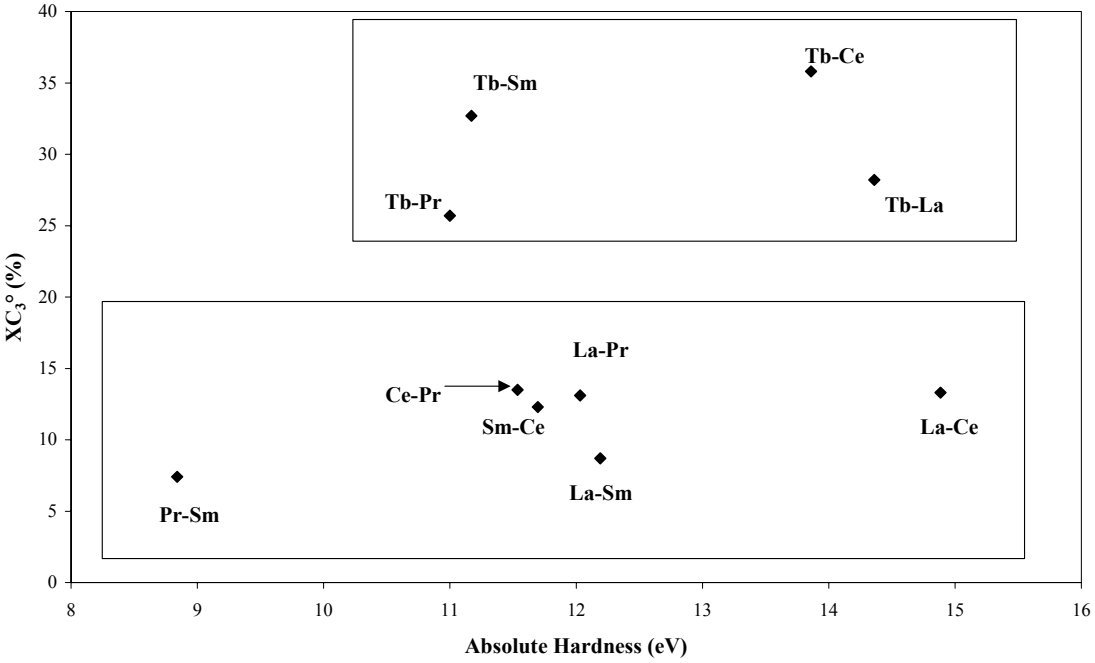

Fig.III.46: Evolution of propane conversion of Ni:Co:Ln:Ln':Mo:Si (Ln, Ln' = La, Ce, Pr, Sm, Tb) catalysts with respect to the absolute hardness of the additional elements, at 753K. (Both $Y^*CO_2/3$ and $XC_3°$ values for the Tb-Ce association have been corrected for the catalyst mass, see table IV.15 in Appendix IV).

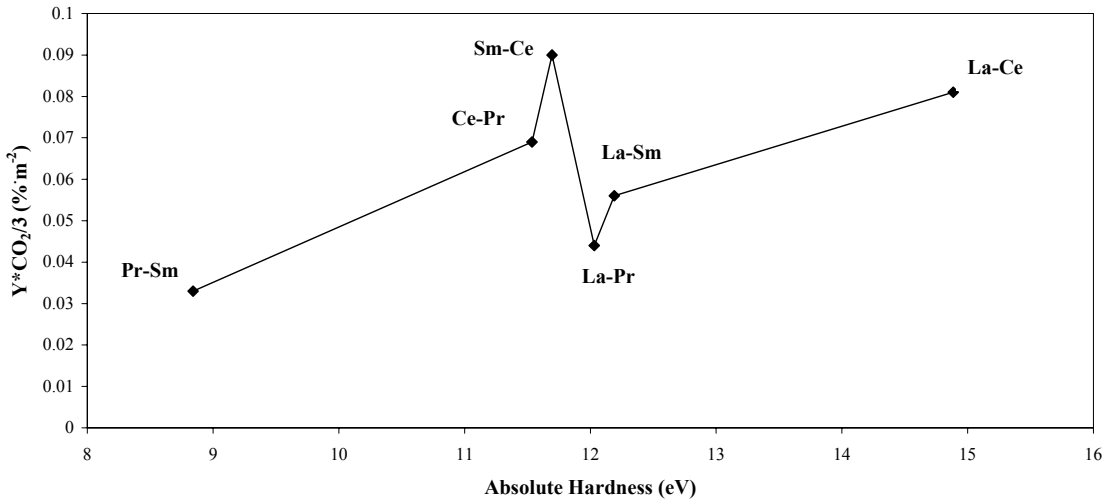

Fig.III.47: Evolution of intrinsic CO_2 yield of Tb- free Ni:Co:Ln:Ln':Mo:Si catalysts with respect to the absolute hardness of the additional elements (at 753 K).

In addition, Tb could also be the lanthanide which is present in higher amount on the surface (even if was impossible to carry out XPS analysis on Tb-based catalysts) and strongly influences the catalytic performances of the catalysts in which it is involved.

III.2.15.3 Redox potential

Fig. III.48 illustrates the correlation between the catalytic activity expressed in terms of intrinsic CO_2 yields of all multimodified Ni and Co molybdates and the average redox potential of the additional elements (table IV.20 in Appendix IV). The most active catalysts are characterized by the highest redox potentials. In these cases, the high overall reducibility of the Tb^{4+}-$Ln^{4+/3+}$ associations increases the availability of the electrophilic species (as O^-), promoting total oxidation. For the associations Tb-free (Ln-Ln') characterized by a low redox potential, the low reducibility limits the transformation of the nucleophilic lattice oxygen species (O^{2-}) into electrophilic species with a consequent decrease of the catalytic activity (low $Y^*CO_2/3$ values). The catalysts containing Tb^{4+} display the best catalytic performances but also the highest production of overoxidation products like CO_2.

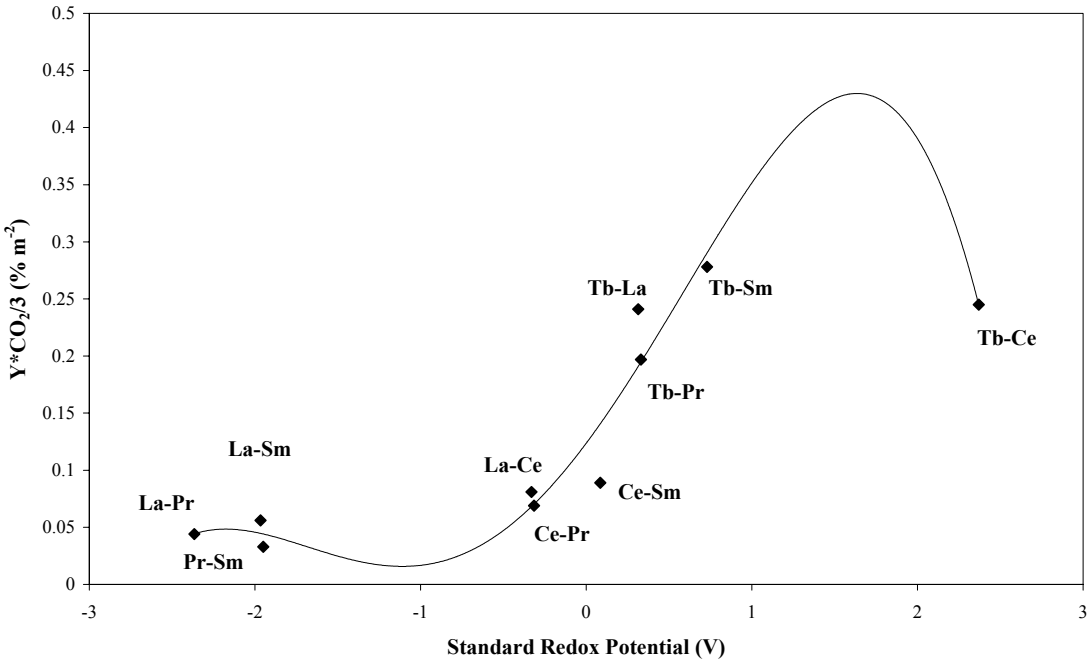

Fig.III.48: Evolution of intrinsic CO_2 yield of Ni:Co:Ln:Ln':Mo:Si (Ln, Ln' = La, Ce, Pr, Sm, Tb) catalysts with respect to the standard redox potential of the additional elements, at 753 K. (The $Y^*CO_2/3$ value for the Tb-Ce association has been corrected for the catalyst mass, see table IV.15 in Appendix IV).

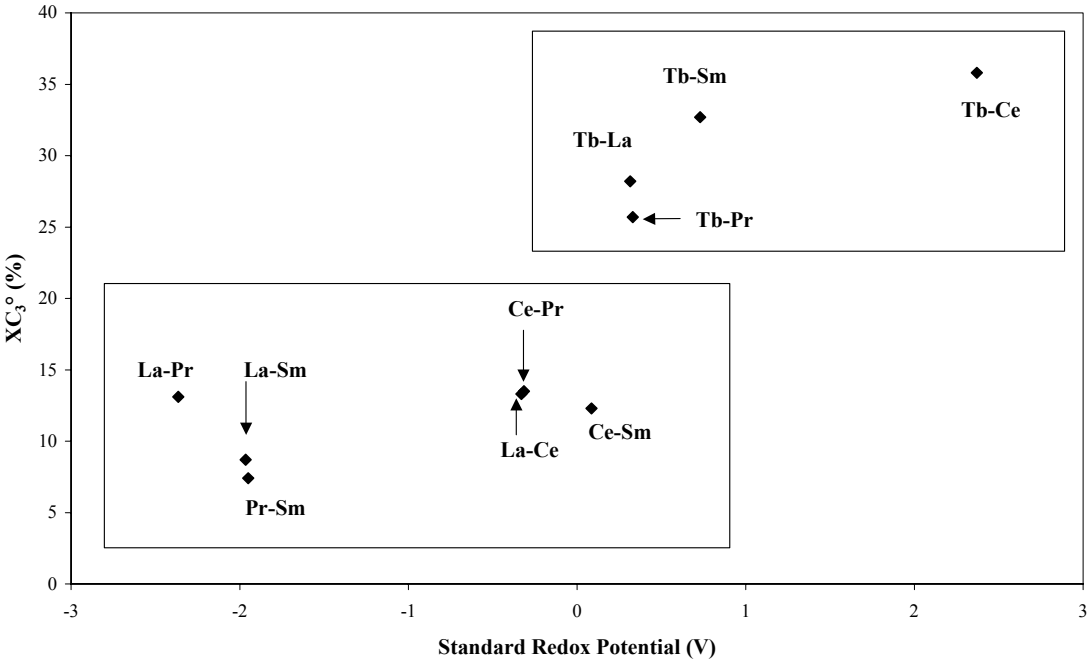

Fig.III.49: Evolution of propane conversion of Ni:Co:Ln:Ln':Mo:Si (Ln, Ln' = La, Ce, Pr, Sm, Tb) catalysts with respect to the standard redox potential of the additional elements, at 753 K. (The $XC_3°$ value for the Tb-Ce association has been corrected for the catalyst mass, see table IV.15 in Appendix IV).

Even if in this case, we can describe in a common picture the catalytic behaviour of all multimodified catalysts, once again two different zones can be distinguished: an upper zone with the most active catalysts and a lower zone with the less active catalysts at low redox potential. The gap appearing between these two classes of catalysts led us to conclude that the influence of Tb on the global catalytic behaviour of the catalysts is critical: Tb^{4+} seems definitely to be the key element of the Tb-Ln-modified catalysts.

Fig.III.49 illustrates the evolution of propane conversion with respect to the average standard redox potential of the additional lanthanides. We observe a relationship very similar to the one observed in the case of intrinsic CO_2 yields. Once again Tb-Ln-modified catalysts are characterized by the highest propane conversion values.

III.2.16 Conclusions

The most important results concerning the catalytic behaviour of all our catalysts are summarized below:

- In the case of silica-dispersed molybdates, the catalytic data emphasize the advantage of using mixed Ni-Co molybdates in comparison with simple Ni or Co molybdates, and also the fact that a higher activity is reached when these active phases are dispersed in a silica matrix, with quite appreciable propene productivities at 753 K. It should be also remembered that the hypothesis of partial encapsulation of the active phase in the silica network was put forward on the basis of the XPS results, and consequently the catalytic behaviour of these samples is not yet fully optimised. However, when comparing catalysts with the same overall composition but prepared by sol-gel or impregnation methods, it comes out that their catalytic behaviour does not follow a specific trend: samples prepared by sol-gel method are sometimes more efficient than those prepared by impregnation, and sometimes not.
- Concerning all other supported catalysts, from the point of view of the catalytic performances expressed in terms of $Y^*C_3^=$, the sol-gel method made possible to prepare alumina-dispersed molybdates that are more active than the corresponding catalysts prepared by impregnation on commercial supports. On the other hand, magnesia-supported molybdates prepared by impregnation display a higher catalytic activity than the analogous ones prepared by sol-gel method. When a mixed Al_2O_3-MgO support is used, the catalysts show slightly better catalytic performances than

the sol-gel prepared MgO-supported molybdates. It was also shown that catalysts characterized by intermediate acid-base properties, like TiO_2- and ZrO_2-based ones, give better catalytic performances than those with high acidity or high basicity.

- Concerning the effect that lanthanides or bismuth can exert on the catalytic performances of nickel and cobalt molybdates, it must be reminded that when solid solutions of β-$NiMoO_4$ and β-$CoMoO_4$ are modified by a lanthanide, a strong enhancement of the catalytic activity and the selectivity towards propene is observed except in the case of Sm. The Tb-modified catalyst is the one displaying the highest propene productivity, but the most selective catalysts are those modified by La or Pr. Incorporation of Ce strongly improves the catalytic activity, more than propene selectivity. The presence of Bi in the catalyst and the subsequent formation of $Bi_2Mo_3O_{12}$ increases the propane conversion but strongly decreases the selectivity towards propene. The catalytic activity, expressed in terms of propene yield, of mixed Ni-Co molybdates modified by two lanthanides is generally enhanced. Also in this case, the presence of Bi in the formulation of the catalyst results in lower propene selectivity. The catalysts modified by Tb are those displaying the highest propene productivity and those modified by Pr and/or La are characterized by the highest propene selectivity.